

LOAD TRANSFER MODELS IN JOINT LINES OF PUNCHED METAL PLATE FASTENERS

Lucas Carvalho Paiva

Thesis submitted to the
School of Technology and Management
Polytechnic Institute of Bragança

in partial fulfilment of the requirements for the Master's Degree in
Construction Engineering

Bragança, November 10, 2019

LOAD TRANSFER MODELS IN JOINT LINES OF PUNCHED METAL PLATE FASTENERS

Lucas Carvalho Paiva

Thesis submitted to the
School of Technology and Management
Polytechnic Institute of Bragança
in partial fulfilment of the requirements for the Master's Degree in
Construction Engineering
in the scope of the double degree program with the
Federal University of Technology – Paraná

Thesis supervised by the Professors
Manuel Teixeira Braz César
Edson Florentino de Souza

Bragança, November 10, 2019

CONTENTS

Contents	i
Abstract	iii
Resumo	iv
Acknowledgements	v
Epigraph	vi
List of Figures	vii
List of Tables	ix
List of Charts	x
Nomenclature	xi
1 Introduction	1
1.1 General aspects	1
1.2 Research objectives	3
1.3 Thesis structure	3
2 Timber as a Structural Element	4
2.1 Introduction	4
2.2 Advantages of timber-based structures	6
2.3 Connection systems	7
2.4 Trussed rafter industry	10
2.4.1 Nail plate trusses manufacturing	12
2.5 Nail plates	14
2.6 Summary	18
3 Design of Nail Plate Connections	19
3.1 Introduction	19
3.2 Nail plate mechanical parameters	20
3.2.1 Anchorage area parameters	21
3.2.2 Net-cross section parameters	21
3.3 Characteristic resistance values	22
3.3.1 Nail plate characteristic values	22
3.3.2 Connection characteristic values	22
3.4 Design according to Eurocode 5	24
3.4.1 Anchorage verification	24

3.4.2	Net-cross section verification	25
3.5	Stress distribution in wood trusses	26
3.6	Rupture lines	29
3.7	Summary	30
4	A Heel Joint Modeling	31
4.1	Introduction	31
4.2	Anchorage area verification	34
4.3	Distribution models	35
4.3.1	Model 1 – Simultaneous line deformation	35
4.3.2	Model 2 – Bending moments transfer	38
4.3.3	Model 3 – Isolated regions	40
4.3.4	Model 4 – Independent force transfer	43
4.4	Comparison and critical combination of force distribution	45
4.5	Summary	48
5	Conclusions and Further Research	49
5.1	Conclusions	49
5.2	Future developments	50
	References	51
A	NPCalc Code	55

ABSTRACT

Timber joints are a key part of timber structures, and their performance is a major requisite to successful timber constructions. Among all the connection types, punched metal plate fasteners are the most economical and efficient, reasons why this connection dominates the prefabricated truss industry. However, the structural load bearing capacity of these timber connections is mechanically complex and difficult to analyse. Besides, the current standards oversimplify many current joint configurations and don't provide a guideline to predict the stress distribution within the plate.

Most research to date has focused on modelling and testing punched metal plate fasteners from a FEM 3-D perspective, accounting for all its parts (timber, plate, teeth and tooth-wood interface) whilst knowledge on the 2-D stress distribution within the plate is limited. The complete joint modeling with a 3-D model based on FEM gives precise results on the mechanical behavior of those plates, but requires more time to model and more computational processing. In a truss design point of view, where many connections need to be verify, a 2-D static model is usually the annalist's choice, and despite the large industrial application of metal plates, the internal force flow still lacks research.

The research reported in this thesis describes four methods to account for the stress distribution in punched metal plate fasteners. Each model is based on a particular plate behavior and aims to identify the critic rupture lines to successfully attend the ultimate limit state criteria.

A heel joint was taken as starting point to study the stress distribution in the rupture lines, and a computational tool (NPCalc) was developed based on the current standards to verify the main connection aspects. The connection was modeled by the four methods and the results were analysed and compared, seeking to identify how the stress flows within the plate once the loads are applied.

Two manual and two numerical methods were presented. The results showed a considerable variability with the model's choice, and the numerical models pointed to be more conservative. However, the simple regions (delimited by only one rupture line) presented equal results regardless the chosen model.

Finally, the conclusions of the elaborated research are presented, discussing the extension of its results and the suggestions for future development, in order to complement the analysis and modeling of wooden trusses with punched metal plate fasteners.

Keywords: timber connections; nail plate trusses; punched metal plate fasteners; stress distribution.

RESUMO

As ligações são um aspecto chave das estruturas de madeira e seu desempenho é um requisito necessário para construções bem-sucedidas. Entre os tipos de ligação já desenvolvidos, as chapas metálicas são as mais econômicas e eficientes, razões pelas quais essa conexão domina o setor de treliças pré-fabricadas. No entanto, a capacidade de carga estrutural dessas conexões é mecanicamente complexa e difícil de análise. Além disso, as normativas atuais simplificam configurações correntes de conexão e não fornecem uma diretriz para prever a distribuição de tensões na placa.

Até o momento, a maioria das pesquisas se concentrou na modelagem e teste de chapas dentadas a partir de uma perspectiva FEM 3-D, respondendo por todas as suas partes (madeira, chapa, dentes e interface dente-madeira), enquanto o conhecimento da distribuição de tensões 2-D dentro do placa é limitada. A modelagem completa da ligação com um modelo 3-D baseado em FEM fornece resultados precisos sobre o comportamento mecânico dessas placas, mas requer tempo para modelar e considerável processamento computacional. Do ponto de vista do projeto de treliças, onde muitas conexões precisam ser verificadas, um modelo estático em 2-D é geralmente a escolha do analista e, apesar da grande aplicação industrial dessas chapas, o conhecimento acerca da distribuição de forças internas ainda requer aprofundamento.

A pesquisa relatada nesta tese descreve quatro modelos para prever a distribuição de tensões nas linhas de ruptura de chapas metálicas dentadas. Cada modelo é baseado em comportamento específico da ligação e tem como objetivo identificar as linhas de ruptura críticas para atender com segurança os critérios do estado limite último.

Uma ligação de extremidade foi tomada como ponto de partida para estudar a distribuição de tensões e uma ferramenta computacional (NPCalc) foi desenvolvida com base nas normativas atuais para verificar os principais aspectos da conexão. A conexão foi modelada pelos quatro métodos desenvolvidos e os resultados foram analisados e comparados, buscando identificar como a tensão na chapa flui após a aplicação das cargas.

Foram apresentados dois modelos manuais e dois modelos numéricos. Os resultados apresentaram grande variabilidade com o modelo escolhido, e os modelos numéricos tenderam a ser mais conservadores. Entretanto, As regiões simples (delimitadas por apenas uma linha de ruptura) apresentaram resultados iguais para todos os modelos testados.

Por fim, são apresentadas as conclusões do trabalho elaborado, discutindo a extensão de seus resultados e as sugestões para desenvolvimento futuro, a fim de complementar a análise e modelagem de treliças em madeira com chapas dentadas.

Palavras-chave: estruturas em madeira; treliças pré-fabricadas; chapa metálica dentada; distribuição de esforços.

ACKNOWLEDGEMENTS

Although presented as an individual project, this dissertation is actually the result of a collaborative process. All the work done and goals achieved would not be possible without the support and encouragement of many people. Therefore, I want to thank those who contributed to this journey.

To my supervisor, Prof. Manuel Teixeira Bráz César, for the availability, support and guidance without which it wouldn't be possible to accomplish the research goals.

To the Polytechnic Institute of Bragança and the Federal Technological University – Paraná, institutions that gifted me great opportunities and experience.

To Eng. Gabryel Smek, for the invaluable friendship and suggestions that contributed to this project.

To all the friends I had the pleasure of meeting in Bragança, through you, I could discover the best of all parts of the world. Your friendship is the best memory of this journey.

Finally, a very special mention to my parents, Jacó and Silvana, who not only never questioned my abilities, but always did their best to support my goals. To both of you I am an eternal debtor.

“You can do anything, but not everything.”

– David Allen

LIST OF FIGURES

1.1	Geometry of a heel joint	3
2.1	Longhouse reconstruction, 3000 BC, [4].	5
2.2	Horyuji Temple, [11, 13].	5
2.3	Prefabricated timber frame with several concealed connections, [24].	8
2.4	Comparison of four high performance connections, [25].	9
2.5	Conventional truss structure, [30].	11
2.6	Nail plate truss structure, [30].	11
2.7	Manufacture of truss frame, [31].	12
2.8	Automated Cut Saw SP720, [32].	13
2.9	Truss assembly, [33].	13
2.10	Plate pressing, [33].	14
2.11	Truss handling, [34].	14
2.12	Common nail plate shapes, [35].	15
2.13	Foschi proposition for the load-slip curve, [37].	16
2.14	Heel joint studied designs, [38].	17
2.15	Overall slip contribution, [39].	17
3.1	Typical nail plate fastener	19
3.2	Nail plate configuration examples	20
3.3	EC5 nail plate notation	21
3.4	Parallel to grain test	23
3.5	Perpendicular to grain test	23
3.6	Anchorage area for multiple member joints	24
3.7	Plane truss modeling evolution, [11].	27
3.8	Heel joint model with fictitious elements, [43].	27
3.9	Truss plate connection modeling by DTU 31.3 2012	28
3.10	Force distribution within the plate	29
3.11	Region with one rupture line	29
3.12	Region with multiple rupture lines	30
4.1	Heel joint dimensions in mm	31
4.2	Force's system in the heel joint	32
4.3	NPCalc starting page	34
4.4	Isolated analysis of region B (M1)	35
4.5	Force distribution in region B (M1)	36
4.6	Force distribution on adjacent lines (M1)	36
4.7	Force distribution on adjacent lines (M2)	38
4.8	Bending moment transference by Model 1	38
4.9	Mechanical model of the rupture line (M3)	40
4.10	Force distribution in region B (M3)	41

4.11	Deformed configuration for AB/BC in mm (M3)	41
4.12	Hyperstatic regions by Model 3	42
4.13	Numerical stress transfer method (M4)	43
4.14	Region B as starting point by Model 4	43
4.15	Critical efforts of rupture lines in kN and kN m	46

LIST OF TABLES

4.1	Acting forces in the region's barycenter	33
4.2	Nail plate mechanical properties	33
4.3	Anchorage checking results	34
4.4	Result of distribution by Model 1	37
4.5	Results of net-cross section verification by Model 1	37
4.6	Result of distribution by Model 2	39
4.7	Results of net-cross section verification by Model 2	39
4.8	Result of distribution by Model 3	42
4.9	Results of net-cross section verification by Model 3	42
4.10	Result of distribution by Model 4	44
4.11	Results of net-cross section verification by Model 4	45
4.12	Net-cross section envelop results	46
4.13	Overall comparison of stress distribution by the four presented models	47

LIST OF CHARTS

4.1	Line AC comparison by Model 1	37
4.2	Line AC comparison by Model 3	42
4.3	Line AC comparison by Model 4	44
4.4	Line AB comparison by Model 4	44
4.5	Line BC comparison by Model 4	44
4.6	Net-cross section capacity overall comparison	45

NOMENCLATURE

CONVENTIONS

H, V	horizontal and vertical directions , global axis.
T, N	tangential and normal directions, local plate axis.
M	bending moment in Z axis (paper plane).

ACRONYMS

ASTM	American Society for Testing and Materials
ANSI	American National Standards Institute
CSA	Canadian Standards Association
DTU	Document Technique Unifié
EC5	Eurocode 5 (EN 1995-1-1:2004)
FEM	Finite element method
ISO	International Organization for Standardization
NPCalc	Nail Plate Calculator
TPI	Truss Plate Institute
ULS	Ultimate limit state

GREEK LETTERS

α	angle between the force and the x-direction (main plate direction)
β	angle between the grain-direction and the force
γ	angle between the x-direction and the rupture line
τ	stress

ROMAN LETTERS

A	area
e	eccentricity

F	force
f	strength
h	relative height
I	inertia
K	stiffness
k	constants
ℓ	rupture line dimension
r	distance from the region barycenter
W	torsion module

LOWER INDICES

0	parallel-to-grain direction
90	perpendicular-to-grain direction
c	compression
d	design value
k	characteristic value
ser	slip
t	tension
v	longitudinal shear

INTRODUCTION

In this thesis, four theoretical models were presented to predict the stress distribution in the rupture lines of punched metal plate fasteners. The main standards were revised and each model, accounted for a specific joint behavior, was analyzed to identify which parameters have direct influence in the stress distribution. This introduction motivates the research and outlines its structure.

1.1 GENERAL ASPECTS

Timber is one of the oldest building materials, probably dating back to prehistory, where fallen trees were used as bridges to access new paths. Due to its availability and variety, this material has various structural applications, such as in use in bridges, trusses, floors, roofs, among others. Few materials have characteristics that enable as many structural applications as wood. In addition, wood adds the concepts of sustainability, being a low aggregate energy structural material, durable (when well designed) and recyclable. Like any raw material, it is necessary to reflect on its possible scarcity, and this is one of the great advantages of wood: if sustainable forest management and good harvesting are practiced, wood becomes indefinitely available.

The usage evolution of the wood as a structural element is, however, conditioned to the knowledge of the physical properties and mechanical behavior of the material. There are many factors that make wood a more complex material than the most common building materials such as concrete, steel and ceramic. Due to its variability, inherent to its growth and development, wood has properties that directly influence its design process, such as moisture content, difference in resistance when loading is applied parallel or perpendicular to the fibers (elevated anisotropy), and even the method adopted to classify their resistance. Structural analysis of wood elements as well as their mechanical modeling is also hampered by nonlinear behavior, creep and biological degradation. [1, 2].

The most important aspect of timber structures is the joint design. The need to study the connections is due to the unavailability of parts that adapt to the design conditions, either due to the high strength required or the structure geometry. The first wooden houses, which appeared around 3500 BC, had a limited width range of 5–7 m, due to simplified adhesive bonding techniques. Mechanical joints date back to 600 BC, and since then the use of these connection types, especially in wooden trusses, has been developing. [3, 4].

Mechanical connections can be divided into two main groups, according to the form of

stress transmission. The group of dowels or pins, such as nails and screws, where force transmission is described by a combination of the behavior between the pins and the wood in contact with the pin rod. The second group includes metal plates, such as rings or shear plates and toothed plates, which transmit stress through the surface contact area of their members. [5, 6].

In general, wood joints are the limiting factor in the structure design. The strength of the structure is usually determined by the strength of its connections. The mechanical behavior of the structure is also characterized by the quantity and type of the connection used.

The mechanical behavior of wood joints is complex and difficult to predict. For instance, the load capacity of a connection with a certain number of connectors is not equal to the product of the resistance of a single connector multiplied by the number of connectors. In most regulations, the reduction in the load capacity is taken into account by the effective number of connectors n_{ef} , which is less than the actual number of connectors n . In European and Brazilian codes, the actual number of connectors is only dependent on n . In codes used in Canada and the United States of America, the spacing between connectors, either between them or relative to edges, is also taken into account. As well in metal plates, many variables can affect the joint stiffness: the size and number of teeth, the orientation of the plate in relation to the wood fibers, the angle of forces applied, the location of the connection in relation to the center of the members axis. In addition, the stress distribution is nonlinear and non-constant across the width and length of the plate. [7, 8].

The proper choice of the type of connection is also a determining factor in the cost evaluation and, most notably, in the execution time of timber projects. The evolution of wood building systems is therefore directly linked to the development of more efficient joining methods, both on-site and in prefabricated parts. [9].

Among the types of mechanical connectors developed, the most efficient and less labor intensive are the punched metal plate fasteners. Such plates are widely used in the production of prefabricated roof trusses, for their low cost and easy production compared to other types of joints. [10].

Punched metal plate fasteners (nail plates) are galvanized steel plates with thicknesses between 0.9–2.5 mm, with teeth perpendicular to the plate with size between 8–15 mm. These plates are pressed on each side of the wood by presses, and the transmission of the bonding forces mobilizes a large portion of the wood area, reason why this connection is more efficient than other types of mechanical joints. The complexity in the design of these connections is due to the stress distribution within the plate. The distribution is nonlinear and non-constant along its length and width. Current standards present the equations for the Ultimate Limit State (ULS) design from the forces acting on the rupture lines, but there is no comprehensive research about the mechanical modeling to obtain these forces [11].

In the present dissertation, four methods are suggested to characterize the stress distribution in the rupture lines of nail plates. A heel joint, illustrated in Figure 1.1, is taken as a starting point for the developed modelings.

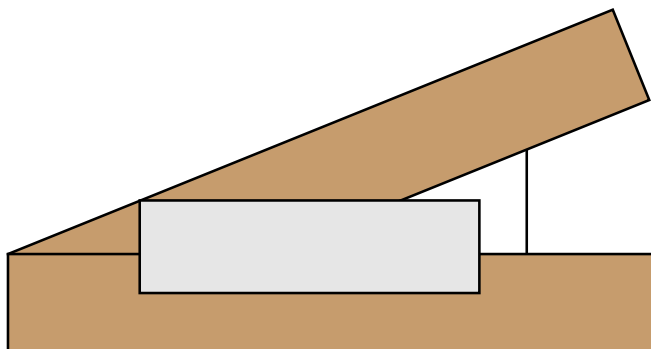


Figure 1.1: Geometry of a heel joint

1.2 RESEARCH OBJECTIVES

The main objectives were:

- Study the design and modeling criteria of nail plate timber connections;
- Propose models to predict the stress distribution in the rupture lines;
- Develop a computational tool to verify nail plate connections.

1.3 THESIS STRUCTURE

The dissertation was structured in 5 chapters. *Chapter 1* gives an introduction and theme's background, the relevance of the study and the defined objectives of the investigation.

Chapter 2 covers the literature review, starting with the main applications of wood as a structural element, focusing on the manufacture of roof trusses. Then, timber joint mechanisms are studied and finally the nail plate joints, their manufacturing process and the state-of-the-art are presented.

Thereafter, *Chapter 3* discusses the design criteria of nail plates. The premises and relevant equations of the main standard resolutions are described. Finally, the truss modeling of prefabricated trusses and the problem of rupture lines are presented.

The formulation of new stress distribution methods is described in *Chapter 4*. In total, four methods are proposed in order to account for the various load behaviours that a nail plate connection may be subjected to.

Chapter 5 presents the conclusions of the studies on the intended objectives. In view of the conclusions, future development lines are suggested.

TIMBER AS A STRUCTURAL ELEMENT

The origins and advantages of using wood as a structural element are discussed. Then, timber connections are presented, highlighting the nail plate joints. The focus of this chapter is to present a brief literature review on the use of wood and to direct the study to the nail plate connections.

2.1 INTRODUCTION

From prehistory to the beginning of the industrial age, wood has always been present in the human relationship with the environment. The use of wood, the oldest of building materials, began a building model that would remain, even after the advent of new materials. Over the millennia, knowledge about the construction and architecture of wooden structures has become a way of connecting people around the world. Wooden constructions developed, regardless of cultural and regional boundaries.

That said, the early construction methods evolved and the knowledge and techniques needed to deal with this material were gradually building an empirical basis. In the beginning, simplified adhesive bonding techniques limited maximum spans, but constant evolution brought new connection methods and new designs. A brief historical review shows that, despite their scarce knowledge of building properties and techniques, prehistoric civilizations were incredibly intelligent in adapting structures to their needs and conditions. Therefore, the evolution of these techniques created an architectural identity (e.g. the Nordic houses and Japanese temples) that was only achieved due to the versatility of this material [12].

The first framed houses arose around 3000 BC. The durability of these constructions did not exceed 20 years, as little was known about structural detailing, especially in bracing and joints. Figure 2.1 illustrates the archaeological reconstruction of a house in Central Europe, dated 3000 BC. Spans were limited to 5–7 m long, and the shape of the triangular truss was at first the simplest solution found [4].

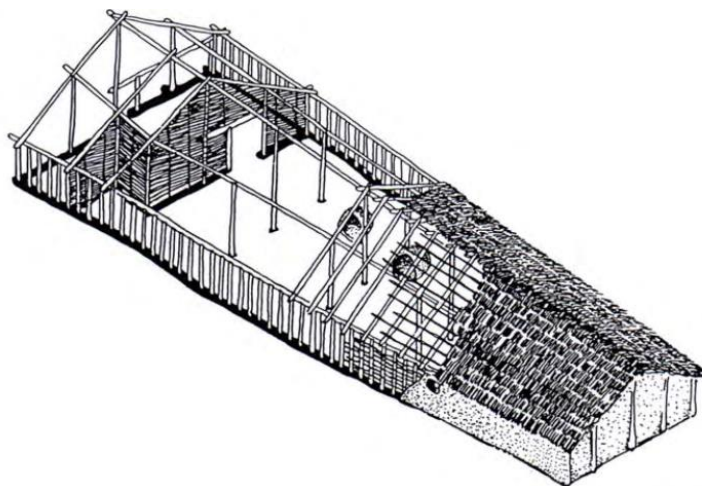


Figure 2.1: Longhouse reconstruction, 3000 BC, [4].

Some regions of Asia have a long relationship with the structural element of wood. In Japan, the oldest structure still in existence, the Horyuji Temple, was built in the 7th century. This building has a double roof and each of the five floors is supported by the central pole [11, 13].

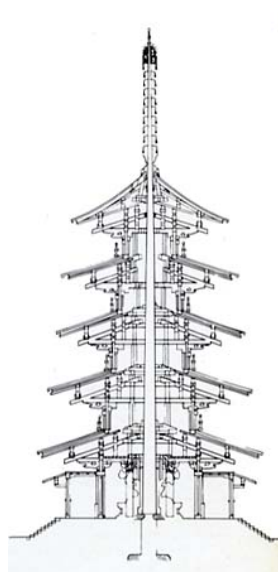


Figure 2.2: Horyuji Temple, [11, 13].

Another important structural application is in bridges structures. Prior to modern steel and concrete constructions, wood was the dominant material in the bridge's scenario. In 55 BC, the Roman Empire built a bridge over the Rhine river. The bridge was 140 m long, 5–6 m wide and would allow two-way traffic. Only 10 days were required for its construction.

One of the oldest existing bridges is located in Switzerland. The Chapel Bridge is 222 m long and was built in 1333. Like many bridges in Switzerland, the structure is covered, which favors its weather protection and aids in protection against biological degradation [14].

Although the history of timber constructions has been set aside with the advent of new building materials (concrete and steel), it is undeniable that historical examples show excellent durability of timber structures when well designed. In this respect, certain timber projects that aim for a long service life systematize the geometry in a way that makes it easy to repair or replace its elements when needed.

Today wood production in the world is estimated at 3.89 bi m³, with approximately 50% of this volume being used as fuel, and construction applications are diverse. Lightweight structures (based on structural wood, composite and laminated panels) are widely used for residential houses, small multi-storey floors and for commercial buildings. Similar elements are also used for wall and floor elements. The best known application is in roof parts. In most steel or concrete constructions, a wood truss roof is usually the most cost-effective choice [15].

Timber-based building systems have great potential for rational use of resources and low aggregate cost. There are numerous successful examples in North America and Northern Europe, where timber constructions exemplify that it is possible to develop light and efficient panels and laminate-based structures. These systems feature simplified construction techniques and are faster to build compared to concrete structures [16].

The fact that wood has been widely used for millennia does not imply that there has been a major scientific advance on the physical and mechanical understanding behavior of the material. In fact, the vast majority of studies and timber construction techniques result of empiricism and from designer's experience.

2.2 ADVANTAGES OF TIMBER-BASED STRUCTURES

Wood is the building material available to most societies. The vast amount of species has made at least one of them adapt to local climate and conditions, which is why this material can be found in all parts of the globe. Wood has already been used for the construction of various engineering works: houses, bridges, war machines, boats, among others. There are numerous advantages to applying this material, as shown in researches by Whitelaw [17], Nolan [18], Townsend and Wagner [19], Adedeji and Ogunsote [20], Smith and Snow [21].

1. It is available in most countries. It can be obtained from local suppliers and transported to the construction site by small vehicles. It is a widely accepted structural material and used in various cultures.
2. The good weight-resistance ratio enables its use in framed structures. Some species have high resistance to biological degradation, corrosion and even good resistance to marine environments. Wood is markedly more resistant to salt corrosion, with less variation in structural properties. It is a durable material and there are several finishing and protection techniques that, in addition to increasing the aesthetic capital of the building, can extend the service life for centuries with minimal maintenance.
3. Workability is a major factor in the rise in the scope of construction. It is possible to shape the material with hand or machine tools, and there are several design options. In addition, due to the wide range of resistances, depending on the species used, it

is possible to find the optimal geometry and strength capacity for the project.

4. It is renewable and biodegradable. It has low aggregate energy and presents good thermal and acoustic performance. Wooden designed houses still remain a model for minimum energy consumption in buildings.

2.3 CONNECTION SYSTEMS

Connections are the main aspect in the design of timber structures. Due to the limitation of the length of the pieces, generally shorter than the required spans, splices and composite arrangements should be used. Timber joints are generally less efficient than corresponding joints between other materials (such as steel) due to the low embedded resistance and low shear strength, especially in perpendicular direction to the fibers. This means that there is a need to increase the connection area, which generally infers geometric changes and, in practice, in the piece length. Joints tend to be less resistant than the connected members themselves, and choosing the best joint type goes beyond simply checking the maximum resistant load. Other aspects such as cost-effective and the production process are equally important. This shows how important is the study of timber connections. [5, 11].

Mechanical connectors have been used for centuries and over 60 different types have been patented in Europe and America. The development of connections was most notable in Europe as a result of World-War-I-related timber demand. The United States then experienced rapid growth at World War II period, with about 1 mi m² built in the first six months of 1942. During this period, there was a large expansion in the timber framed structure's market, which motivated the development of more efficient connection techniques, both mechanically and in the manufacture itself [22].

Thomas [23] briefly reviewed major mechanical connectors such as nails, screws, bolts, shear rings, and metal plates. Some advantages of nail plate joints were highlighted: high efficiency in terms of load capacity, simplicity and automated fabrication process, good fire resistance and reduced amount of steel used in joints. The main disadvantage is the need for special tools for crafting, especially in small works.

Bainbridge and Mettem [24] studied various types of fixed covered joints (which can transfer bending moments), illustrated in Figure 2.3. In the analysis of timber structures, the links are generally modelled as hinges, which reduces the complexity of the analysis and generally leads to a more conservative model. The study addressed conventional technologies and new connections not yet on the market. The authors comment that the use of conventional connections is inefficient, and may result in heavy and poorly optimized structures.

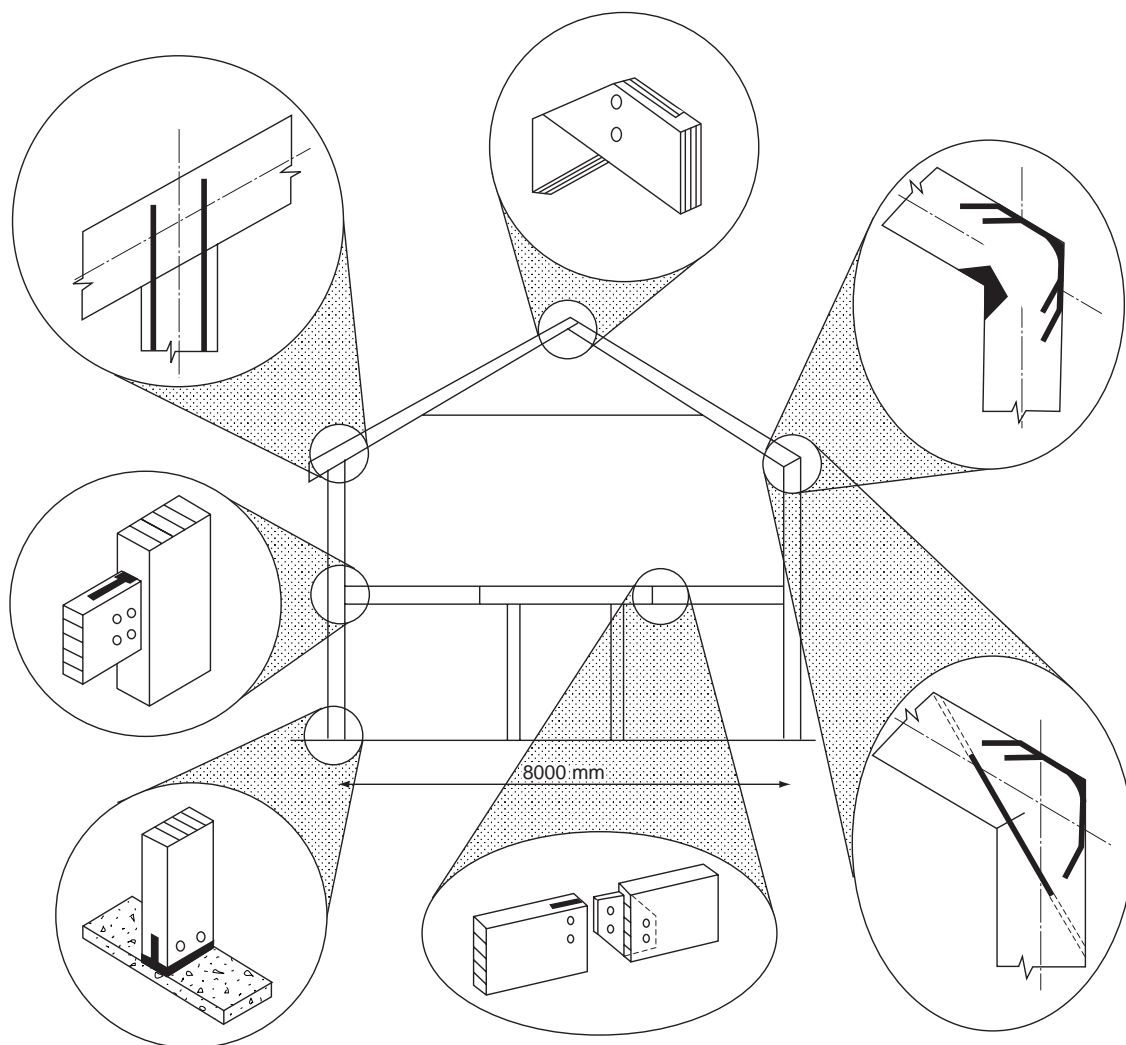


Figure 2.3: Prefabricated timber frame with several concealed connections, [24].

Claisse e Davis [25] performed tests on four types of high performance joints. As in the current design methodology, timber sections are generally governed by the joint section necessity, thus more efficient joints can increase stiffness and also reduce sections and therefore the overall weight of the structure. The connections studied were: conventional bolts (for reference value), injected resin steel dowels, nail plates and glass polymer reinforced (GRP) pins. The most efficient connections were nail plates and GRP reinforced pins. The stiffness of the GRP reinforced connections were clearly higher than the others, but from the load capacity point of view, the nail plates presented the highest average. Figure 2.4 shows the maximum load values of the four studied connections.

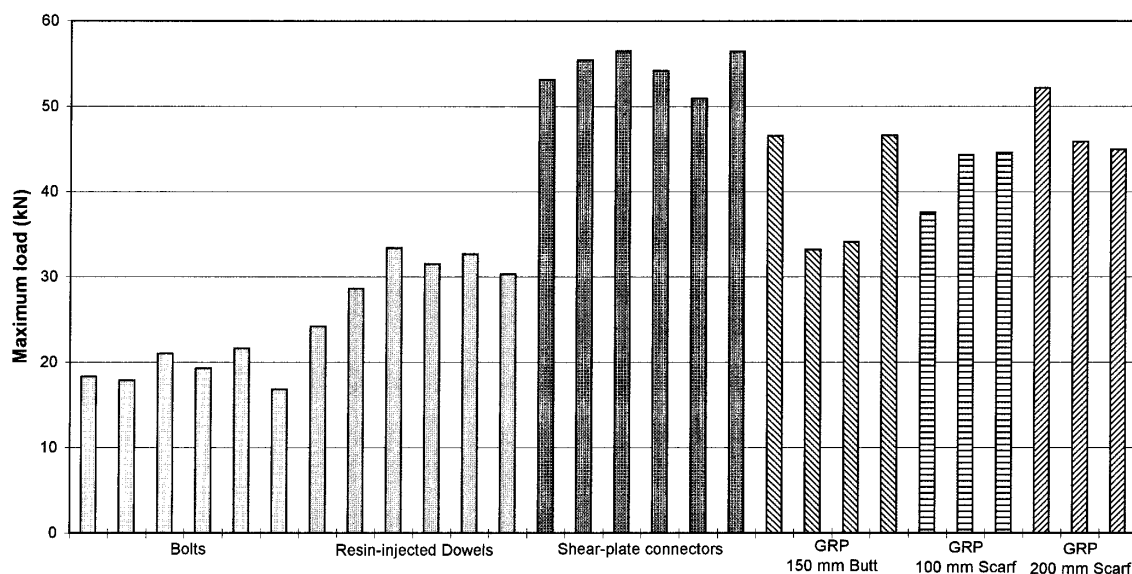


Figure 2.4: Comparison of four high performance connections, [25].

Faherty [22] summarized the analysis and design criteria for the main connections. Some relevant factors that influence the performance of mechanical connections were highlighted:

1. Thickness: Experimental tests were conducted in two modes: parallel and perpendicular loading to the fibers. It was observed that the rupture mode also depends on the thickness. In general, the critical load increases linearly with thickness to a certain extent of proportionality;
2. End margin: Two dimensions of shear rings have been tested. Load capacity remained constant with increasing end spacing beyond the reference value (15 cm). For smaller spacings, the reduction in load capacity decreased almost proportionally with the decrease in spacing;
3. Edge margin: There was an increase of the maximum load the greater the lateral spacing adopted. For minimum distances, the pieces broke when the maximum load was reached, and for maximum distances, the maximum load was reached before the wood failure;
4. Moisture content: The tested scenarios were: green wood¹, treated and then connected and treated before making the connection. Specimens with untreated wood had a maximum load of about 2/3 of those obtained with treated wood. Similarly, the connection in already treated wood presented higher strengths. The drying process causes a rearrangement of the fibers and the spaces between the connections weaken the embedded strength. The series of tests shows that joint strength increases as moisture decreases and stiffness properties, both elastic and inelastic, are little affected;
5. Steel Resistance: joints have been tested with three steel grades: 435 MPa, 500 MPa and 700 MPa. The tests showed that the stiffness and strength of the joints are

¹green wood refers to the recent cut, with no time for drying and evaporation. The m.c. considered for this type of test is 100%.

governed by the mechanical properties of the wood, and not by steel quality.

2.4 TRUSSED RAFTER INDUSTRY

Prefabricated roof trusses have been used in America, Europe and the United Kingdom since the mid-1960s. Over the past 30 years, 50 million roofs have been manufactured in the United Kingdom. In 1978, US sales were estimated at \$1.5 billion, in which \$100 million representing just the nail plates. Its use is known for residences, but applications are increasing their spectrum for long-span buildings such as schools, institutes and industries. Interestingly, the success of this industry branch is not as published and technical reports on technology and manufacturing methods are scarce [26].

Prior to the expansion of the prefabricated industry, the manufacturing process with pin type connectors was time consuming and labor intensive. Technical advancement in the US began in the study of the feasibility of producing stamped tooth plates (nail plates). These connections proved superior from the point of view of maximum load capacity and it was rarely necessary to increase the dimensions of the parts for the purpose of fitting the connection. Traditional connections with nails or screws still required some form of notch in the connection area, which eventually constrained edge spacing. This drawback was generally bypassed by increasing shear planes by duplicating certain elements in the roof truss. Due to their high performance, the nail plates also had less need for edge spacing, resulting in smaller timber sections and lighter trusses [27].

Conventional roofing structures, Figure 2.5, are composed of structural elements (truss) that withstand the stresses required and weft elements (purlins, rafters and bracing) that support the roofing materials. Its manufacturing process was on site, using metal notches and pins such as nails and screws. The classic geometry of the scissors requires some duplicate element in a sandwich shape. In Figure 2.5 the webs are doubled and allow the other elements to be connected by at least one shear plane.

The prefabricated system, Figure 2.6, with the use of nail plates, presents some key differences. In the truss, all members must have same thickness and are all in the same plane. There are no duplicate elements, as nail plates do not require shear planes outside the connection plane. The structure consist of trusses equally spaced between 0.6–2 m, depending on the particularities of the project. The weft elements are reduced to only slats (for ceramic tiles) or purlins (for fiber cement slates). Increasing the amount of trusses compensates for the decrease in weft elements. However, the sections of the truss parts are considerably thinner, which can reduce the overall frame weight by up to 40% compared to the conventional system. [28, 29].

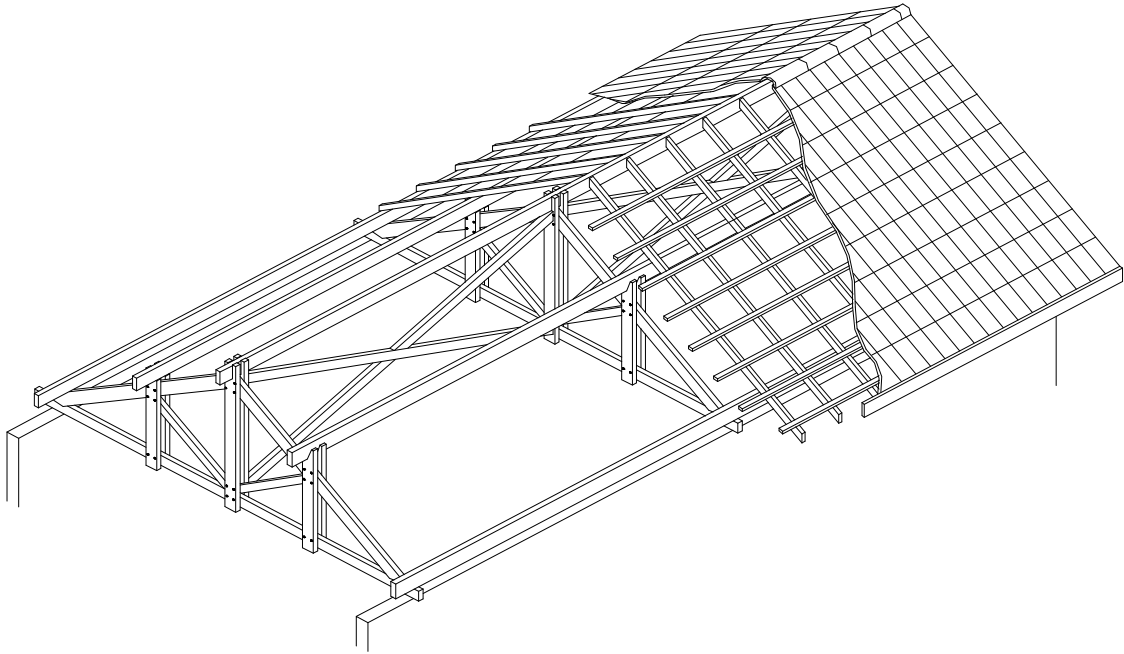


Figure 2.5: Conventional truss structure, [30].

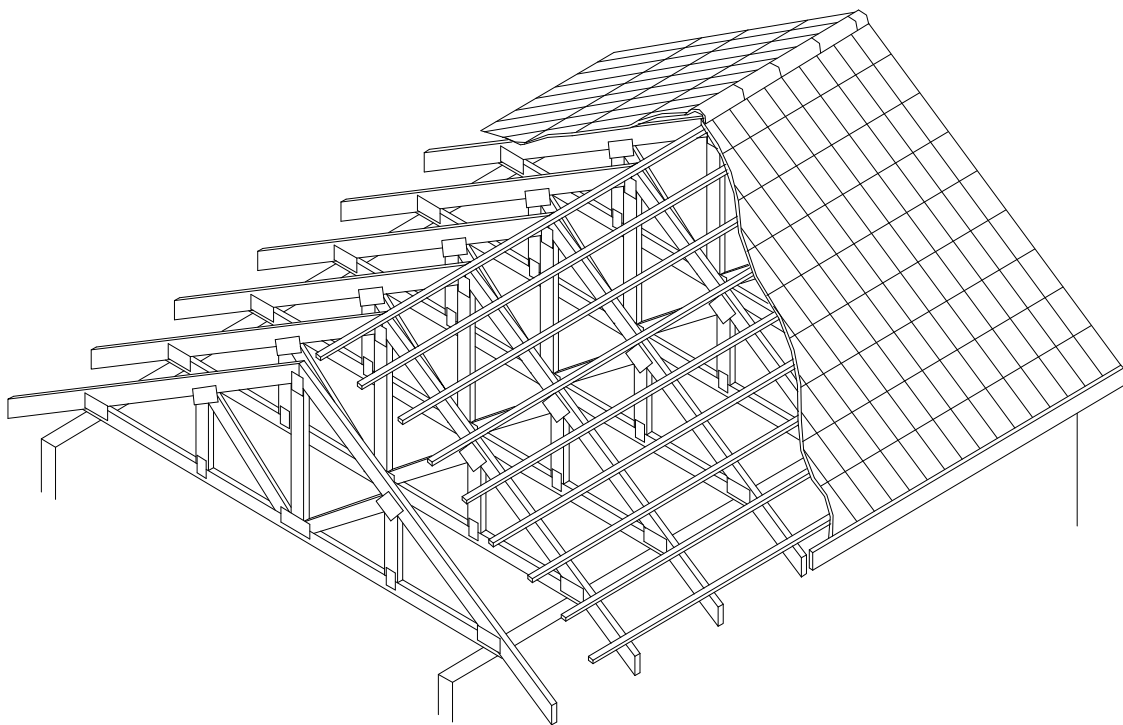


Figure 2.6: Nail plate truss structure, [30].

2.4.1 NAIL PLATE TRUSSES MANUFACTURING

The prefabricated truss production line consists of a series of saws, guides and presses, as shown in Figure 2.7. The relevant stages of the process are described in the following.

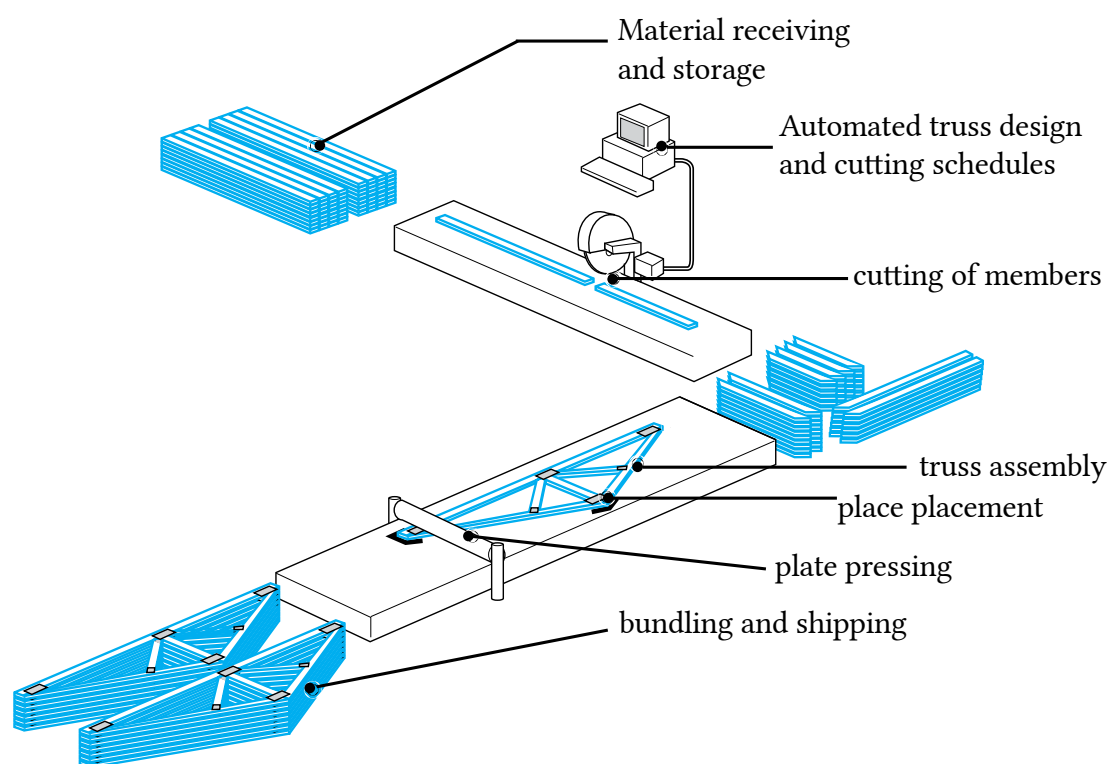


Figure 2.7: Manufacture of truss frame, [31].

The first step is the elaboration of the truss model design. The project can be done by the customer or the manufacturer. There are many factors to consider in a prefabricated roof design: the amount sloping regions and the geometric arrangement of trusses, spacing and bracing, load redistribution elements, among others. Companies that manufacture trusses generally have specialized software for detailing and designing these structures. By the mid-1970s, computer development was still limited, and the first calculation programs of the time were parameterized for each truss type, and design options were predefined. The simplified model of calculation considered, for deformation purposes, that the multiple trusses operated as a beam with several sections. Today the stiffness matrix method allows to calculate any truss configuration for any load configuration. Truss members are considered as uniform linear bars, and the joints are treated as rigid, transmitting bending moments. Unless previously specified, trusses are designed with pinned supports. It is therefore necessary to specify the vertical and horizontal bracing of the wall-roof interface [27].

With the project, the elaboration of the wood pieces begins. A series of guides and saws are used to shape the truss members. This process is virtually all computerized. Modern cutting tables feature laser mapping and a rolling system for serial part cutting, as shown in Figure 2.8:

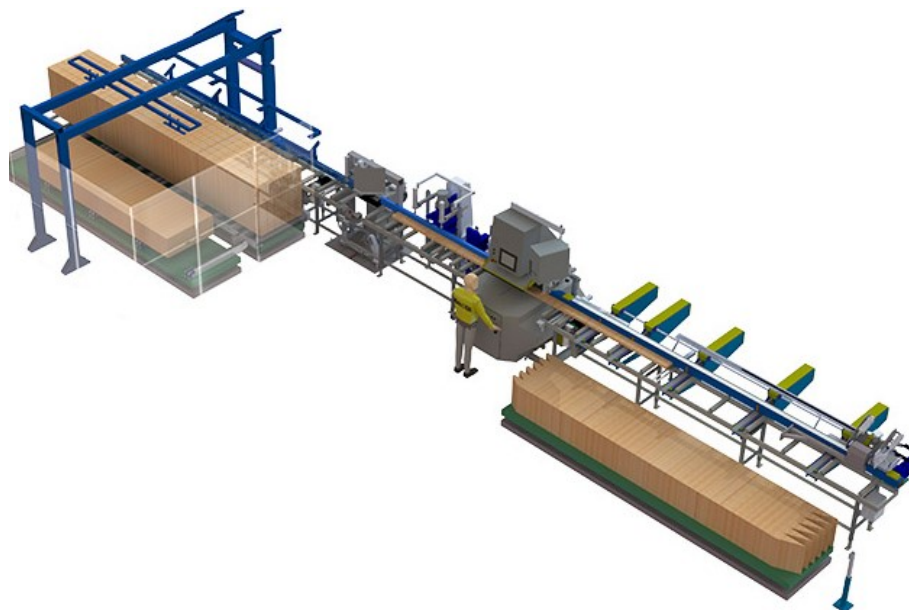


Figure 2.8: Automated Cut Saw SP720, [32].

The next step is assembling the truss profile. The positioning take place on tables with the structure shape. Again, there are a number of machines that have automated most of the work, using laser guides and rolling pins, illustrated in Figure 2.9:

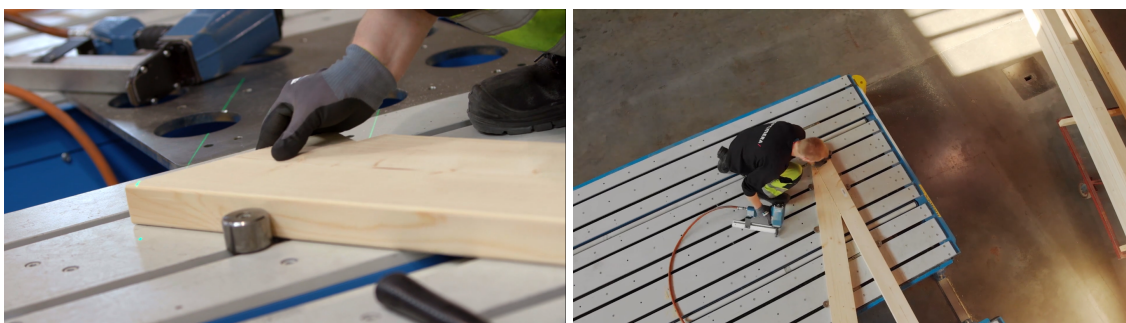


Figure 2.9: Truss assembly, [33].

With the truss arrangement set, the next step is the plate placement and pressing. Nail plate connections require a specific calculation for pressing. If the pressure is too high, it is possible that the wood may suffer some mechanical damage, compromising the stiffness of the connection. Similarly, if the pressure is too low, the plate may exhibit slippage or teeth withdrawal in the section. There are other less commonly used techniques for on site pressing, such as portable hydraulic presses or the use of hammers combined with a metal plate that covers the entire plate. An example of automatic press is illustrated in Figure 2.10:

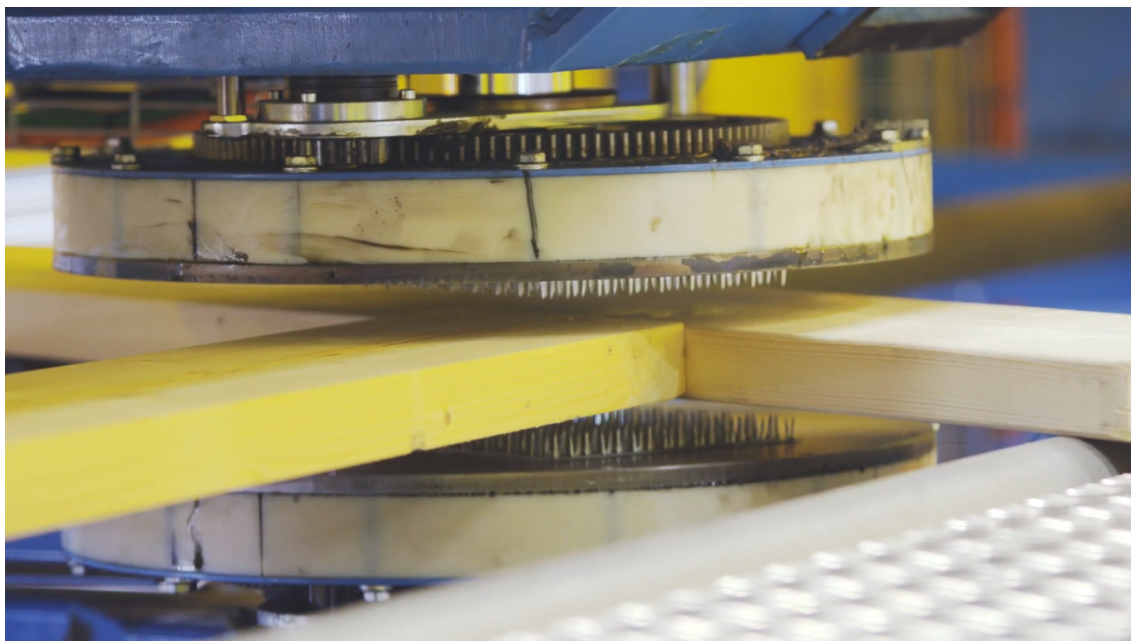


Figure 2.10: Plate pressing, [33].

Last but not least, it is necessary to lift and stack the fabricated truss. This step requires a correct maneuver when lifting (either out of the factory or on-site mounting) because the acting loads are inverse to the main calculated design conditions. Special care is taken to avoid undesigned overloads, and a current solution is to distribute the lifting load with the help of a bar, as in Figure 2.11:

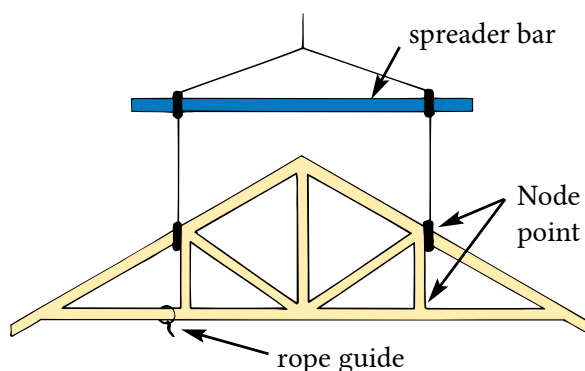


Figure 2.11: Truss handling, [34].

2.5 NAIL PLATES

Nail plates originated after World War II, during which time conscious use of resources (especially steel) became relevant. The first nail plate was invented and patented in Florida in 1952. The purpose of the fabrication process was to make it possible to produce a plate of the required size while stamping it, and this created a new horizon in the wood truss industry. This migration from making on-site connections to factories has led to greater quality control and consistency in the structural performance of wood trusses. Another important aspect was the decrease in the demand for qualified labor to craft the

connections, since the joint assembly was automated. Today, more than 90% of residences and apartments in the United States use this prefabricated roof truss technology. The figure 2.12 represents some common types of nail plates [35].

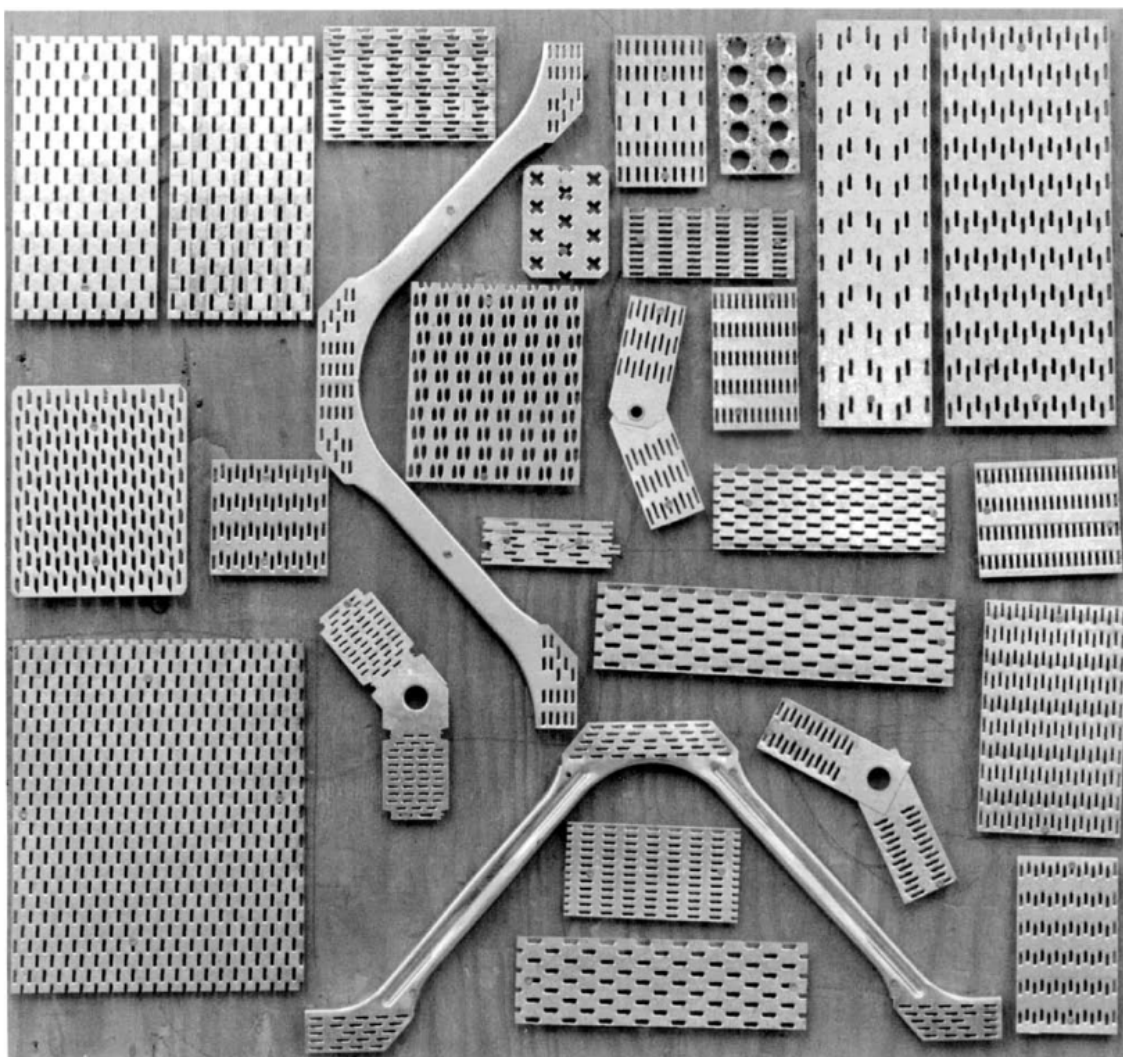


Figure 2.12: Common nail plate shapes, [35].

Mirsa and Esmay [36] conducted one of the first analytical studies for stress distribution in nail plates using the principle of minimal complementary energy. The modeling considered only one plate geometry, and the analysis was restricted to the consideration of the linear-elastic behavior. The theoretical curves predicted the maximum stress in cases where the failure mode was due to wood failure and suggested some propositions about the stress distribution on the plates, but did not fit the experimental data very well. One of the reasons was the linear-elastic approach and the consideration of the rigid behavior of the plate.

One of the first FEM (Finite Element Method) approaches was proposed by Foschi [37], and many subsequent studies were based on the expressions developed in this work. The 2-D structural formulation assumed that, in the teeth-wood interface area, both plate and wood could be treated as rigid elements, connected by nonlinear springs. The stiffness of these springs was approximated by considerations of plate geometry and tooth orientation in relation to wood-grain direction. The load-slip relationship under

lateral loading was characterized by a three-parameter experimental model, as shown in Figure 2.13:

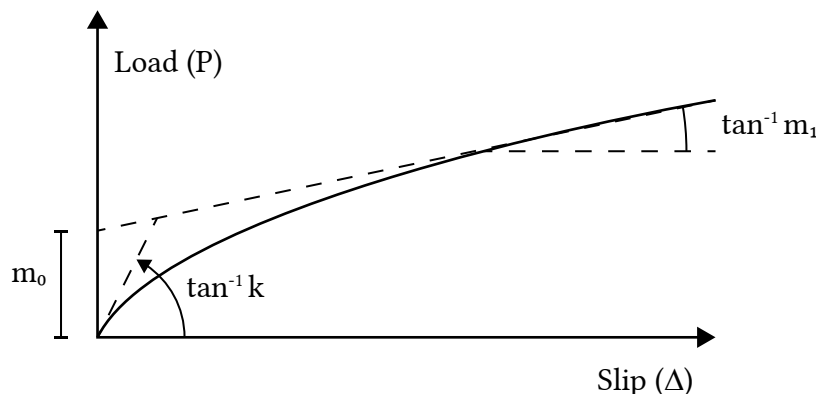


Figure 2.13: Foschi proposition for the load-slip curve, [37].

$$P = (m_0 + m_1 |\Delta|) \left(1 - e^{-k|\Delta|/m_0}\right) \quad (2.1)$$

where:

- P joint load;
- k initial curve slope;
- m_1 asymptotic slope;
- m_0 intersection of the asymptote with the load axis;
- Δ joint slip.

The properties k , m_1 e m_0 are derived from four basic tests, combining the orientation of the applied force with the grain-direction in relation to the longest plate length, and the intermediate values for arbitrary orientations were obtained from Hankinson's interpolation.

Lau [38] studied the heel joints illustrated in Figure 2.14. The red dots indicate where the displacement measurement was taken, and it has been found that the positioning of the plate can generate a high frictional force on the notch details of the heel joint, as well as change the rupture mode. Three rupture modes were identified: wood failure at the teeth-interface, teeth withdrawal and plate buckling. In cases where the axis of the plate was oriented in the main axis of the tensioned member – (a) and (b) – the criterion was mostly the teeth withdrawal, and in cases where the axis was oriented in the compressed member – (c) and (d) – buckling was more pronounced. In addition, two plate dimensions were evaluated. The increase in plate length considerably affected the teeth withdrawal mode, but had no marked relevance in buckling cases.

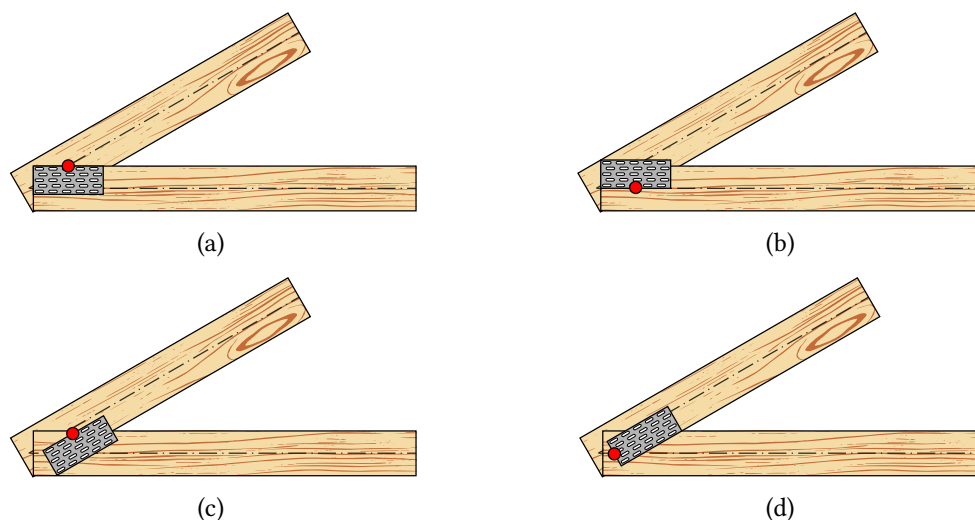


Figure 2.14: Heel joint studied designs, [38].

Cramer [39] also addressed the nail plate modeling, and took into consideration the joint eccentricity and the semi-rigid nonlinear behavior of the connection. Each tooth was modeled as a group of three springs, two translational and one rotational, positioned at the center of gravity of the tooth-plate contact area. The following rupture/deformation modes were studied simultaneously: tooth deformation, wood deformation and steel deformation. The parametric study of loads presented the following interactions, illustrated in Figure 2.15, where the first two columns refer to the smallest plate (76.2x88.9 mm), and the last two columns, the largest plate (127x254 mm). The difference in material behavior is due to relative stiffness. Analysis has shown that the premise of the rigid behavior of the tooth-wood interface is reasonable for small plates but inaccurate for relatively large plates. In addition, the deformations in the teeth were not uniform for the larger plates.

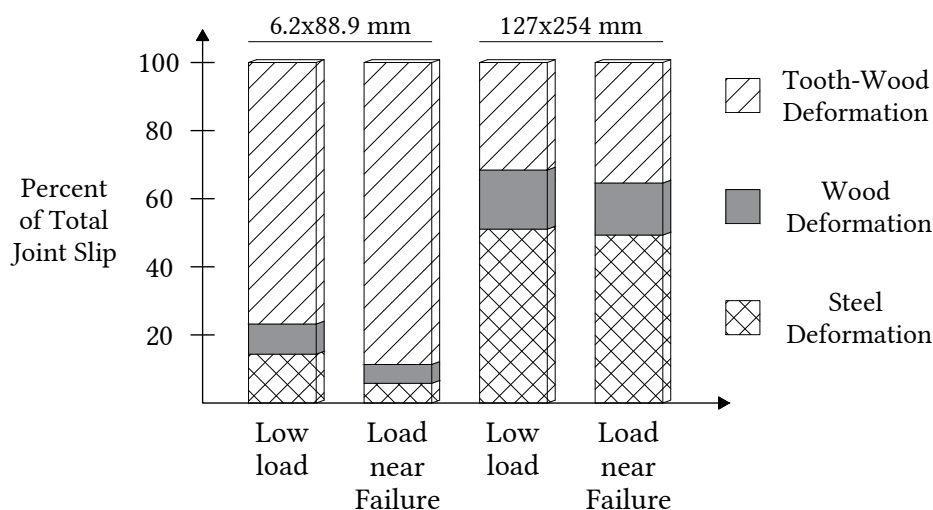


Figure 2.15: Overall slip contribution, [39].

Gebremedhin [26, 40] developed two theoretical models for the calculation of joint stiffness, a linear 2-D model based on FEM, and another based on the theory of elasticity. The FEM model used a mesh composed of 3-node triangular elements and the results of stiffness values were overestimated. The elasticity model considered that each tooth

acted as a cantilever beam, where the wood-deformation was converted into reaction in the teeth. Experimental results were performed to validate the modeling results. The elasticity model predicted the experimental results more accurately, however, this method needs a previous variable, the modulus of elasticity of the tooth-wood interface.

Groom [41] produced a theoretical model that accurately predicted the maximum limit states of different connection types. The method was based on the theory of elasticity and included the inelastic behavior of the teeth and took into account the variation of the moment of inertia along the tooth length. The test approach was an incremental loading, where each load increment was processed assuming that at these intervals the joint behavior was linear. The linear responses were then accumulated for each increment. The model was able to accurately predict the load-slip curves considering various types of geometric combinations.

Vatovec [42] used ANSYS software to analyze the connections. In this study, a nonlinear 3-D modeling was idealized, and each tooth was considered as a node composed of three nonlinear springs. The nail plate was modeled without gaps between the teeth. The model calculated the axial stress-strain curves accurately, but the authors reported that the rotational parameters were not validated due to lack of sufficient boundary conditions.

2.6 SUMMARY

The advantages that have popularized the use of wood as a structural material since prehistory are still valid today. The contemporary need for the use of sustainable and renewable materials once again brings relevance to the study of wood. In addition, the market's need to provide increasingly efficient and cost-effective structures also enhances their use: lightweight and timber frame designs are on the rise due to their low cost and fast installation.

The success of the wood construction industry and its constant expansion is directly linked to the development of new connection techniques. In this sense, there is a clear need to understand and study the physical and mechanical behavior of this material, which still has its foundation in empirical results. The success of nail plate connections in the prefabricated truss business is visible, accompanied by the dominance of this segment in roof trusses all around the world. Almost fully automated fabrication and high mechanical performance are the main factors that distinguish the nail plates from other connections.

The mechanical behavior of nail plate joints is complex and depends on several factors such as geometry, number of teeth, load and grain-direction orientations. The main focus of studies and modeling in the literature is on the tooth-wood interface, where the mechanical properties of the wood and the geometric compatibility of the deformations make the analysis intricate. It is clear that the advantages offered by nail plate connections carry with them a high complexity in their modeling.

DESIGN OF NAIL PLATE CONNECTIONS

The main factors that influence the connection's strength and stiffness are listed. The methods used to establish the basic plate properties are described, as well as the standard's formulations that define the minimum anchorage areas and the ULS verification. Finally, the structural models that characterize the stress distribution in nail plate trusses are discussed. This chapter presents the calculation procedure that will be the focus of modeling in the following chapters.

3.1 INTRODUCTION

Nail plates are described in EN 1075 *Timber Structures – Test Methods – Joints made with punched metal plate fasteners* as a plate with teeth “punched-out” of the plate in one direction, that stick out forming a right angle. The Figure 3.1 details a common nail plate design.

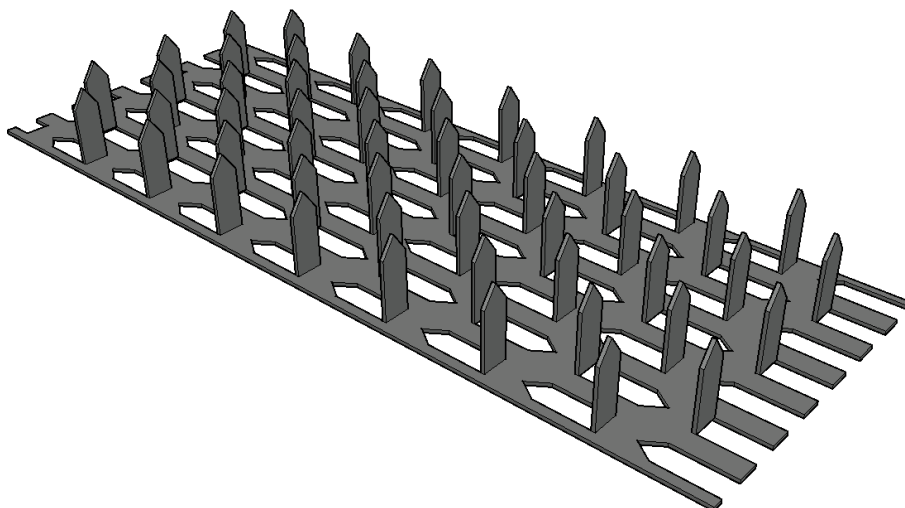


Figure 3.1: Typical nail plate fastener

These plates are usually made of stainless or galvanized steel. Nail plates allow the connection of two or more pieces of wood that are the same thickness in a symmetrical connection, with one plate on each side. There are several possible connection configurations, as shown in Figure 3.2.

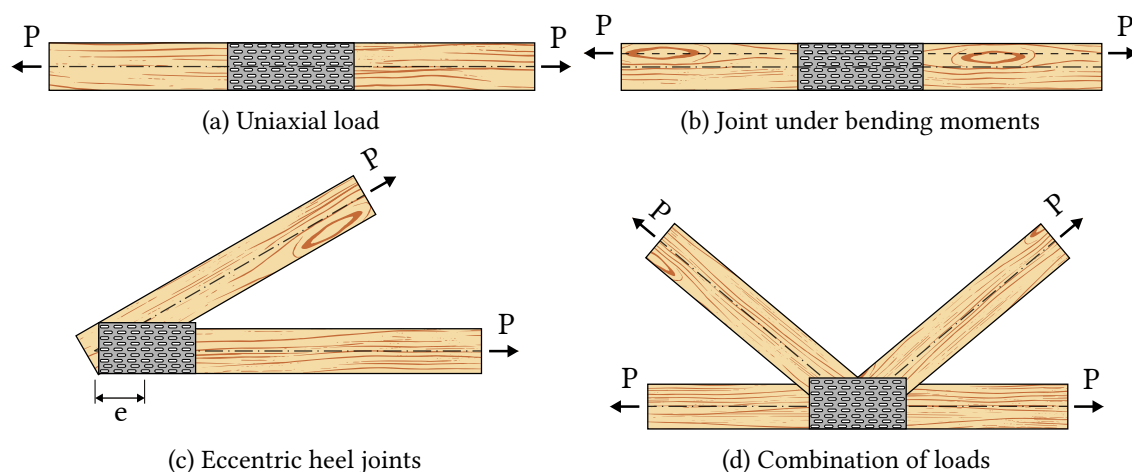


Figure 3.2: Nail plate configuration examples

Nail plates come in a variety of plate shapes and multiple tooth designs that cover a wide variety of connections. However, the factors that influence the connection performance are constant, which allows the establishment of general analysis criteria for these joints.

The main current standards dealing with testing and verification procedures are from American and European institutes. The American Society of Testing and Materials (ASTM) E489 describes the methods for determining the tensile strength properties of the plate, and resolutions E767 and D1761 address the shear strength criteria. The Truss Plate Institute (TPI) brings in ANSI resolution 2014 general rules for checking and designing, specifying the quality of materials and other rules for the prefabricated truss industry. Some other standards such as the Canadian CSA S347 and the ISO 8969 provide methods for evaluating the resistance of only certain specific configurations or only take axial actions into account.

Most current standards simplify the general design conditions. In most cases, joints are subject to some kind of load combination or eccentricity and ASTM resolutions only describe axial loads. There is a normative deficit not only from the perspective of load representativeness, but also from geometric configurations, as for example common cases illustrated in Figures 3.2c and 3.2d. It is necessary to study a way of generalizing these connections tests, involving the geometrical plate parameters, orientation and loading combinations, or, alternatively, to develop a mechanical analysis method based on these parameters [38].

The European standard EN 1995-1-1:2004 (EC5) is the main reference for the plate design. Reference is made to two other standards that presents the tests for determining the mechanical properties of the plates and other parameters, namely EN 1075 and EN 14250. The standard provides the designing equations but makes no mention of the modeling criteria, focus of the present dissertation.

3.2 NAIL PLATE MECHANICAL PARAMETERS

The stress is initially transmitted from the wood to the teeth in the anchorage area of the first connected element, then from the teeth to the plate through the rupture

line and finally to the teeth of the other connected member. The load capacity of the connection is then defined by two failure criteria: the load-bearing capacity of the teeth in the anchorage area is reached or the load capacity of the net- cross-section area of the plate in the rupture line between members. In the following, the parameters that interfere with each failure criterion is revised. Figures, equations and notation are adapted from EC5.

3.2.1 ANCHORAGE AREA PARAMETERS

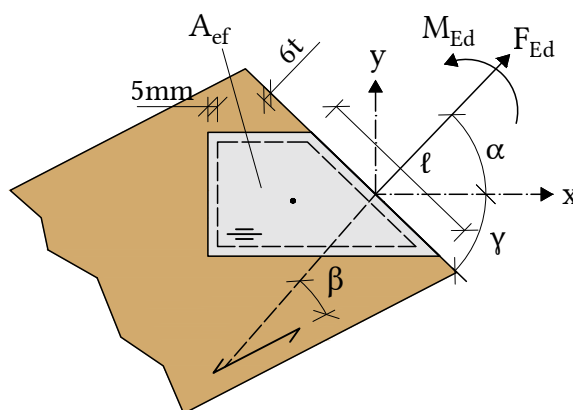


Figure 3.3: EC5 nail plate notation

- A_{ef} effective anchorage area. The effective area is calculated by subtracting 5 mm from the adjacent edges of the wood section and $6t$ in the end grain direction parallel to the fibers, with t the plate thickness;
- r_{max} distance between the center of gravity of the plate and the farthest point from the center. I_p is the polar moment of inertia of the effective area around its center. r_{max} and I_p are parameters used when there are bending moments acting on the rupture lines.

3.2.2 NET-CROSS SECTION PARAMETERS

- α angle between the direction of the applied force and the main direction of the plate x (the main direction of the plate is the top capacity direction, usually parallel to the teeth-direction). It has influence on the embedment area of the wood (where the stress transmission to the teeth occurs) and in the bending moment resistance;
- β angle between the rupture line force direction and the grain-direction. Affects the embedment parameters that will be described below in the plate properties;
- γ angle between the main plate direction and the rupture line. This angle affects the net-cross section area in the connection line;
- l rupture line length. The projected lengths, parallel and perpendicular to the main direction of the plate transfer the forces between the connected pieces of wood;

- the strength properties of the steel.

3.3 CHARACTERISTIC RESISTANCE VALUES

3.3.1 NAIL PLATE CHARACTERISTIC VALUES

According to EC5, the following characteristic strength values are needed to the design procedure:

- $f_{a,0,0,k}$ characteristic nail load-bearing capacity per unit of area, for $\alpha = 0^\circ$ and $\beta = 0^\circ$. A commonly used unit is N/mm^2 ;
- $f_{a,90,90,k}$ characteristic nail load-bearing capacity per unit of area, for $\alpha = 90^\circ$ and $\beta = 90^\circ$. N/mm^2 ;
- $f_{t,0,k}$ characteristic plate tension capacity per length unit (in the main direction), $\alpha = 0^\circ$. N/mm ;
- $f_{c,0,k}$ characteristic plate compression capacity per length unit, $\alpha = 0^\circ$. N/mm ;
- $f_{v,0,k}$ characteristic plate shear capacity per length unit, $\alpha = 0^\circ$. N/mm ;
- $f_{t,90,k}$ characteristic plate tension capacity per length unit (perpendicular to the main direction), $\alpha = 90^\circ$. N/mm ;
- $f_{c,90,k}$ characteristic plate compression capacity per length unit, $\alpha = 90^\circ$. N/mm ;
- $f_{v,90,k}$ characteristic plate shear capacity per length unit, $\alpha = 90^\circ$. N/mm ;

Each of these properties have tests detailed in EN 1075. The values for 5% of the statistical distribution (characteristic values) are transformed into design values by a modification factor k_{mod} and by a partial factor of material property γ_M .

3.3.2 CONNECTION CHARACTERISTIC VALUES

From the nail plate parameters, the connection strength parameters are defined. The parallel to grain anchorage resistance ($\beta = 0^\circ$), $f_{a,\alpha,0,k}$, is obtained by the test illustrated in Figure 3.4a. A bilinear function is adapted, based on the plate coefficients k_1, k_2 e α_0 (parameters given by the plate manufacturer) illustrated in Figure 3.4b:

$$f_{a,\alpha,0,k} = \begin{cases} f_{a,0,0,k} + k_1 \cdot \alpha, & \text{when } \alpha \leq \alpha_0, \\ f_{a,0,0,k} + k_1 \cdot \alpha + k_2 \cdot (\alpha - \alpha_0), & \text{when } \alpha_0 \leq \alpha \leq 90^\circ. \end{cases} \quad (3.1)$$

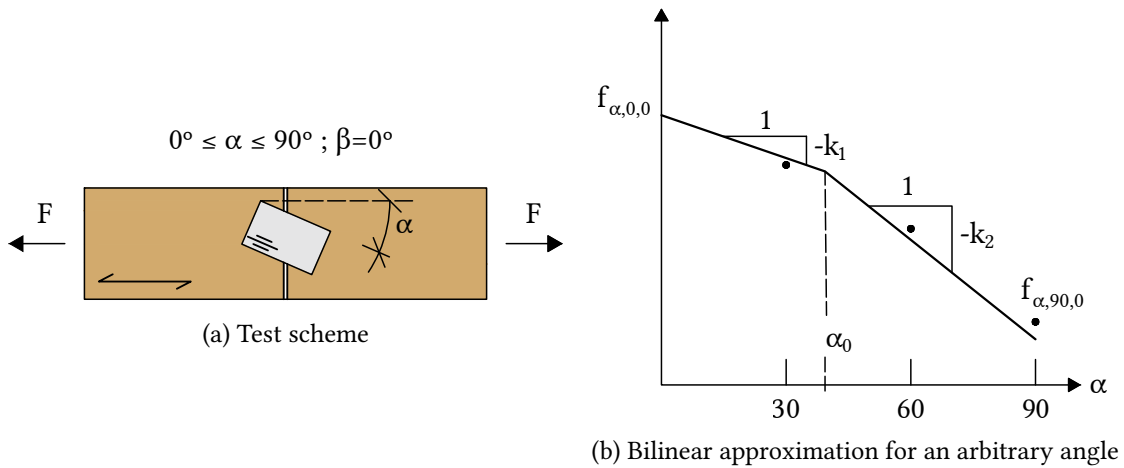


Figure 3.4: Parallel to grain test

Perpendicular to grain resistance ($\alpha = 0^\circ$), $f_{a,0,\beta,k}$, is obtained by testing a T-connection, as shown in Figure 3.5a. To the perpendicular direction, a sine approximation is used, Figure 3.5b:

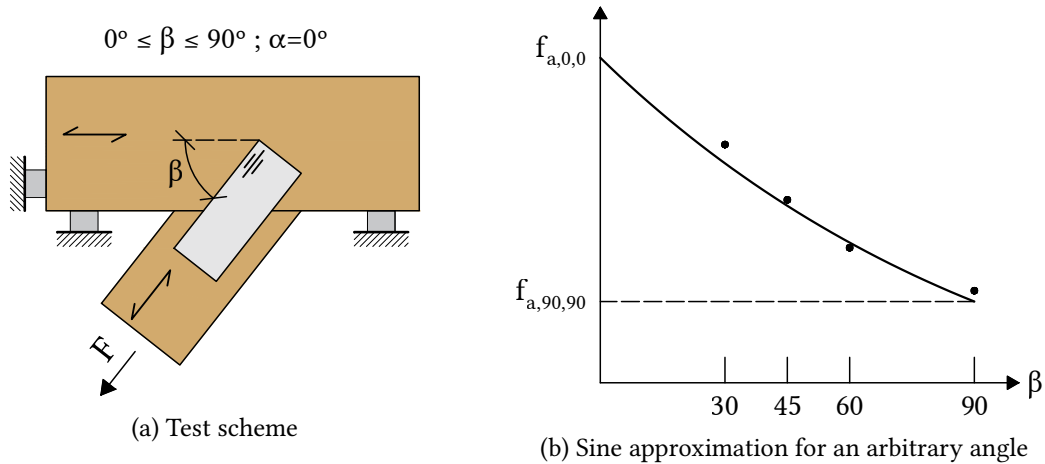


Figure 3.5: Perpendicular to grain test

Once defined these two functions, which represent the relationship between $f_{a,0,0}$ and $f_{a,90,90}$, EC5 proposes an interpolating function for arbitrary anchorage strength per plate area $f_{a,\alpha,\beta,k}$:

$$f_{a,\alpha,\beta,k} = \begin{cases} \max \left\{ \begin{aligned} & f_{a,\alpha,0,k} + (f_{a,\alpha,0,k} - f_{a,90,90,k}) \cdot \frac{\beta}{45^\circ} \\ & f_{a,0,0,k} + (f_{a,0,0,k} - f_{a,90,90,k}) \cdot \sin[\max(\alpha, \beta)] \end{aligned} \right. & , \text{ for } \beta \leq 45^\circ, \\ f_{a,0,0,k} + (f_{a,0,0,k} - f_{a,90,90,k}) \cdot \sin[\max(\alpha, \beta)], & \text{ for } 45^\circ < \beta \leq 90^\circ. \end{cases} \quad (3.2)$$

3.4 ULTIMATE LIMIT STATE DESIGN ACCORDING TO EUROCODE 5

3.4.1 ULS ANCHORAGE AREA CAPACITY

The anchorage area is subject to stresses that occur in the effective area of the plate as defined above. More complex joint configurations require individual checks for each plate area, as illustrated in Figure 3.6:

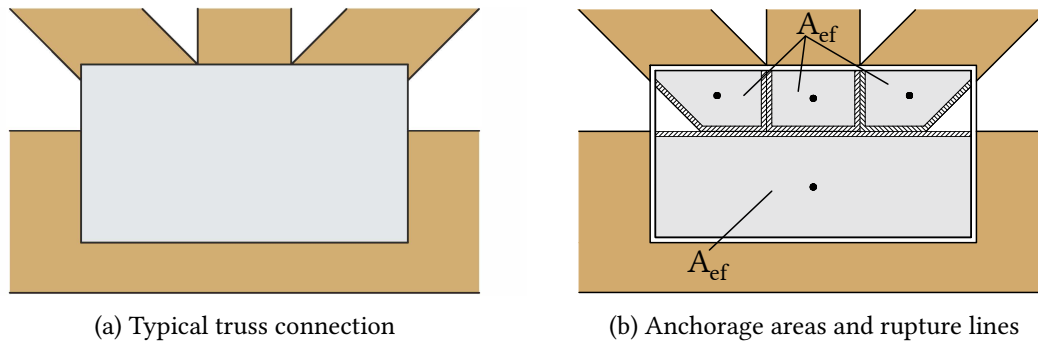


Figure 3.6: Anchorage area for multiple member joints

The stresses due to acting forces F_{Ed} and bending moments M_{Ed} are evaluated as follows:

$$\tau_{F,d} = \frac{F_{A,Ed}}{A_{ef}} \qquad \tau_{M,d} = \frac{M_{A,Ed}}{W_p} \qquad (3.3)$$

where:

- $F_{A,Ed}$ Design load applied to the anchorage area barycenter;
- $M_{A,Ed}$ Design bending moment in the barycenter;
- W_p Effective area torsion modulus.

W_p corresponds to the torsion modulus of the effective section, actuated for a bending moment in its plane, being calculated by the expression:

$$W_p = \int_{A_{ef}} r \, dA$$

where the integration domain is the effective area and r is the distance from the elementary area to the barycenter. The torsion modulus can be conservatively evaluated by the expression:

$$W_p = \frac{A_{ef} \cdot \sqrt{\left(\frac{A_{ef}}{h_{ef}}\right)^2 + h_{ef}^2}}{4} \qquad (3.4)$$

where h_{ef} the highest height perpendicular to the largest side of the plate.

The ultimate limit state condition of the anchorage is then defined by the following relation:

$$\left[\frac{\tau_{F,d}}{f_{a,\alpha,\beta,d}} \right]^2 + \left[\frac{\tau_{M,d}}{f_{a,0,0,d}} \right]^2 \leq 1 \quad (3.5)$$

3.4.2 ELS RUPTURE LINE CAPACITY

To check the rupture line, EC5 reduces the acting forces on orthogonal components. x and y :

$$F_{x,Ed} = F_{Ed} \cdot \cos \alpha \pm 2 \cdot F_{M,Ed} \cdot \sin \gamma \quad (3.6)$$

$$F_{y,Ed} = F_{Ed} \cdot \sin \alpha \pm 2 \cdot F_{M,Ed} \cdot \cos \gamma \quad (3.7)$$

It is also necessary to define the strength capacities in the directions x and y . These expressions depend on the type of stress that acts in the section. The following formulas are for tension loads, $F_{x,Ed} > 0$ and $F_{y,Ed} > 0$ (the compression cases use the same equation, only requiring a substitution for the respective compression strength values):

$$F_{x,Rk} = \max \left\{ \begin{array}{l} |f_{t,0,k} \cdot \ell \cdot \sin(\gamma - \gamma_0 \cdot \sin(2 \cdot \gamma))| \\ |f_{v,0,k} \cdot \ell \cdot \cos \gamma| \end{array} \right. \quad (3.8)$$

$$F_{y,Rk} = \max \left\{ \begin{array}{l} |f_{t,90,k} \cdot \ell \cdot \cos \gamma| \\ k \cdot f_{v,90,k} \cdot \ell \cdot \sin \gamma \end{array} \right. \quad (3.9)$$

where k the parameter that takes into account the influence of axial stress on bearing shear strength y , evaluated by:

$$k = \begin{cases} 1 + k_v \cdot \sin(2\gamma), & \text{if } F_{x,Ed} > 0, \\ 1, & \text{if } F_{x,Ed} \leq 0. \end{cases} \quad (3.10)$$

the constants γ_0 e k_v determined by the plate manufacturer (similarly to k_1 , k_2 and α_0).

The equation to be satisfied to ensure the strength of the plate in the rupture line section is defined by the interaction of the stress and strength portions:

$$\left[\frac{F_{x,Ed}}{F_{x,Rd}} \right]^2 + \left[\frac{F_{y,Ed}}{F_{y,Rd}} \right]^2 \leq 1 \quad (3.11)$$

3.5 STRESS DISTRIBUTION IN WOOD TRUSSES

As noted, in order to design a nail plate connection it is necessary to evaluate the distribution of stresses in two steps: the forces transmitted from the wood (where the loads are actually applied) to the center of gravity of the effective areas, through which the anchorage area checking is carried out, Section 3.4.1, and then from the center of gravity to the breaking lines, where the net-cross steel section is checked, Section 3.4.2.

Unlike usual pinned joints where truss modeling is designed with hinged nodes that do not transmit bending moments and the axial stresses of the bars are directly the stresses on the pin shear plane, nail plate joints require a more elaborate approach to include the transmission of bending moments and take into account the plate geometry in the modeling.

Nail plate connection design is generally supported by experimental testing. Variables such as plate geometry, plate orientation in relation to fibers, loads, tooth geometry, among others, cause the cost of testing to be high if all variables are parameterized. A more efficient solution is to develop an analytical method based on known parameters such as the mechanical properties of the plate, the wood and the loading conditions. With the experimental support, the analysis parameters are adjusted and then the developed numerical model can be expanded to analyze more joint configurations.

The mechanical behavior modeling of the plate can be divided into two main groups: a 3-D mechanical model, characterizing the plate, the teeth, the wood and defining elements of plate-wood interaction and a 2-D structural model focused on the stress distribution to meet the ULS design criteria. Each of these models has a purpose. The 3-D model, which the vast majority of literature deals with, aims to understand how stress flows along the plate. This analysis yields important results that define the best plate geometry and the most optimal shape of the teeth, where the deformations and critical stress concentrations occur, and how to implement a more efficient design. The 2-D model, scarcely grounded in the literature and focus of the present dissertation, allows a plane analysis of the stress distribution that provides the necessary results for the plate designing. This model is divided into two steps: a plane modeling that transmits the stresses of the wood to the plate and a second modeling starting from the loads in the geometric center of the plate to the rupture lines.

Roof trusses are structures that require some care in their analysis and there are some geometric details that cannot be overlooked. The real model is 3-D, with three-dimensional bar elements and the connection of the elements must take into account the rigidity of the connection and all the inherent eccentricities of the truss construction process. Truss structures may be subject to axial loading, bending moments and torsion. The complete solution of a 3-D model involving all these variables would take a high computational time, both from the design model and the numerical solution. Today, computer programs use 3-D modeling to design architecture and avoid geometric incompatibilities between elements, but the structural analysis of each truss is simplified by a static 2-D model.

Over the past few decades, truss modeling has shown an advance in modeling considerations, as illustrated in Figure 3.7. The early models considered linear bars and joints, with reduced node loads, and had an easy-to-solve system compatible with the processing power and calculation tools of the 1980s. Model 2 has some improvements, such as

auxiliary bar elements that simulate the existing eccentricities and the distributed load model now in the bar elements [11].

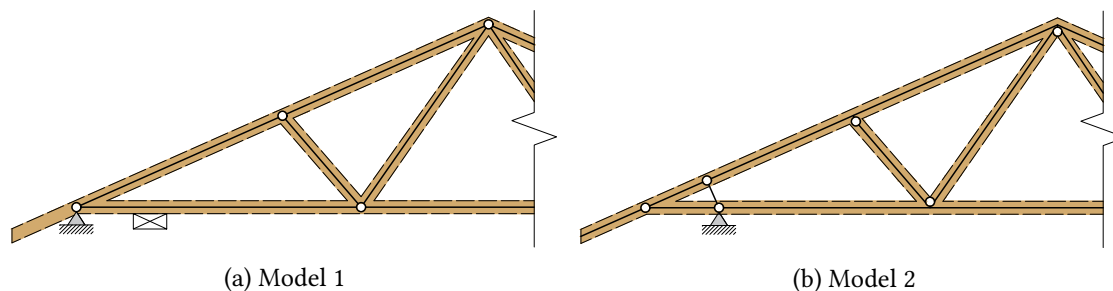


Figure 3.7: Plane truss modeling evolution, [11].

The distribution of bending moments in the end joints is particularly important and has been the subject of research by Lau [38] and Riberholt [43]. More sophisticated models have been developed, as in Figure 3.8. In this model, only forces perpendicular to the wedge contact area are transferred by the fictitious elements. Axial forces are transmitted by the axes of the actual bars.

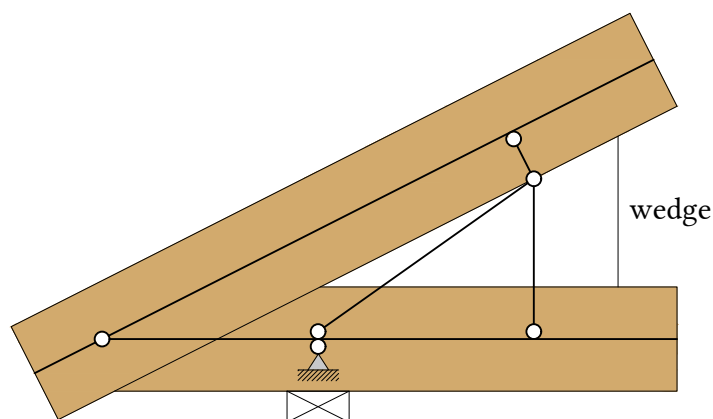


Figure 3.8: Heel joint model with fictitious elements, [43].

All previous models have imperfections in common. First, the forces on each plate in the respective contact areas are not directly given and still need to be calculated. Second, the deformation of each joint is not included in the overall deflection of the truss model, since the supports considered are simply adopted as hinges. To account for the deformations of the structure in the calculation of connections, spring elements were introduced. Three independent springs represent two translations and one rotation at each node. Springs may be linear or nonlinear, and their stiffness depends on the geometric and mechanical properties of the plate. An approach that takes into account the two observations cited is presented in the following.

Mechanical modeling for the transmission of forces to the geometric center of the plate regions is documented in the third part of the French standard DTU 31.3 2012. The method is based on the proposition that the wood pieces are disconnected from each other, and the connection is made through the plate stiffness. The mechanical model consists of the axes of the timber elements and the geometric centers of the plate regions. A series of fictitious bar elements are used to simulate the stress flow that occurs at the tooth-wood

interface. The connection model is characterized by the following steps, illustrated in Figure 3.9:

- The lines representing the axes of the timber elements are designed;
- The geometric centers of each region is determined;
- Fictitious lines are drawn perpendicular to the timber axes, which intersect the geometric centers;
- The geometric centers are also connected to each other by fictitious lines. These bars have springs at their ends, stiffnesses which define their translation and rotation. The calculation of the spring stiffness depends on the mechanical properties of the plate and is described in EC5;
- The structural model is calculated and the product of the stiffness by their deformation results in the forces that are transmitted to the geometric centers.

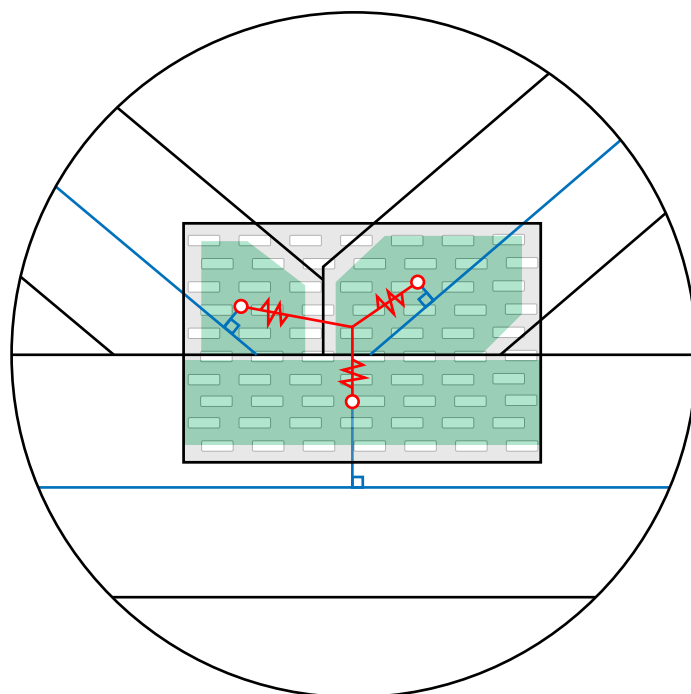


Figure 3.9: Truss plate connection modeling by DTU 31.3 2012

The stiffness of the springs used at the ends of the fictitious elements is defined by the mechanical and geometrical properties of the plate and the parameter used is the slip modulus, K_{ser} , provided by the plate manufacturer:

$$\begin{aligned} K_{x,y} &= K_{ser} \cdot 2 \cdot A_{ef} \\ K_{\varphi} &= K_{ser} \cdot 2 \cdot I_p \end{aligned} \quad (3.12)$$

With the efforts in the barycenter of the regions it is possible to calculate the anchorage strength and to proceed to the next step, the stress distribution to the rupture lines.

3.6 RUPTURE LINES

The stresses in the barycenter of the plate regions are illustrated in Figure 3.10a. The task is to carry the nodal loads in the barycenter to the breaking lines to obtain the force variables F_d and bending moment M_d as proposed by EC5. The result would be the composition illustrated in Figure 3.10b. The problem is markedly statically indeterminate and there are no boundary conditions defined.

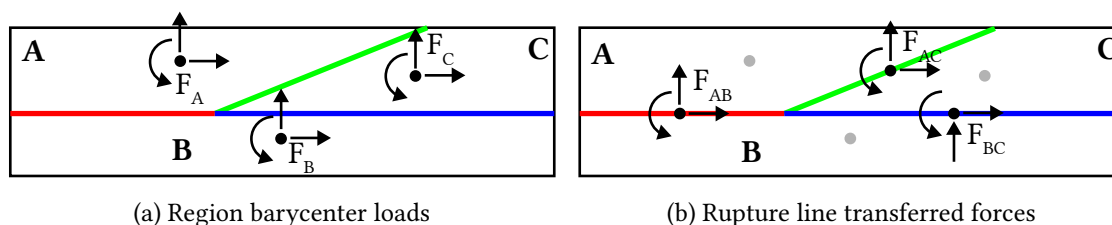


Figure 3.10: Force distribution within the plate

The ambiguity of the system suggests that there is more than one solution. The problem must be addressed from the point of view of possible modes of rupture, which in turn depend on considerations about the operation of the connection as a whole. From a sizing point of view, it is necessary to ensure that all rows check for the ultimate limit state.

The American (TPI) and Canadian (CSA) standards provide other equations for rupture line verification, but only for a region delimited by a single rupture line, as in Figure 3.11. An example would be two timber pieces with purely axial loads. EC5 can also be used by simply applying the principle of superposition to obtain the stresses at the rupture line.

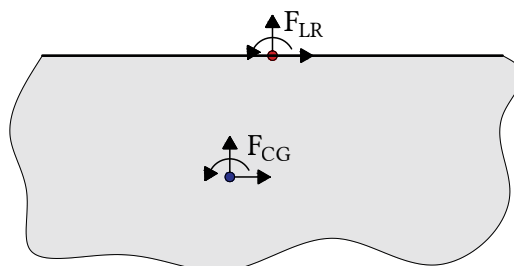


Figure 3.11: Region with one rupture line

This model is trivial and represents only a small portion of the possible connections that exist in a truss, where it is common to find three or more bars connected by a plate, that is, connections where there are multiple rupture lines per plate region, as illustrated in Figure 3.12. These cases are hyperstatic and their structural modeling requires some boundary definition. In addition, the actions of adjacent regions must be taken into account. Due to the boundary conditions, the solution will differ depending on the method chosen for analysis and also on the arbitrary region chosen as the starting point of the solution.

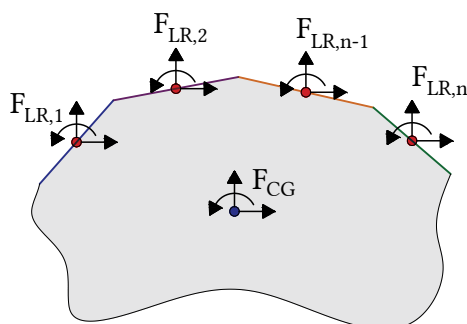


Figure 3.12: Region with multiple rupture lines

3.7 SUMMARY

Nail plate connections design requires the definition of an anchorage area, which ensures the transmission of stresses from wood to plate, and a net-cross section of steel, which supports the passage of stress to the other connected member. Six resistance parameters are individually defined by tests regulated by EN 1075.

Each connection region shall meet the safety check of its respective forces at the center of gravity for the anchorage area criterion. The strength according to the net-cross section area criterion at each rupture line shall be deduced in terms of two orthogonal components to the main direction of the plate.

The advancement of truss models seek to improve the distribution of stresses, especially for bending moments, as eccentricities are inherent in current constructive geometries. In addition, one should look for the best model that describes the timber-connection interaction. Nail plates require modeling to take into account not only truss geometry but also plate geometry, and numerous experiments show that this joint type is capable of transmitting bending moments. The consideration of each nodal deformation should also be included in the overall truss model, and a possible solution is the model proposed by DTU 31.3 2012.

The distribution of forces on the rupture lines is the major difficulty of these connections. The problem is hyperstatic and the ambiguity of solutions varies with the choice of boundary conditions and the arbitrariness of the initially verified region. The safety criterion of structures requires that checks be made for the most critical load combination. The next chapter deals with the modeling of a heel joint where various methods for determining the stress distribution on the rupture lines are studied.

A HEEL JOINT MODELING

A heel joint is studied. Initially, the geometry and mechanical properties of the proposed problem are defined. This Chapter begins from the loads applied at the barycenter of the plate regions and presents four approaches to predict the stress distribution to the rupture lines, two manual and two numerical. A computational tool was developed to verify the studied connection. Major results as the main standards verification are discussed.

4.1 INTRODUCTION

In the previous chapter, the theoretical foundations that allow the verification and design of nail plate connections were reviewed. The rupture modes and load capacity equations that should be verified were presented and lastly a mechanical model capable of transporting the stresses of the timber members to the barycenter of the plate regions was proposed. These propositions will be applied to verify the following connection. The studied connection consists of two timber elements with dimensions in the plane of 160 mm and a wedge, connected by a commercial plate with dimensions 152x559x1.5 mm, with geometry illustrated in Figure 4.1:

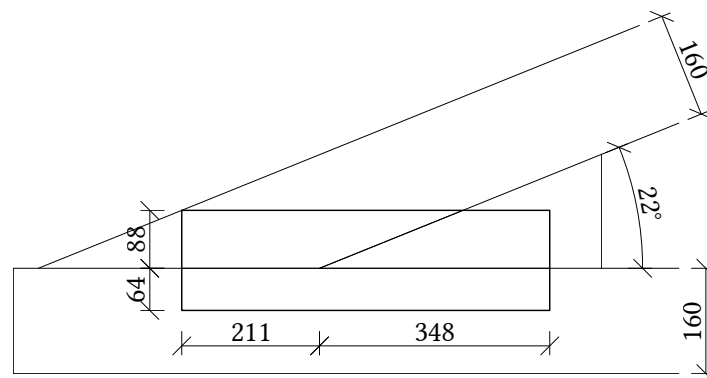


Figure 4.1: Heel joint dimensions in mm

The following conventions will be used from this section:

- The forces in the region barycenter are on the global axes and are denoted by V_{\star} , H_{\star} e M_{\star} ;
- The forces on the rupture lines are described in terms of the main axes of the rupture line direction and are denoted by T_{\star} , N_{\star} e M_{\star} ;

- Positive signal convention follows the structural static analysis definitions.

Before starting to study the distribution models, it is necessary to define the system of forces/reactions that must be in equilibrium. As the joint geometry is contained in the overall truss deformation model, the external forces are the loads applied to the wood and the reactions on the model supports are responsible for the static equilibrium. The forces are then transferred to the barycenter and the anchorage area together with the net-cross steel section transfer the forces through the rupture lines. In the heel joints, often there is also a portion of force transferred by friction and compression in the wedge region, but these forces will not be part of the scope of this work. Due to the ability of the plates to transfer bending moments, the equations involving the rupture lines will be several times statically indeterminate. The Figure 4.2 summarizes these observations:

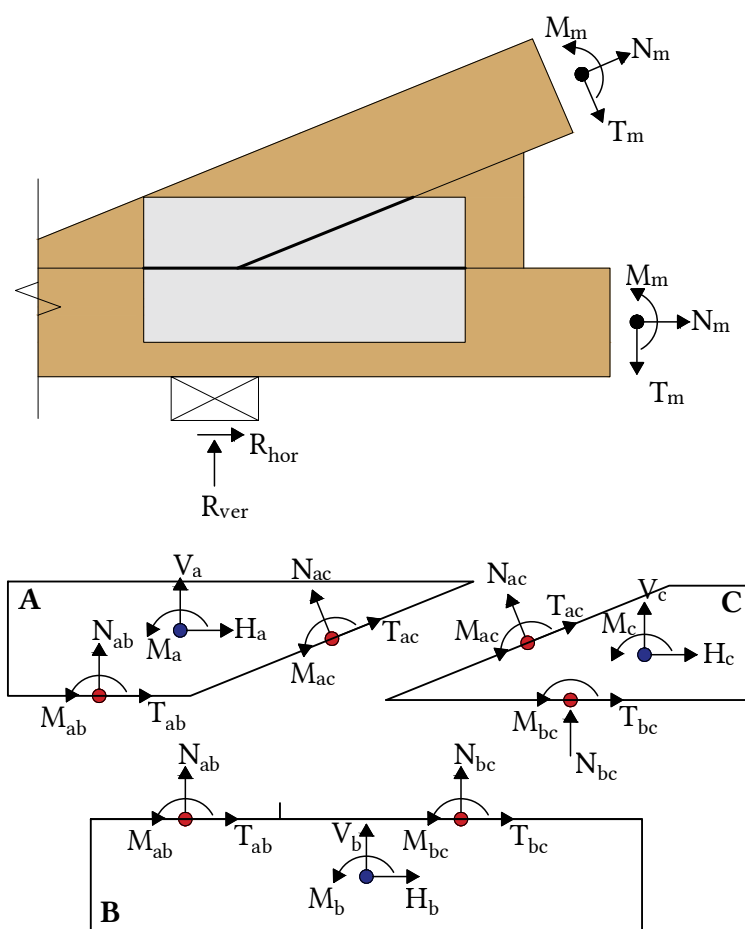


Figure 4.2: Force's system in the heel joint

The mechanical modeling to obtain the stresses according to DTU 31.3 has its main values summarized in Table 4.1 and plate properties, given by the manufacturer, are described in Table 4.2:

Table 4.1: Acting forces in the region's barycenter

Region	H	V	M
	kN	kN	kN m
A	-28.2	7.67	-0.7
B	26.2	-6.34	-0.2
C	2.22	-1.51	-0.22

Table 4.2: Nail plate mechanical properties

Characteristic strengths			Constants		
Prop.	Value	Unit	Prop.	Value	Unit
$f_{a,0,0,k}$	2.31	N/mm ²	K_{ser}	3.5	N/mm mm ²
$f_{a,90,90,k}$	1.3	N/mm ²	a_0	38	°
$f_{t,0,k}$	320	N/mm	γ_0	16	°
$f_{c,0,k}$	210	N/mm	k_1	-0.022	N/° mm ²
$f_{v,0,k}$	106	N/mm	k_2	0.0031	N/° mm ²
$f_{t,90,k}$	200	N/mm	k_v	0.7	-
$f_{c,90,k}$	151	N/mm			
$f_{v,90,k}$	87	N/mm			

A computational tool named NPCalc was developed by the author to automate the normative checking regarding the design process according to EC5, starting from the geometric and mechanical variables of the connection. The program was written in Xojo, which is a IDE¹ based on Visual Basic. The choice of this platform was due to the ease of programming the user interface, which in general has as complex formulation as the main code of the program itself. The program have four tabs: two for the plate and geometry data entry and two for the main verification criteria, illustrated in Figure 4.3. The plate and geometry tabs receive the specifications of plate strengths (as given in Table 4.2) and the geometric configuration of the desired connection. With these parameters, the program can evaluate the connection strengths, and once given the acting loads at the geometric center/rupture lines, it can perform the verification according to EC5. By now, the heel joint model illustrated in Figure 4.1 is available, however the code was structured based on object-oriented principles, which makes the verification functions and data entry parameterized, thus easy to re-use and expand.

The equations and theories of future methods will be described and the developed tool will be used to the calculations.

¹An Integrated Development Environment is a platform that allows the development of a program in its two main parts: the user interface (front end) and the source code that runs in the background (back end).

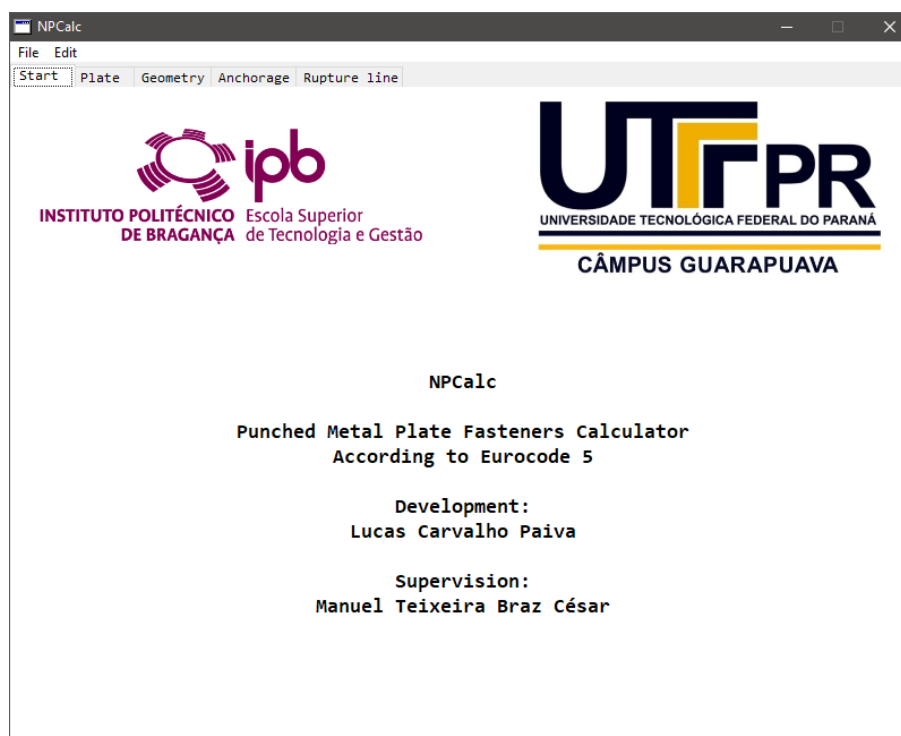


Figure 4.3: NPCalc starting page

The next sections deal with checking the proposed connection. A quick verification of the anchorage area is performed and after its validation the distribution models for the rupture lines are presented.

4.2 ANCHORAGE AREA VERIFICATION

All three regions of the connection were verified according to the procedure described in Section 3.4.1. Equation 3.5, which defines the ultimate resistance criterion of the anchorage area, was applied to quantify the three regions of the studied joint. Table 4.3 summarizes the strength and stress parameters that composes the equation.

Table 4.3: Anchorage checking results

Region	$\tau_{F,d}$	$f_{a,\alpha,\beta,d}$	$\tau_{M,d}$	$f_{a,0,0,d}$	%
	kN/m ²	kN/m ²	kN/m ²	kN/m ²	
A	1170.7	1176.3	455.5	1599.2	107%
B	817.3	1415.7	43.1	1599.2	33%
C	157.1	1206.0	271.9	1599.2	4%

The anchorage area strength criterion has a good safety margin, except for Region A. However, a 7% is numerically acceptable, while considering only the force request component $\tau_{F,d}$ is close to the calculated resistance. The NPCalc tool can then be used to evaluate the influence of any parameter in a practical way. An example of the calculation report generated by the NPCalc tool is shown in Listing 4.1:


```

1 Connection dimensions (see label ref):
2 dim_a := 0.16 [m]
3 dim_b := 0.16 [m]
4 dim_c := 0.88 [m]
5 dim_d := 0.64 [m]
6 dim_e := 0.35 [m]
7 dim_f := 0.21 [m]
8 dim_g := 22.0 [deg]
9
10 *****
11
12 Design resistances:
13 fa00d := fa00k*Kmod/gM
14 fa00d = 2.31e+6*0.9/1.3 = 1.599231e+6 [N/m2]
15 faabd := faabk*Kmod/gM
16 faabd = 1.699136e+6*0.9/1.3 = 1.176325e+6 [N/m2]
17
18 Anchorage checking region A:
19 A_anch := (Tfd/faabd)^2+(Tmd/fa00d)^2
20 A_anch = (1.170659e+6/1.176325e+6)^2 + (4.554641e+5/1.599231e+6)^2 = 1.072 [--]
21 A_anch := A_anch*100
22 A_anch = 107.15 %

```

Listing 4.1: NPCalc Report example of anchorage checking

4.3 DISTRIBUTION MODELS

The next sections present the stress distribution propositions. More than just a hyperstatic problem, solving these connections is, in fact, to propose boundary conditions that make the variable problem solvable based on the connection's working concepts.

4.3.1 MODEL 1 – SIMULTANEOUS LINE DEFORMATION

The first model admits that the forces in the wood are applied slowly and gradually and the stress transfer occurs in the plate such that the deformation of all rupture lines are occurring simultaneously. This proposition leads to the conclusion that adjacent lines share the same force action and the solution of one region can be transferred to the others by superposition. Upon inspection, region B can be isolated first, as in Figure 4.4:

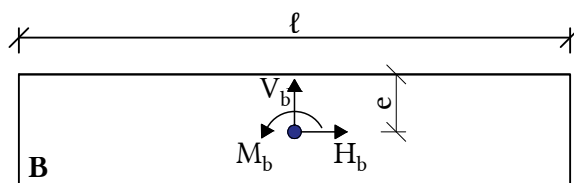


Figure 4.4: Isolated analysis of region B (M1)

The loads can then be transferred to the center of the rupture line by applying the principle of superposition of effects, in the following formulation:

$$\sigma_{N,m} = \frac{4 \cdot (M_b + H_b \cdot e)}{\ell^2}$$

$$\sigma_{N,v} = \frac{V_b}{\ell} \tag{4.1}$$

$$\sigma_{T,h} = \frac{H_b}{\ell}$$

In order to transmit the stresses to the adjacent lines, the forces were uniformly distributed along the line according to a perfectly-plastic behavior, that is, so that in each section of the line the uniform load is the result of permanent deformation, or, in load terms, each section has the same (maximum) value. The result can be viewed in Figure 4.5:

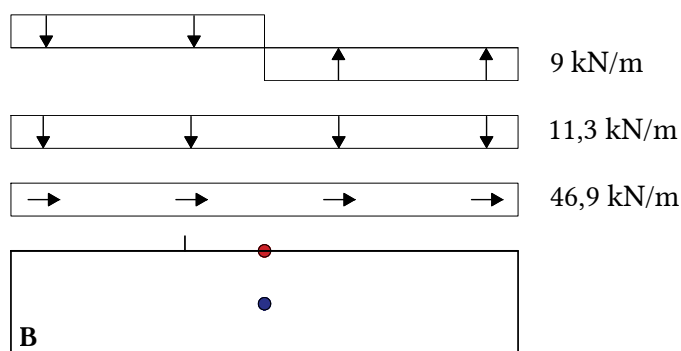


Figure 4.5: Force distribution in region B (M1)

The acting moment in the center and the moment generated by the eccentric force were converted to a distributed torque. Therefore, the adjacent lines of regions A and C can then be calculated once known the distribution that will match the loads of region A (N_{ab} , T_{ab} e M_{ab}) and in region C (N_{bc} , T_{bc} e M_{bc}), as illustrated in Figure 4.6:

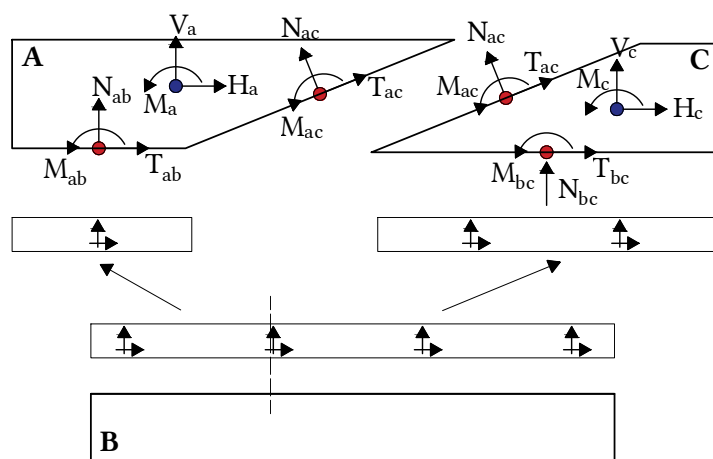


Figure 4.6: Force distribution on adjacent lines (M1)

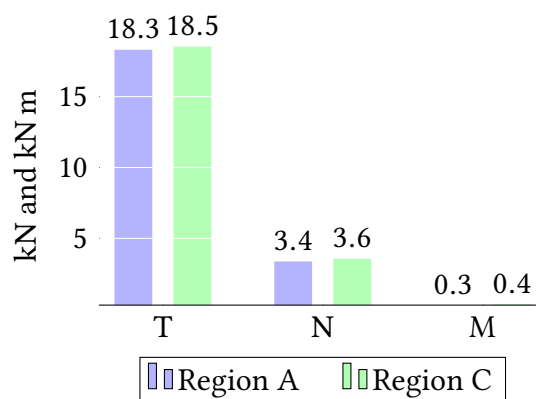
Table 4.4 summarizes the concentrated loads on the rupture lines:

Table 4.4: Result of distribution by Model 1

Region	Line	T	N	M
		kN	kN	kN m
A	AB	-4.29	9.89	0
	AC	18.31	-3.37	0.29
B	AB/BC	26.20	-6.34	0.70
C	BC	-2.05	16.31	0.17
	AC	18.53	-3.55	0.35

As the efforts acting on the anchorage zones are in equilibrium and assuming a simultaneous deformation between all lines, the load results in the inclined line AC were expected to be numerically equal for either initially evaluated region, as shown in Chart 4.1:

Chart 4.1: Line AC comparison by Model 1



With the distribution results, the NPCalc tool is then used to verify the safety criterion of the net-cross section described in Section 3.4.2. The equation criterion 3.11 has its parameters calculated and the summary of the results can be found in Table 4.5:

Table 4.5: Results of net-cross section verification by Model 1

Region	Line	$F_{x,Ed}$	$F_{x,Rd}$	$F_{y,Ed}$	$F_{y,Rd}$	%
		kN	kN	kN	kN	
A	AB	3.39	17.20	9.89	32.46	15%
	AC	19.23	19.16	5.66	36.15	103%
B	AB/BC	26.20	45.58	8.84	86.00	34%
C	BC	2.05	28.38	17.29	53.54	11%
	AC	19.65	19.16	6.31	36.15	108%

4.3.2 MODEL 2 – BENDING MOMENTS TRANSFER

The first model used the superposition principle to replace the acting bending moment in an equivalent distributed torque, to determine the acting loading on the adjacent lines to region B. Model 2 starts from an analogous premise with a second approach to transfer adjacent loads. The overall effect of the line will be distributed proportionally to the length of the adjacent line so that each line receives a bending moment portion applied to its center of gravity. Figure 4.7 illustrates this mechanism.

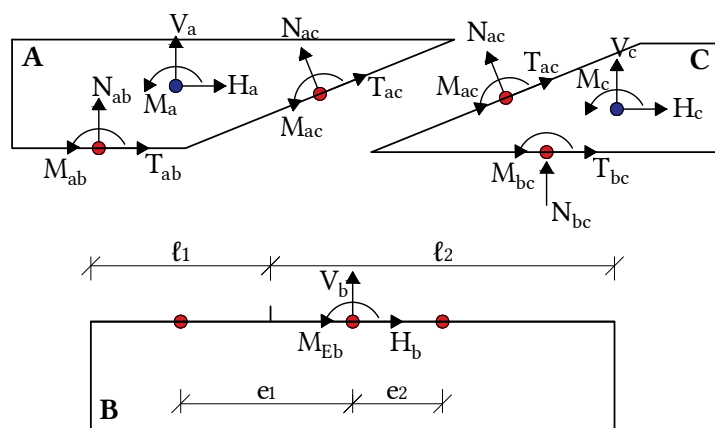


Figure 4.7: Force distribution on adjacent lines (M2)

This procedure attempts to compensate for the loss/variation in the bending moment effect transfer between lines that occurs in the first model, which is arbitrarily defined by the geometric relationship between the centers of gravity of the line, as shown in Figure 4.8:

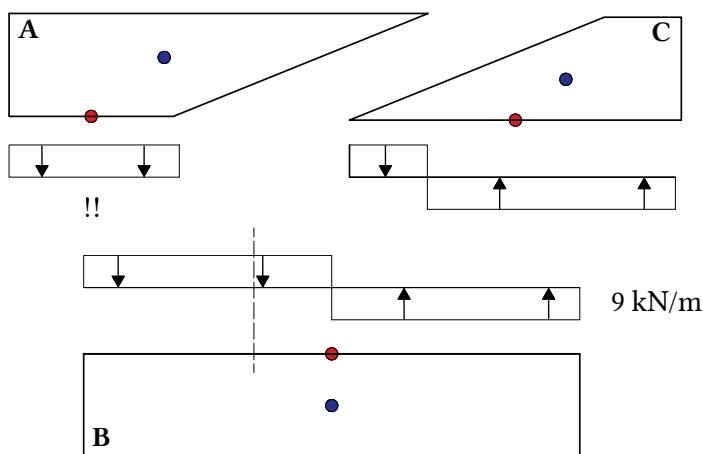


Figure 4.8: Bending moment transference by Model 1

Using the distances illustrated in Figure 4.7, the proportions can be defined:

$$\delta_A = \frac{\ell_1}{\ell} \qquad \delta_B = \frac{\ell_2}{\ell} \qquad (4.2)$$

The forces were transferred quantitatively by the following expressions:

$$\begin{aligned}
 N_{ab} &= \delta_A \cdot V_b & N_{bc} &= \delta_B \cdot V_b \\
 T_{ab} &= \delta_A \cdot H_b & T_{bc} &= \delta_B \cdot H_b \\
 M_{ab} &= \delta_A \cdot M_{Eb}
 \end{aligned}
 \tag{4.3}$$

To respect the moment equilibrium between the distributed forces, the eccentricities in Figure 4.7 were considered:

$$M_{bc} = M_{ab} + M_{Ed} - N_{ab} \cdot e_1 + N_{bc} \cdot e_2 \tag{4.4}$$

With the adjacent lines calculated, the inclined line AC could then be determined for both regions A and C, and the results are shown in Table 4.6:

Table 4.6: Result of distribution by Model 2

Region	Line	T	N	M
		kN	kN	kN m
A	AB	-3.80	15.72	0.42
	AC	12.48	-3.87	-0.28
B	AB/BC	26.20	-6.34	0.70
C	BC	-2.54	10.48	0.11
	AC	12.70	-4.05	-0.22

As noted, the rupture segment AB now has a positive bending moment of 0.42 kN m, which was null in Model 1, even though the initial calculated line AB/BC was submitted to a bending forces. Besides, the inclined line AC also presented close values from either starting region.

The NPCalc tool is then applied and the results of ULS verification are presented in Table 4.7:

Table 4.7: Results of net-cross section verification by Model 2

Region	Line	$F_{x,Ed}$	$F_{x,Rd}$	$F_{y,Ed}$	$F_{y,Rd}$	%
		kN	kN	kN	kN	
A	AB	3.80	17.2	19.70	32.46	42%
	AC	13.37	19.16	6.08	36.15	51%
B	AB/BC	26.20	45.58	8.84	86.00	34%
C	BC	2.54	28.38	11.11	53.54	5%
	AC	13.40	19.16	5.79	36.15	51%

4.3.3 MODEL 3 – ISOLATED REGIONS

The manual models (Models 1 and 2) assume that the lines deform simultaneously due to a gradual transfer of forces. However, it is possible that only one region of the connection is initially requested, so it is necessary to study each region separately and to verify that there is no rupture occurring for each region alone. Since only region B has a single rupture line, manual methods would not solve the other regions, so a numerical method is recommended.

The proposed modeling for the case of regions with multiple rupture lines is based on the researches of Foschi [37] and Gebremedhin [26] and follows the coming premises, illustrated in Figure 4.9:

1. The rupture line has a rigid behavior, which means that there must be no relative rotation between adjacent nodes, but rather a global rotation of the line (if subjected to bending actions);
2. The line is divided into n finite elements of uniform length. The length of the finite element was set at 10 mm and the arrangement of the nodes was thought such that the adjacent lines had the same node configuration scheme;
3. For each node, a pair of linear springs is used to describe the vertical and horizontal translation components of the node.

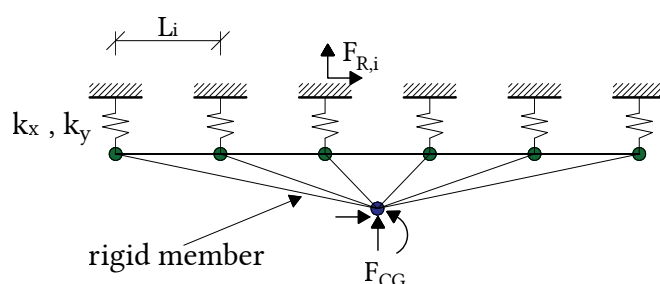


Figure 4.9: Mechanical model of the rupture line (M3)

The commercial software chosen to proceed with the modeling was the Midas/Gen packages, for some main reasons. The consideration of a rigid element requires an exact formulation of geometric constraints or, as in most programs, a numerical approximation called the penalty method, where rigid elements are arbitrarily assigned high rigidity values. Midas/Gen packages have a tool named *rigid link*, initially designed to simulate rigid diaphragm slab behavior, which uses a geometric constraint between a group of nodes (slave nodes) in relation to a main node (master node). This method not only accounts for a precise rigid behavior, but reduces the degree of freedom of the overall model, since the rigid members behave as boundary elements. Another useful tool is used to model the springs. Spring supports are considered free degrees of freedom in the matrix formulation, and the nodal solution of these nodes returns a slip value. Midas/Gen software has a boundary element called *elastic link*, which encompasses only independent spring stiffness parameters for each axis. This allows a spring element (with definite stiffness in both main directions) to be attached to a fixed support, where the reactive forces of this restraint are the direct result of the spring's slip product by its stiffness, saving an extra processing step [44].

The spring coefficient used is as described in Equation 3.12, which depends on the plate slip modulus:

$$K_{x,y} = K_{ser} \cdot 2 \cdot A_{ef}$$

As a starting point for an evaluation of the method, the region B is studied, where it is also possible to determine the distribution manually, and therefore enable a qualitative comparison:

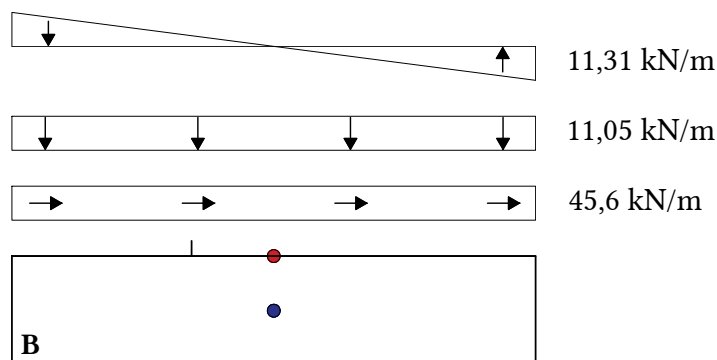


Figure 4.10: Force distribution in region B (M3)

It is noted that the numerical method produces a result equivalent to the previously described manual models, but qualitatively distinct. The distribution of the acting moment is actually elastic. This result is obtained by analyzing the deformed configuration of the continuous line, illustrated in Figure 4.11:

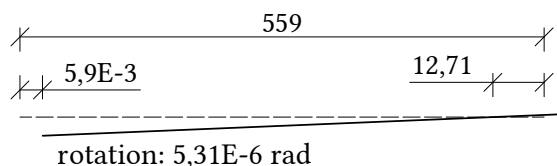


Figure 4.11: Deformed configuration for AB/BC in mm (M3)

To make possible a comparison between previous methods, the discrete result from the numerical modeling was evaluated according to its areas of influence. Assuming that the line operates as a rigid element, the rotation parameter is constant along the line. As a consequence of the linear nature of the springs, the deformations follow a linear rule and therefore the reactions on the nodes result in a triangular shape. Because the numerical method initially calculates the displacement of the structure and only later turns the result into force actions, there is a qualitative variation of the normal loads. The neutral axis of the bending moment is not in the center but shifted to the right (12.71 mm from the right node). This phenomenon was not observed in manual methods because consideration of the horizontal force eccentricity H_b affected only the bending moment value acting at the center of the line, not the overall rotation of the line axis, as detected by the numerical method.

As this numerical approach does not impose a maximum number of rupture lines per region, Regions A and C can also be modeled, as shown in Figure 4.12:

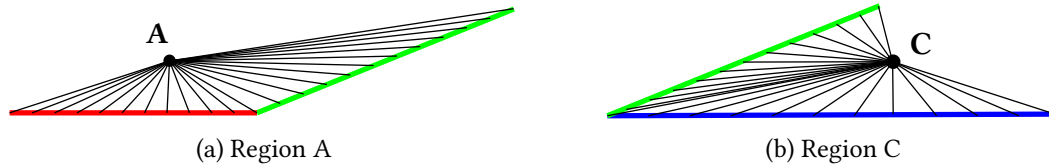


Figure 4.12: Hyperstatic regions by Model 3

the equivalent stress distribution in the line’s geometric center is listed in Table 4.8:

Table 4.8: Result of distribution by Model 3

Region	Line	T	N	M
		kN	kN	kN m
A	AB	5.49	-13.68	-0.12
	AC	2.08	-14.74	-0.26
B	AB/BC	26.02	-6.28	1.18
C	BC	-1.40	1.01	-0.35
	AC	-0.17	1.19	-0.06

As illustrated in Chart 4.2 and presented in Table 4.9, the evaluation of isolated regions can lead to very distinct values in adjacent lines:

Chart 4.2: Line AC comparison by Model 3

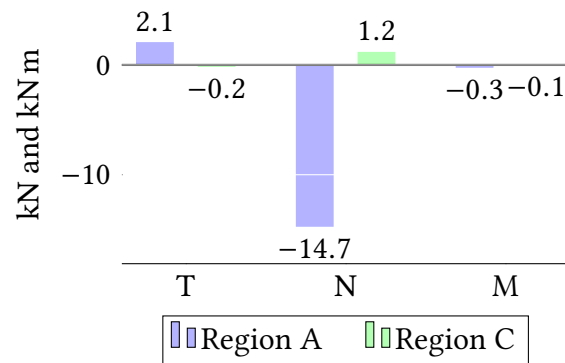


Table 4.9: Results of net-cross section verification by Model 3

Region	Line	$F_{x,Ed}$	$F_{x,Rd}$	$F_{y,Ed}$	$F_{y,Rd}$	%
		kN	kN	kN	kN	
A	AB	5.49	17.20	14.82	32.46	31%
	AC	2.91	19.16	16.79	36.15	24%
B	AB/BC	26.02	45.58	10.50	86.00	34%
C	BC	1.40	28.38	3.02	53.54	1%
	AC	0.36	19.16	1.66	36.15	1%

4.3.4 MODEL 4 – INDEPENDENT FORCE TRANSFER

The previous model was based on the analysis of a single isolated region, which should be in equilibrium with the rest of the plate and thus the verification could be done for each independent region. Model 4 provides for an extension of this verification, where adjacent lines that have not reached the ultimate limit state have their forces transferred to each other. This proposition seeks to compensate for the interaction between adjacent lines that is not part of the previous model considerations. The assumption of isolated regions, if verified, generates a rearrangement of efforts that is illustrated in Figure 4.13:

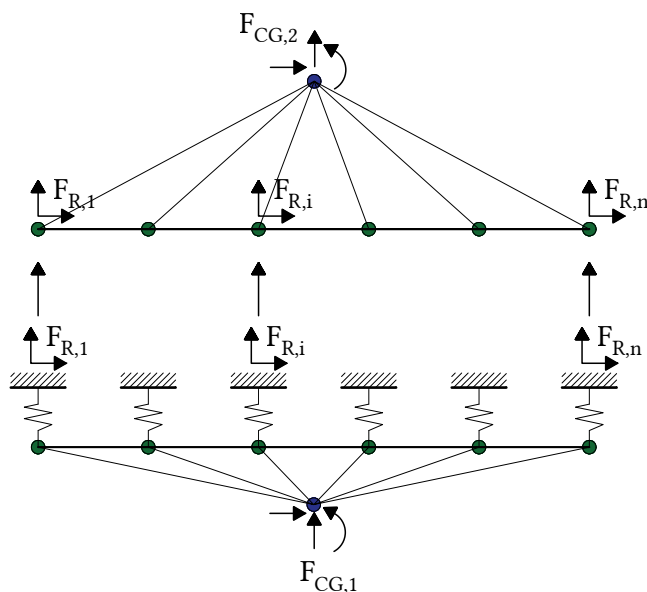


Figure 4.13: Numerical stress transfer method (M4)

Model 4 calculation starts for each isolated region and there are n transfer combinations. Since each region has its own internal forces, the choice's arbitrariness of the two initial regions chosen as starting point generates distinct stress distributions. Figure 4.14 illustrates the case where region B is initially evaluated, then the adjacent efforts are passed to the other regions, and finally the inclined line AC is solved:

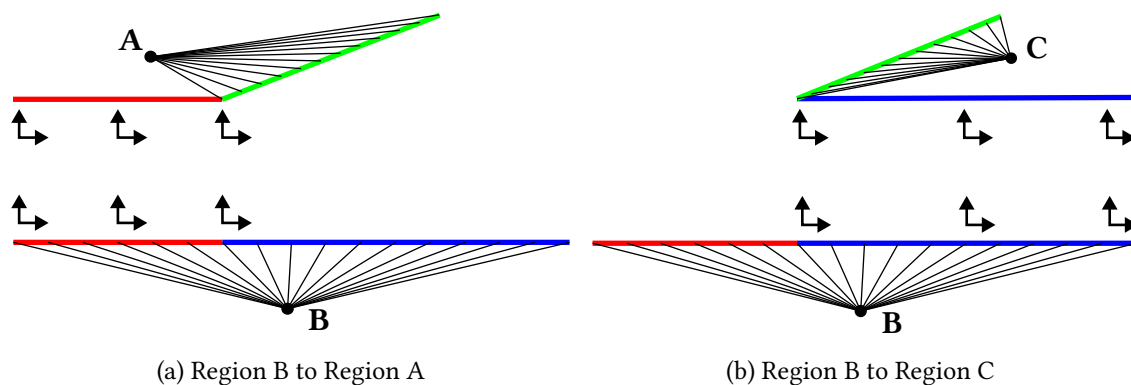


Figure 4.14: Region B as starting point by Model 4

Table 4.10 summarize the efforts for each one of the three rupture lines. The results refer to the highest values, given the starting region:

Table 4.10: Result of distribution by Model 4

Initial Region	Line	T	N	M
		kN	kN	kN m
A	AB	5.49	-13.68	-0.12
	BC	-17.41	-7.71	0.03
	AC	2.08	-14.74	0.29
B	AB/BC	26.02	-6.28	1.18
	AC	-18.86	3.94	-1.69
C	AB	-25.32	7.12	1.24
	BC	-1.40	1.01	-0.35
	AC	-0.17	1.19	-0.06

Each combination in Model 4 leads to distinct values for every line. Graphs 4.3, 4.4 and 4.5 illustrate the same lines through different regions:

Chart 4.3: Line AC comparison by Model 4

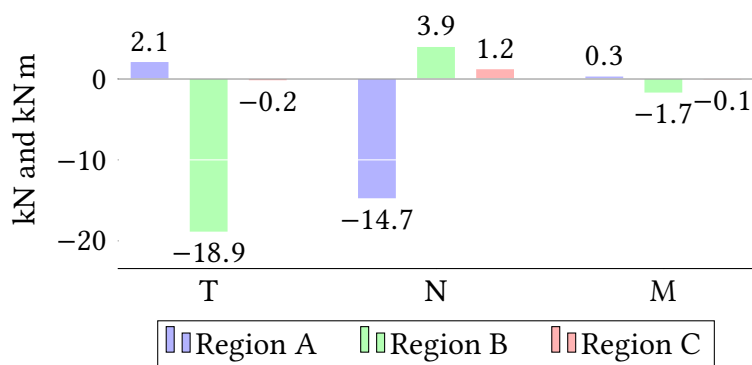


Chart 4.4: Line AB comparison by Model 4

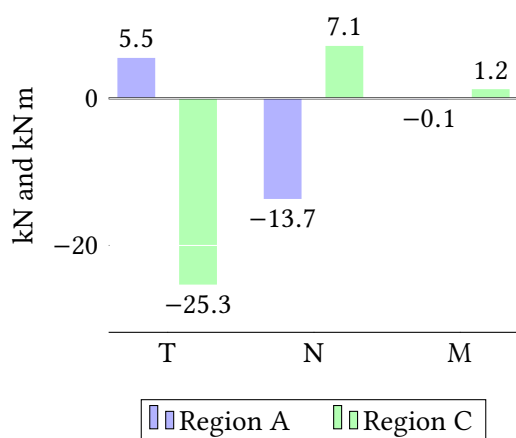
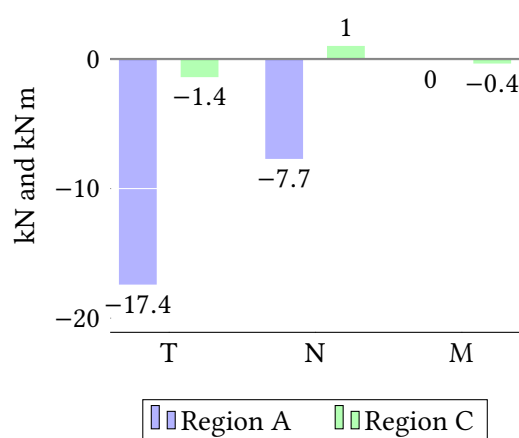


Chart 4.5: Line BC comparison by Model 4



Since in this model the forces are obtained independently for each region, each portion of the horizontal line has distinct values, so it is necessary to evaluate the distribution separately. Results are summarized in Table 4.11:

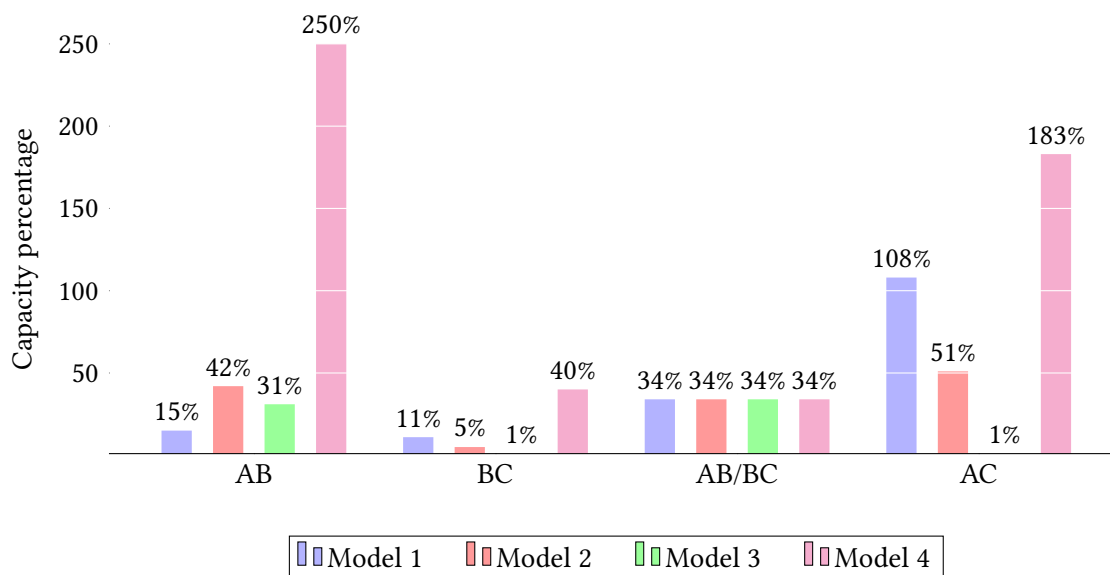
Table 4.11: Results of net-cross section verification by Model 4

Initial Region	Line	$F_{x,Ed}$	$F_{x,Rd}$	$F_{y,Ed}$	$F_{y,Rd}$	%
		kN	kN	kN	kN	
A	AB	5.49	17.20	14.82	32.46	31%
	BC	17.41	28.38	7.88	53.54	40%
	AC	3.00	19.16	17.03	36.15	25%
B	AB/BC	26.02	45.58	10.5	86.00	34%
	AC	24.25	19.16	17.28	36.15	183%
C	AB	25.32	17.20	18.87	32.46	250%
	BC	1.40	28.38	3.02	53.54	1%
	AC	0.36	19.16	1.66	36.15	1%

4.4 COMPARISON AND CRITICAL COMBINATION OF FORCE DISTRIBUTION

Graph 4.6 compares the EC5 verification for each one of the four lines studied. Some methods evaluate the same line multiple times, thus the highest value was taken:

Chart 4.6: Net-cross section capacity overall comparison



The following observations can be obtained from the Graph above:

- All methods leads to very distinct values for regions with more than one rupture line;
- Model 4 tends to be the most conservative;
- Regions with one rupture line (AB/BC) present the same value for all methods.

The four modeling performed can be combined from the perspective of the most critical effort in each section, shown in Figure 4.15:

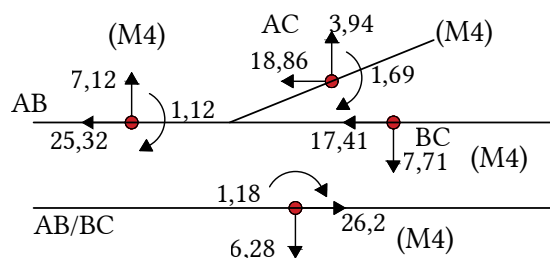


Figure 4.15: Critical efforts of rupture lines in kN and kN m

Not only the efforts vary with the type of analysis, but also the rupture lines. In models where isolated regions are analyzed, the horizontal line is divided, which is why there are two results in this failure mode: one for each portion of the line and one for when the horizontal line as a whole is analyzed by region B. Finally, Table 4.12 shows the line checking for the envelope results by all four models:

Table 4.12: Net-cross section envelop results

Line	Method	Fx	Fx	Fy	Fy	%
		kN	kN	kN	kN	
AB	4	25.32	17.20	18.87	32.46	250%
BC	4	17.41	28.38	7.88	53.54	40%
AB/BC	4	26.02	45.58	10.5	86.00	34%
AC	4	24.25	19.16	17.28	36.15	183%

Finally, to provide a quick way to compare the stresses in each rupture line, Table 4.13 summarizes the results of the force distribution for each model:

Table 4.13: Overall comparison of stress distribution by the four presented models

Line	Model 1			Model 2			Model 3			Model 4		
	T	N	M	T	N	M	T	N	M	T	N	M
	kN	kN	kN m	kN	kN	kN m	kN	kN	kN m	kN	kN	kN m
AB	-4.29	9.89	0	-3.8	15.72	0.42	5.49	-13.68	-0.12	-25.32	7.12	1.24
BC	-2.05	16.31	0.17	-2.54	10.48	0.11	-1.4	1.01	-0.35	-17.41	-7.71	0.03
AB/BC	26.2	-6.34	0.7	26.2	-6.34	0.7	26.02	-6.28	1.18	26.02	-6.28	1.18
AC	-18.53	3.55	-0.35	12.48	-3.87	-0.28	2.08	-14.74	-0.26	2.08	-14.74	0.29

4.5 SUMMARY

The studies covered in this chapter allow the conclusions of the following corollaries:

1. The force distribution varies quantitatively and qualitatively with the chosen analysis method;
2. Manual modeling suggests a plastic stress distribution, while numerical modeling follows an elastic pattern when modeled by linear springs;
3. Regions with one rupture line present close values to both manual and numerical models.

With regard to the conclusions presented, the developed manual methods are only valid when there is a region delimited by a single line of rupture and cannot be applied to completely hyperstatic cases. Numerical methods do not have this limitation, but depend on the consideration of rigid elements, which limits the options of commercial software that have the exact formulation of these elements.

CONCLUSIONS AND FURTHER RESEARCH

The main objectives are addressed in this conclusion. The first objective was to make a normative review and to define the main methods of verification to the ultimate limit state for nail plate connections. The other two objectives were to present methods to predict the distribution of internal forces on the plate and develop an automatic calculation tool to systematize the checking. Here, extensions that the proposed tasks have reached are discussed and guidelines for future research are proposed.

5.1 CONCLUSIONS

At the beginning of the dissertation, it was mentioned that the greatest difficulty of nail plates connections was in determining the forces acting on the rupture lines, both from the modeling and normative scarcity point of view.

Firstly, it was compiled the necessary information about these joints and their analysis methods. The existing modeling procedures were studied and the conclusions obtained for the stress distribution in relation to the methods used.

The main current standard has been revised and its equations have been presented. It was identified how to obtain the plate calculation parameters and how to model the truss to obtain the forces acting on the geometric center of the regions, then proceed with the stress distribution.

About the proposed methods:

- To make the system solution possible, it was necessary to impose boundary conditions on the rupture lines. For this, the premises used were based on the studied literature. The literature models were based on a mechanical construction involving all the components of the connection (the wood, the plate, the teeth and the tooth-wood interface). The set of hypotheses from these documents were then brought from another perspective: a 2-D model that allows to evaluate the distribution of forces with frame-type elements (bars, springs and rigid elements);
- Each method established a simplification of actions based on how the connection works and how the forces are transmitted on prefabricated trusses. Each isolated method does not aim to evaluate the exact distribution of all lines as a whole, but seeks to identify, for each mode, one or a group of critical lines. In this sense, the final result of the verification is considered as the envelope of all the described methods;

- Although exemplified in the case of an heel joint, the developed methods can be extended to more types of joint configurations, bearing in mind the limitations of each method. Similarly, the NPCalc tool was developed according to the principles of object orientation, and by adjusting the input parameters, the same code can be applied to other connection types and configuration.

5.2 FUTURE DEVELOPMENTS

To continue the research initiated in this dissertation, two segments can be highlighted that should be developed, in a qualitative approach, to ensure a more complete analysis of the connection systems. One component is associated with the developed modeling and the other related to the NPCalc software.

In relation to the manual modelings, it is intended to extend the verification to regions with more than one rupture line, replacing the system with a fictitious equivalent line. Manual models provide a quick check and allow to evaluate the direct influence of stresses without the need to initially calculate the slip values.

The numerical modeling has two main boundary elements that can be extended. The first is the rigid operation of the line through the rigid link tool. It is intended to study an alternative way to simulate the rigid behavior with displacement constraints, so that it is possible to extend numerical verification to more commercial software. The second is the springs used to describe the plate stiffness. It is intended to develop a formulation involving a nonlinear spring coefficient that more accurately reflects the behavior of the tooth-wood interface and, in addition, to develop an equivalent spring system at the key node points of the line, in order to simplify its modeling and implementation.

About the NPCalc tool, it is intended to expand the calculation to more connection types and include the numerical models for stress distribution. It is also intended to use the computational structure already developed to maximize the anchoring and steel net section verification functions to determine the optimum geometry and strength parameters for the studied joint.

REFERENCES

- [1] Michael S. Mamlouk and John P. Zaniewski. *Materials for Civil and Construction Engineers*. 3rd ed. Pearson, 2010 (cit. on p. 1).
- [2] Wood Handbook. “Wood as an engineering material”. In: *General Technical Report FPL-GTR-190, Department of Agriculture, Forest Service, Forest Products Laboratory: USA* (2010) (cit. on p. 1).
- [3] Michael R. O’Halloran. “Changing nature of wood-based structural materials”. In: *Elsevier* 6.3 (1992), pp. 139–143 (cit. on p. 1).
- [4] Petr Kuklík. *History of timber structures*. 1st ed. Education Materials for Designing and Testing Timber Structures, 2008. Chap. 1 (cit. on pp. 1, 4, 5).
- [5] P. Racher. *Mechanical timber joints-General. Timber Engineering STEP 1 – Basic of design, material properties, structural component and joints*. Almere Centrum Hout, 1995 (cit. on pp. 2, 7).
- [6] J. Natterer. “Quality criteria for timber design”. In: *Elsevier* 6.3 (1992), pp. 133–137 (cit. on p. 2).
- [7] André Johannes Maria Jorissen. “Double shear timber connections with dowel type fasteners”. PhD thesis. Delft University, The Netherlands, 1998 (cit. on p. 2).
- [8] Saadettin Murat Onat. “Feasibility of using metal Plate Connected Timberstrand LSL joints in the truss fabrication industry”. In: *Journal of Bartın Faculty of Forestry* 18.1 (2016), pp. 1–12 (cit. on p. 2).
- [9] Robert Kliger. *Design of timber Structures*. 2nd ed. Swedish Forest Industries Federation, 2016. Chap. 1 (cit. on p. 2).
- [10] Edward E. Callahan and Pamela W. Dinsmore. *Metal Plate Connected Wood Truss Handbook: A Comprehensive Guide to the Design and Use of Metal Plate Connected Wood Trusses in Construction Today*. Wood Truss Council of America, 1993 (cit. on p. 2).
- [11] Sven Thelandersson and Hans J. Larsen. *Timber engineering*. John Wiley & Sons, 2003 (cit. on pp. 2, 5, 7, 27).
- [12] Thomas Herzog et al. *Timber construction manual*. Walter de Gruyter, 2012 (cit. on p. 4).
- [13] Jonathan Edward Kidder. *The art of Japan*. Outlet, 1985 (cit. on p. 5).
- [14] Werner Stadelmann and Nerses Sehbenderyan. *Wooden Bridges in Switzerland (in german)*. Bündner Monatsblatt, 1990 (cit. on p. 5).
- [15] Food and Agriculture Organization of The United Nations. *The Global Forest Resource Assessment*. Technical report. 2018. URL: <http://www.fao.org/home/en/> (cit. on p. 6).

- [16] Jarosław Malesza and Czesław Miedziałowski. “Current directions in development of modern wood-framed houses”. In: *Procedia Engineering* 172 (2017), pp. 701–705 (cit. on p. 6).
- [17] S. Whiltelaw. “Architects love Timber”. In: *Australian Forest Industries Journal* 2.2 (1990), pp. 57–62 (cit. on p. 6).
- [18] N. Gregory. “The Culture of Using Timber as a Building Material in Australia”. In: *The Pacific Timber Engineering Conference* (1994) (cit. on p. 6).
- [19] Phil Townsend and Chris Wagner. “Timber as a Building Material-An environmental comparison against synthetic building materials”. In: *National Association of Forest Industries Ltd* (2002), p. 8 (cit. on p. 6).
- [20] Y.M.D. Adedeji and Olu Ola Ogunsote. “Modern Techniques of Using Timber in Building Structures and Components in Nigeria”. In: *Proceedings of conference, Department of Architecture, Federal University of Technology, Akure*. 2005 (cit. on p. 6).
- [21] Ian Smith and Monica A. Snow. “Timber: An ancient construction material with a bright future”. In: *The Forestry Chronicle* 84.4 (2008), pp. 504–510 (cit. on p. 6).
- [22] Keith Faherty. “Timber Connectors”. In: *Mechanical Connections in Wood Structures* (1995), pp. 173–218 (cit. on pp. 7, 9).
- [23] K. Thomas. “Mechanical Fasteners”. In: *The Structural Engineer* 60A.2 (1982), pp. 47–51 (cit. on p. 7).
- [24] R.J. Bainbridge and C.J. Mettem. “A review of moment-resistant structural timber connections”. In: *Proceedings of the Institution of Civil Engineers-Structures and Buildings* 128.4 (1998), pp. 323–331 (cit. on pp. 7, 8).
- [25] Peter A. Claisse and Tim J. Davis. “High performance jointing systems for timber”. In: *Construction and Building Materials* 12.8 (1998), pp. 415–425 (cit. on pp. 8, 9).
- [26] K.G. Gebremedhin and P.L. Crovella. “Load distribution in metal plate connectors of tension joints in wood trusses”. In: *Transactions of the ASAE* 34.1 (1991), pp. 281–0287 (cit. on pp. 10, 17, 40).
- [27] J.D. Bellamy. “The trussed rafter industry: An introduction for engineers”. In: *Proceedings of the Institution of Civil Engineers-Structures and Buildings* 104.1 (1994), pp. 51–59 (cit. on pp. 10, 12).
- [28] Julio Cesar Molina and Carlito Calil Junior. “Sistema construtivo em Wood Frame para casas de madeira”. In: *Ciências Exatas e Tecnológicas, Londrina* 31.2 (2010), pp. 143–156 (cit. on p. 10).
- [29] Walter Pfiel and Michele Pfiel. *Estruturas de madeira*. LTC, 2003 (cit. on p. 10).
- [30] Henrique Partel. “Sistema informatizado para projeto de estruturas industrializadas de madeira para telhados”. MA thesis. Universidade de São Paulo, 2000 (cit. on p. 11).
- [31] Canada Wood. *Wood Trusses: Strength, Economy, Versatility*. Technical report. 2010. URL: <https://canadawood.org/technical-publications/> (cit. on p. 12).
- [32] Randek ©. *Randek CUT SAW SP720*. Technical report. 2019. URL: <http://www.randek.com/en/products/cut-saws/crosscut-saw-spl728> (cit. on p. 13).

- [33] Randek ©. *AutoEye Truss System SF022*. Technical report. 2019. URL: <http://www.randek.com/en/products/roof-truss-system/autoeyetruss-system-sf022> (cit. on pp. 13, 14).
- [34] Wolf Systems ©. *Trussed Rafter - Technical Manual*. Technical report. 2004. URL: <https://www.wolfssystem.co.uk/> (cit. on p. 14).
- [35] Rakesh Gupta, Milan Vatovec, Thomas H. Miller, et al. “Metal-plate-connected wood joints: a literature review”. In: *Forest Research Laboratory Oregon State University* (1996) (cit. on p. 15).
- [36] R.D. Misra and M.L. Esmay. “Stress distribution in the punched metal plate of a timber joint”. In: *Transactions of the ASAE* 9.6 (1966), pp. 839–842 (cit. on p. 15).
- [37] Ricardo O. Foschi. “Analysis of wood diaphragms and trusses. Part II: Truss-plate connections”. In: *Canadian Journal of Civil Engineering* 4.3 (1977), pp. 353–362 (cit. on pp. 15, 16, 40).
- [38] Peter W.C. Lau. “Factors affecting the behaviour and modelling of toothed metal-plate joints”. In: *Canadian Journal of Civil Engineering* 14.2 (1987), pp. 183–195 (cit. on pp. 16, 17, 20, 27).
- [39] S.M. Cramer, D. Shrestha, and W.B. Fohrell. “Theoretical consideration of metal-plate-connected wood-splice joints”. In: *Journal of Structural Engineering* 116.12 (1990), pp. 3458–3474 (cit. on p. 17).
- [40] K.G. Gebremedhin, M.C. Jorgensen, and C.B. Woelfel. “Load-slip characteristics of metal plate connected wood joints tested in tension and shear”. In: *Wood and fiber science: journal of the Society of Wood Science and Technology* (1992) (cit. on p. 17).
- [41] Leslie Groom and Anton Polensek. “Nonlinear modeling of truss-plate joints”. In: *Journal of structural engineering* 118.9 (1992), pp. 2514–2531 (cit. on p. 18).
- [42] M. Vatovec, T.H. Miller, and Rakesh Gupta. “Modeling of metal-plate-connected wood truss joints”. In: *Transactions of the ASAE* 39.3 (1996), pp. 1101–1111 (cit. on p. 18).
- [43] H. Riberholt. “Guidelines for static models of trussed rafters”. In: *Int. Council for Research and Innovation in Building and Construction. Working Commission W18-Timber Structures* (1982) (cit. on p. 27).
- [44] Midas Information Technology. *Midas/GEN – Analysis Manual*. 2014. URL: http://manual.midasuser.com/EN_TW/Gen/830/index.htm (cit. on p. 40).

TECHNICAL STANDARDS

- [45] EN 1995-1-1. *Eurocode 5: Design of timber structures – Part 1-1: General – Common rules and rules for buildings*. European Committee for Standardization, 2004.
- [46] EN 1075. *Timber structures – Test methods – Joints made with punched metal plate fasteners*. European Committee for Standardization, 1999.

- [47] EN 14250. *Timber structures. Product requirements for prefabricated structural members assembled with punched metal plate fasteners*. European Committee for Standardization, 2010.
- [48] NF DTU 31.3. *Timber structures connected with metal plate fasteners or gussets – Part 3: Design requirements*. Association Française de Normalisation, 2012.
- [49] ASTM E489. *Standard Test Method for Tensile Strength Properties of Metal Connector Plates*. American Society for Testing and Materials, 1997.
- [50] ASTM E767. *Standard Test Method for Shear Strength Properties of Metal Connector Plates*. American Society for Testing and Materials, 2001.
- [51] ASTM D1761. *Standard Test Methods for Mechanical Fasteners in Wood*. American Society for Testing and Materials, 2012.
- [52] ANSI/TPI. *National design standard for metal-plate connected wood truss construction*. Truss Plate Institute, 1995.
- [53] CSA S347. *Method of test for evaluation of truss plates used in lumber joints*. Canadian Standards Association, 1980.
- [54] ISO 8969. *Timber Structures – Testing of punched metal plate fasteners and joints*. International Organization for Standardization, 2011.

APPENDIX **A****NPCALC CODE**

The following code is a compact instruction to fully allow the program's replication, in front-end and back-end development. The IDE version of this project is the Xojo 2019r.1.1 running in Windows 10.

Project: NPCalc

Date: quinta-feira, 10 de outubro de 2019 14:20:03

App

Class App

Inherits Application

Constants

Const kEditClear As String = "&Delete"

Const kFileQuit As String = "&Quit"

Const kFileQuitShortcut As String = ""

End Class

MainMenuBar

MainMenuBar

FileMenu

SpecialMenu = 0

Text = &File

Index = -2147483648

AutoEnable = 1

Visible = True

FileQuit

SpecialMenu = 0

Text = #App.kFileQuit

Index = -2147483648

ShortcutKey = #App.kFileQuitShortcut

Shortcut = #App.kFileQuitShortcut

AutoEnable = 1

Visible = True

EditMenu

SpecialMenu = 0

Text = &Edit

Index = -2147483648

AutoEnable = 1

Visible = True

EditUndo

SpecialMenu = 0
Text = &Undo
Index = -2147483648
ShortcutKey = Z
Shortcut = Cmd+Z
MenuModifier = True
AutoEnable = 1
Visible = True

EditSeparator1

SpecialMenu = 0
Text = -
Index = -2147483648
AutoEnable = 1
Visible = True

EditCut

SpecialMenu = 0
Text = Cu&t
Index = -2147483648
ShortcutKey = X
Shortcut = Cmd+X
MenuModifier = True
AutoEnable = 1
Visible = True

EditCopy

SpecialMenu = 0
Text = ©
Index = -2147483648
ShortcutKey = C
Shortcut = Cmd+C
MenuModifier = True
AutoEnable = 1
Visible = True

EditPaste

SpecialMenu = 0
Text = &Paste
Index = -2147483648
ShortcutKey = V
Shortcut = Cmd+V
MenuModifier = True
AutoEnable = 1
Visible = True

EditClear

```
SpecialMenu = 0
Text = #App.kEditClear
Index = -2147483648
AutoEnable = 1
Visible = True
```

```
EditSeparator2
SpecialMenu = 0
Text = -
Index = -2147483648
AutoEnable = 1
Visible = True
```

```
EditSelectAll
SpecialMenu = 0
Text = Select &All
Index = -2147483648
ShortcutKey = A
Shortcut = Cmd+A
MenuModifier = True
AutoEnable = 1
Visible = True
```

MW

Class MW

Inherits Window

Events

```
Sub Open()
    'verif_cap_res_tipo1
    'verif_cap_res_tipo2(-25320, -7120, 1240, 0, 0.211) 'AB -- A
    'verif_cap_res_tipo2(2080, -14740, -260, 0.383972, 0.235) ' AC -- A
    'verif_cap_res_tipo2(26020, -6280, 1180, 0, 0.559) 'AB/BC -- B
    'verif_cap_res_tipo2(-17410, -7710, 30, 0.383972, 0.235) 'BC -- C
    'verif_cap_res_tipo2(-18860, 3940, -1690, 0, 0.348) ' AC -- C
```

End Sub

MW Control TabPanel1:

```
Sub Open()
    Me.Caption(0)="Start"
    Me.Caption(1)="Plate"
```



```
Me.Caption(2)="Geometry"  
Me.Caption(3)="Anchorage"  
Me.Caption(4)="Rupture line"  
End Sub
```

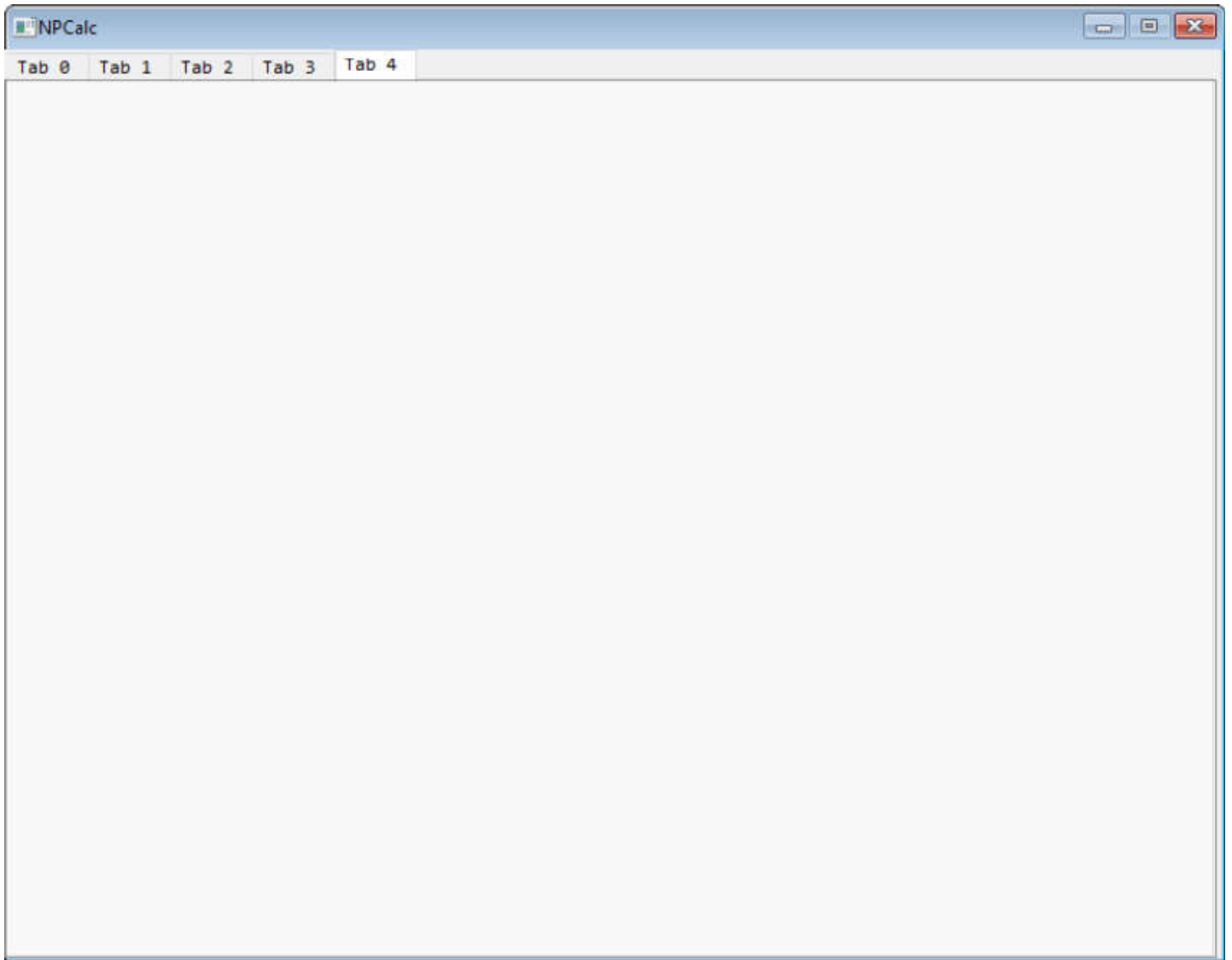
MW Control Pag01:

MW Control Pag11:

MW Control Pag21:

MW Control Pag31:

MW Control Pag41:



End Class

Pag0

Class Pag0

Inherits ContainerControl

Pag0 Control TextArea1:

```
Sub Open()  
    Me.TextSize=18  
    me.Bold=true  
End Sub
```

Pag0 Control logo_ipb:

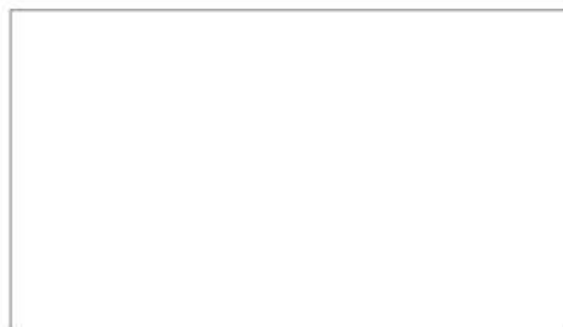
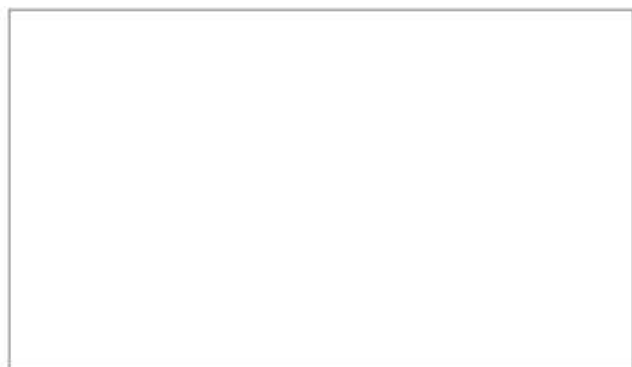
```
Sub Paint(g As Graphics, areas() As REALbasic.Rect)  
    g.DrawPicture(ScaleImage(IMG_logo_ipb, Me.Width, Me.Height), 0, 0)
```

End Sub

Pag0 Control logo_utfpr:

```
Sub Paint(g As Graphics, areas() As REALbasic.Rect)  
    g.DrawPicture(ScaleImage(IMG_logo_utfpr, Me.Width, Me.Height), 0, 0)
```

End Sub



NPCalc

Punched Metal Plate Fasteners Calculator
According to Eurocode 5

Development:
Lucas Carvalho Paiva

Supervision:
Manuel Teixeira Braz César



End Class

Pag1

Class Pag1

Inherits ContainerControl

Methods

Sub prop_materiais()

 'Receber as propriedades dos materiais e coeficientes

 'Chapa

 t=Cdbl(Pag1.prop_t.Text)

 kser=Cdbl(Pag1.prop_kser.Text)

 fa00k=Cdbl(Pag1.prop_fa00k.Text)

 fa9090k=Cdbl(Pag1.prop_fa9090k.Text)

 k1=Cdbl(Pag1.prop_k1.Text)

 k2=Cdbl(Pag1.prop_k2.Text)

 α0=Cdbl(Pag1.prop_α0.Text)

 fc0k=Cdbl(Pag1.prop_fc0k.Text)

 fc90k=Cdbl(Pag1.prop_fc90k.Text)

 ft0k=Cdbl(Pag1.prop_ft0k.Text)

 ft90k=Cdbl(Pag1.prop_ft90k.Text)

 fv0k=Cdbl(Pag1.prop_fv0k.Text)

 fv90k=Cdbl(Pag1.prop_fv90k.Text)

 γ0=Cdbl(Pag1.prop_γ0.Text)

 kv=Cdbl(Pag1.prop_kv.Text)

 'Coeficientes

 γM=Cdbl(Pag1.prop_γM.Text)

 kmod=Cdbl(Pag1.prop_kmod.Text)

End Sub

Pag1 Control GroupBox1:

Pag1 Control prop_t:

Pag1 Control prop_fa00k:

Pag1 Control prop_fa9090k:

Pag1 Control Label1:

Sub MouseEnter(index as Integer)

 Dim legenda As Text

```
Select Case Label1(index).index
Case 0
  legenda="plate thickness"

Case 1
  legenda="Slip modulus"

Case 2
  legenda="força resistente de ancoragem, para  $\alpha = 0^\circ$  e  $\beta = 0^\circ$ "

Case 3
  legenda="força resistente de ancoragem, para  $\alpha = 0^\circ$  e  $\beta = 90^\circ$ "

Case 7
  legenda="força resistente de tração, paralelo às fibras"

Case 8
  legenda="força resistente de tração, perpendicular às fibras"

Case 9
  legenda="força resistente de compressão, paralelo às fibras"

Case 10
  legenda="força resistente de compressão, perpendicular às fibras"

Case 11
  legenda="força resistente de embutimento, paralelo às fibras"

Case 12
  legenda="força resistente de embutimento, perpendicular às fibras"

End Select
```

```
legenda_propriedades.Text=legenda
```

```
End Sub
```

Pag1 Control prop_fc0k:

Pag1 Control prop_ft90k:

Pag1 Control prop_ft0k:

Pag1 Control prop_fv90k:

Pag1 Control prop_fv0k:

Pag1 Control prop_fc90k:

Pag1 Control GroupBox2:

Pag1 Control prop_γ0:

Pag1 Control prop_kv:

Pag1 Control prop_kser:

Pag1 Control prop_α0:

Pag1 Control prop_k2:

Pag1 Control prop_k1:

Pag1 Control legenda_propiedades:

Pag1 Control GroupBox3:

Pag1 Control prop_γM:

Pag1 Control prop_kmod:

Characteristic Strengths		
t	<input type="text"/>	m
F,a,θ,θ,k	<input type="text"/>	N/m ²
F,a,9θ,9θ,k	<input type="text"/>	N/m ²
F,t,θ,k	<input type="text"/>	N/m ²
F,t,9θ,k	<input type="text"/>	N/m ²
F,c,θ,k	<input type="text"/>	N/m ²
F,c,9θ,k	<input type="text"/>	N/m ²
F,v,θ,k	<input type="text"/>	N/m ²
F,v,9θ,k	<input type="text"/>	N/m ²

Constants		
K,ser	<input type="text"/>	N/m.m ²
aθ	<input type="text"/>	°
γθ	<input type="text"/>	°
K1	<input type="text"/>	N/° . m ²
K2	<input type="text"/>	N/° . m ²
Kv	<input type="text"/>	-

Coeficientes		
γM	<input type="text"/>	-
Kmod	<input type="text"/>	-

mostrar aqui a legenda das propriedades

End Class

Pag2

Class Pag2

Inherits ContainerControl

Methods

Sub dimensoes_tipo1()

 'Ligaç o Tipo 1 - Duas pe as em liga o de extremidade

 'Receber as dimens es da liga o

 dim_a=Cdbl(Pag2.dim_a.Text)

 dim_b=Cdbl(Pag2.dim_b.Text)

 dim_c=Cdbl(Pag2.dim_c.Text)

 dim_d=Cdbl(Pag2.dim_d.Text)

 dim_e=Cdbl(Pag2.dim_e.Text)

 dim_f=Cdbl(Pag2.dim_f.Text)

 dim_g=Cdbl(Pag2.dim_g.Text)

End Sub

Pag2 Control Canvas1:

Sub Paint(g As Graphics, areas() As REALbasic.Rect)

 g.DrawPicture(ScaleImage(IMG_ligacao_1, Me.Width, Me.Height), 0, 0)

End Sub

Pag2 Control PopupMenu1:

Sub Change()

 Canvas1.visible=True

 Canvas1.Invalidate

End Sub

Pag2 Control dim_a:

Pag2 Control dim_b:

Pag2 Control dim_c:

Pag2 Control dim_d:

Pag2 Control dim_e:

Pag2 Control dim_f:

Pag2 Control dim_g:

Pag2 Control Label1:

Pag2 Control Label2:

Pag2 Control Label3:

Pag2 Control Label4:

Pag2 Control Label5:

Pag2 Control Label6:

Pag2 Control Label7:

Pag2 Control Label8:

Pag2 Control Label9:

Pag2 Control Label10:

Pag2 Control Label11:

Pag2 Control Label12:

Pag2 Control Label13:

Pag2 Control Label14:

Tipo 1 - Duas peças em ligação de extremidade

a mm

b mm

c mm

d mm

e mm

f mm

g g

End Class

Pag3

Class Pag3

Inherits ContainerControl

Pag3 Control Canvas1:

```
Sub Paint(g As Graphics, areas() As REALbasic.Rect)
    g.DrawPicture(ScaleImage(IMG_esforcos_cg_tipo1, Me.Width, Me.Height), 0, 0)
End Sub
```

```
Sub Open()
    Me.Invalidate
```

```
End Sub
```

Pag3 Control cg_Ha:

Pag3 Control Label1:

Pag3 Control Label2:

Pag3 Control cg_Va:

Pag3 Control Label3:

Pag3 Control Label4:

Pag3 Control cg_Ma:

Pag3 Control Label5:

Pag3 Control Label6:

Pag3 Control cg_Hb:

Pag3 Control Label7:

Pag3 Control Label8:

Pag3 Control cg_Vb:

Pag3 Control Label9:

Pag3 Control Label10:

Pag3 Control cg_Mb:

Pag3 Control Label11:

Pag3 Control Label12:

Pag3 Control cg_Hc:

Pag3 Control Label13:

Pag3 Control Label14:

Pag3 Control cg_Vc:

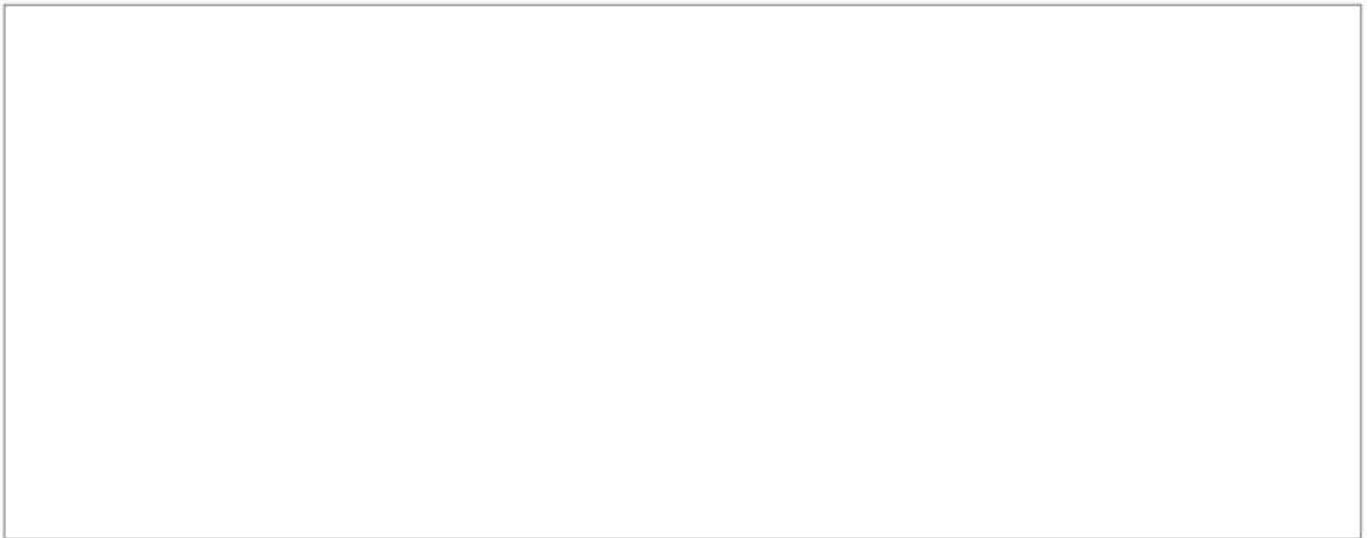
Pag3 Control Label15:

Pag3 Control Label16:

Pag3 Control cg_Mc:

Pag3 Control Label17:

Pag3 Control Label18:



Ha kN

Hb kN

Hc kN

Va kN

Vb kN

Vc kN

Ma kN.m

Mb kN.m

Mc kN.m

End Class

Pag4

Class Pag4

Inherits ContainerControl

Pag4 Control Canvas1:

```
Sub Paint(g As Graphics, areas() As REALbasic.Rect)
    g.DrawPicture(ScaleImage(IMG_esforcos_linha_tipo1, Me.Width, Me.Height), 0, 0)
End Sub
```

```
Sub Open()
    Me.Invalidate
```

End Sub

Pag4 Control TextField1:

Pag4 Control Label1:

Pag4 Control Label2:

Pag4 Control TextField2:

Pag4 Control Label3:

Pag4 Control Label4:

Pag4 Control TextField3:

Pag4 Control Label5:

Pag4 Control Label6:

Pag4 Control TextField4:

Pag4 Control Label7:

Pag4 Control Label8:

Pag4 Control TextField5:

Pag4 Control Label9:

Pag4 Control Label10:

Pag4 Control TextField6:

Pag4 Control Label11:

Pag4 Control Label12:

Pag4 Control TextField7:

Pag4 Control Label13:

Pag4 Control Label14:

Pag4 Control TextField8:

Pag4 Control Label15:

Pag4 Control Label16:

Pag4 Control TextField9:

Pag4 Control Label17:

Pag4 Control Label18:

Pag4 Control TextField10:

Pag4 Control Label19:

Pag4 Control Label20:

Pag4 Control TextField11:

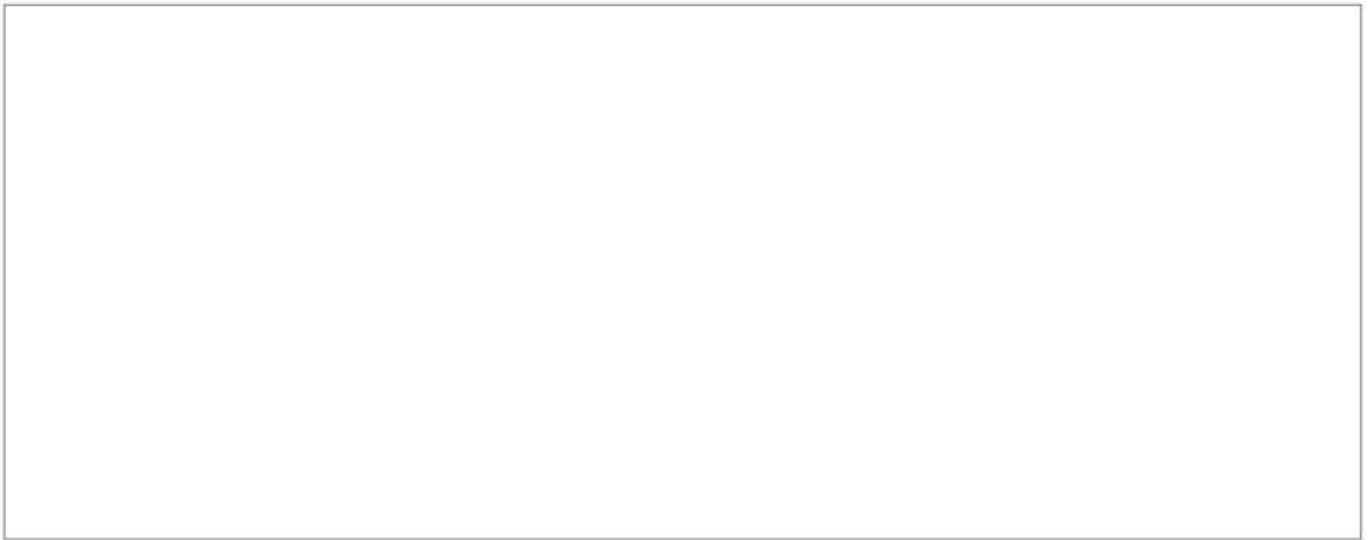
Pag4 Control Label21:

Pag4 Control Label22:

Pag4 Control TextField12:

Pag4 Control Label23:

Pag4 Control Label24:



Hab	<input type="text"/>	kN	Hac	<input type="text"/>	kN	Hbc	<input type="text"/>	kN	Habbc	<input type="text"/>	kN
Vab	<input type="text"/>	kN	Vac	<input type="text"/>	kN	Vbc	<input type="text"/>	kN	Vabbc	<input type="text"/>	kN
Mab	<input type="text"/>	kN.m	Mac	<input type="text"/>	kN.m	Mbc	<input type="text"/>	kN.m	Mabbc	<input type="text"/>	kN.m

End Class

Imagens

IMG logo utfpr

Any 313 @1x
640 x Any
Any
W x H = 640.00 x 313.00
Orientation = Any
Platform = Any
PP1 = 72

Any 626 (640 x 313 @2x)
1280 x Any
Any
W x H = 640.00 x 313.00
Orientation = Any
Platform = Any
PP1 = 144

Any 939 (640 x 313 @3x)
1920 x Any
Any
W x H = 640.00 x 313.00
Orientation = Any
Platform = Any
PP1 = 216

IMG logo ipb

Any 219 @1x
741 x Any
Any
W x H = 741.00 x 219.00
Orientation = Any
Platform = Any
PP1 = 72

Any 438 (741 x 219 @2x)
1482 x Any
Any
W x H = 741.00 x 219.00
Orientation = Any
Platform = Any
PP1 = 144

Any 657 (741 x 219 @3x)
2223 x Any
Any
W x H = 741.00 x 219.00
Orientation = Any
Platform = Any
PP1 = 216

IMG ligacao 1

Any 1318 @1x
3172 x Any
Any
W x H = 3172.00 x 1318.00
Orientation = Any
Platform = Any
PP1 = 72

Any 2636 (3172 x 1318 @2x)
6344 x Any
Any
W x H = 3172.00 x 1318.00
Orientation = Any
Platform = Any
PP1 = 144

Any 3954 (3172 x 1318 @3x)
9516 x Any
Any
W x H = 3172.00 x 1318.00
Orientation = Any
Platform = Any
PP1 = 216

IMG esforcos cg tipo1

Any 1324 @1x
3682 x Any
Any
W x H = 3682.00 x 1324.00
Orientation = Any
Platform = Any
PP1 = 72

Any 2648 (3682 x 1324 @2x)
7364 x Any
Any
W x H = 3682.00 x 1324.00
Orientation = Any

Platform = Any

PP1 = 144

Any 3972 (3682 x 1324 @3x)

11046 x Any

Any

W x H = 3682.00 x 1324.00

Orientation = Any

Platform = Any

PP1 = 216

IMG esforcos linha tipo1

Any 1383 @1x

3259 x Any

Any

W x H = 3259.00 x 1383.00

Orientation = Any

Platform = Any

PP1 = 72

Any 2766 (3259 x 1383 @2x)

6518 x Any

Any

W x H = 3259.00 x 1383.00

Orientation = Any

Platform = Any

PP1 = 144

Any 4149 (3259 x 1383 @3x)

9777 x Any

Any

W x H = 3259.00 x 1383.00

Orientation = Any

Platform = Any

PP1 = 216

MetodosGlobais

Module MetodosGlobais

Methods

Function ScaleImage(p as Picture, maxWidth as Integer, maxHeight as Integer) As Picture

If p <> Nil Then

```

// Calculate the scale ratio
Dim ratio As Double = Min(maxHeight / p.height, maxWidth / p.width)

// Create a new picture to return
Dim newPic As New Picture(p.width * ratio, p.height * ratio)

// Draw picture in the new size
newPic.graphics.DrawPicture(p, 0, 0, newPic.width, newPic.height, 0, 0, p.width, p.height)

Return newPic

End If
End Function

Function StrF(extends t as double) As String
'Controle do formato numérico exportado em .txt

If Abs(t) < 0.01 Or Abs(t) > 10000 Then
Return Str(t, "-#.0#####e")
Else
Return Str(t, "-####.0##")
End
End Function

End Module

```

MetodosCalculo

Module MetodosCalculo

Constants

```
Const kPi = 3.14159265358979323846264338
```

Methods

```
Sub verif_cap_res_tipo1()
'Verificação da capacidade resistente da ligação

'Ligação Tipo 1 - Duas peças em ligação de extremidade
```

```
*****
```

```
'Definição de variáveis
```

```
Dim Va, Ha, Ma, Vb, Hb, Mb, Vc, Hc, Mc As Double
Dim Aef, Ix, Iy, Ip, rmax, WelB, hef, d, Wpl,  $\alpha$ pl, Ku, K $\phi$ , Kx As Double
Dim Fed, Tfd, WplB, Tmd,  $\alpha$ ,  $\beta$  As Double
```

```
Dim Acapres, Bcapres, Ccapres As Double
Dim Mcentro, SigmaM, SigmaF, SigmaT, a As Double
Dim Lef, FxEd1, FxEd2, FyEd1, FyEd2, FxEd, FyEd, FmEd As Double
Dim fn0k, fn90k, k,  $\gamma$  As Double
Dim FxRk, FxRd, FyRk, FyRd As Double
Dim Acapcha, Bcapcha, Ccapcha As Double
```

```
*****
```

```
'Valores do exemplo resolvido (SI)
```

```
Dim f As FolderItem
Dim x As TextOutputStream
f = GetSaveFolderItem("", "relatorio-tipo1.txt")
x = TextOutputStream.Create(f)

Dim data As Xojo.Core.Date = Xojo.Core.Date.Now
x.WriteLine(data.ToText)
```

```
x.WriteLine("RELATÓRIO DE CÁLCULO")
x.WriteLine("Tipo de ligação: duas peças em extremidade (heel joint)")
x.WriteLine
x.WriteLine("*****")
x.WriteLine("*****")
```

```
x.WriteLine
x.WriteLine("Dimensões da ligação (ver legenda):")
```

```
'dim_a=0.160 'm
x.WriteLine("dim_a := "+ dim_a.StrF + " [m]")
'dim_b=0.160 'm
x.WriteLine("dim_b := "+ dim_b.StrF + " [m]")
'dim_c=0.88 'm
x.WriteLine("dim_c := "+ dim_c.StrF + " [m]")
'dim_d=0.64 'm
x.WriteLine("dim_d := "+ dim_d.StrF + " [m]")
'dim_e=0.350 'm
x.WriteLine("dim_e := "+ dim_e.StrF + " [m]")
'dim_f=0.210 'm
x.WriteLine("dim_f := "+ dim_f.StrF + " [m]")
'dim_g=22 'deg
x.WriteLine("dim_g := "+ dim_g.StrF + " [deg]")
```

```
x.WriteLine
x.WriteLine("Propriedades da chapa:")
```

```
t=0.0015 'm
x.WriteLine("t := "+ t.StrF + " [m] - espessura")
kser=3500000 'N/m3
x.WriteLine("kser := "+ kser.StrF + " [N/m3] - modulo de escorregamento")
```

```

fa00k=2310000 'N/m2
x.WriteLine("fa00k := "+ fa00k.StrF + " [N/m2] - tensão resistente de ancoragem, para  $\alpha = 0^\circ$  e  $\beta = 0^\circ$  ")
fa9090k=1300000 'N/m2
x.WriteLine("fa9090k := "+ fa9090k.StrF + " [N/m2] - tensão resistente de ancoragem, para  $\alpha = 90^\circ$  e  $\beta = 90^\circ$  ")
k1=-22000 'N/deg.m2
x.WriteLine("k1 := "+ k1.StrF + " [N/deg.m2] - constante1")
k2=3100 'N/deg.m2
x.WriteLine("k2 := "+ k2.StrF + " [N/deg.m2] - constante2")
 $\alpha$ 0=38 'deg
x.WriteLine("alpha := "+ alpha0.StrF + " [deg] - constante3")

x.WriteLine
x.WriteLine("Propriedades da madeira:")

ft0k=320000 'N/m
x.WriteLine("ft0k := "+ ft0k.StrF + " [N/m2] - tensão resistente de tração, paralelo às fibras")
ft90k=200000 'N/m
x.WriteLine("ft90k := "+ ft90k.StrF + " [N/m2] - tensão resistente de tração, perpendicular às fibras")
fc0k=210000 'N/m
x.WriteLine("fc0k := "+ fc0k.StrF + " [N/m2] - tensão resistente de compressão, paralelo às fibras")
fc90k=151000 'N/m
x.WriteLine("fc90k := "+ fc90k.StrF + " [N/m2] - tensão resistente de compressão, perpendicular às fibras")
fv0k=106000 'N/m
x.WriteLine("fv0k := "+ fv0k.StrF + " [N/m2] - tensão resistente de embutimento, paralelo às fibras")
fv90k=87000 'N/m
x.WriteLine("fv90k := "+ fv90k.StrF + " [N/m2] - tensão resistente de embutimento, perpendicular às fibras")
 $\gamma$ 0=16 'deg
x.WriteLine("gamma0 := "+ gamma0.StrF + " [deg] - ângulo característico da chapa")
kv=0.7
x.WriteLine("kv := "+ kv.StrF + " [--] - fator de redução para peças entalhadas")
kmod=0.9
x.WriteLine("kmod := "+ kmod.StrF + " [--] - fator de redução")
 $\gamma$ M=1.3
x.WriteLine("gammaM := "+ gammaM.StrF + " [--] - coeficiente de segurança")

x.WriteLine
x.WriteLine("Esforços solicitantes no CG dos nós:")

Va=7670 'N
x.WriteLine("Va := "+ Va.StrF + " [N] - força vertical.")
Ha=-28200 'N
x.WriteLine("Ha := "+ Ha.StrF + " [N] - força horizontal")
Ma=700 'N*m
x.WriteLine("Ma := "+ Ma.StrF + " [N*m] - momento")

x.WriteLine("")

Vb=-6340 'N
x.WriteLine("Vb := "+ Vb.StrF + " [N] - força vertical.")

```



```

Hb=26200 'N
x.WriteLine("Hb := "+ Hb.StrF + " [N] - força horizontal")
Mb=200 'N*m
x.WriteLine("Mb := "+ Mb.StrF + " [N*m] - momento")

x.WriteLine("")

Vc=-1510 'N
x.WriteLine("Vc := "+ Vc.StrF + " [N] - força vertical.")
Hc=2220 'N
x.WriteLine("Hc := "+ Hc.StrF + " [N] - força horizontal")
Mc=220 'N*m
x.WriteLine("Mc := "+ Mc.StrF + " [N*m] - momento")

x.WriteLine("")
x.WriteLine("Obs: convenção positiva para cima, direita e anti-horária.")

*****
'ZONA SUPERIOR ESQUERDA (NÓ A)

'Características geométricas e mecânicas da zona

x.WriteLine("")
x.WriteLine("*****")
x.WriteLine("")
x.WriteLine("ZONA SUPERIOR ESQUERDA (NÓ A)")
x.WriteLine("")
x.WriteLine("Propriedades geométricas da zona:")

Aef= 0.024964117 'm2
x.WriteLine("Aef := "+ Aef.StrF + " [m2] - Área efetiva")
Ix= 0.000011543 'm4
x.WriteLine("Ix := "+ Ix.StrF + " [m4] - Inércia na direção principal")
Iy=0.000247901 'm4
x.WriteLine("Iy := "+ Iy.StrF + " [m4] - Inércia na perpendicular à direção principal")
Ip=Ix+Iy 'm4
x.WriteLine("Ip := Ix+Iy - momento polar de inércia")
x.WriteLine("Ip = "+ Ix.StrF + " + " + Iy.StrF + " = " + Ip.StrF+ " [m4] ")
rmax=0.2532159 'm
x.WriteLine("rmax := "+ rmax.StrF + " [m] - maior distância até o CG da zona")
WelB=Ip/rmax 'm3
x.WriteLine("WelB := Ip/rmax - módulo de rigidez elástico")
x.WriteLine("WelB = "+ Ip.StrF + "/" + rmax.StrF + " = " + WelB.StrF + " [m3] ")
hef=0.079 'm
x.WriteLine("hef := "+ hef.StrF + " [m4] - maior altura efetiva de ancoragem perpendicular ao maior lado")
d=Sqrt( (Aef/hef)^2+hef^2 ) 'm
x.WriteLine("d := Sqrt((Aef/hef)^2+hef^2) - EN 1995-1-1 8.49")
x.WriteLine("d = Sqrt((" + Aef.StrF + "/" + hef.StrF + ")^2 + " + hef.StrF + "^2) = " + d.StrF + " [m4]")
Wpl=ae*d/4 'm3
x.WriteLine("Wpl := Aef*d/4 - Momento plástico EN 1995-1-1 8.48")

```

```

x.WriteLine("Wpl = " + Aef.StrF + "*" + d.StrF + "/4 = " + Wpl.StrF + " [m3]")
αpl=Min(Wpl/WelB,1.5)
x.WriteLine("αpl := Min(Wpl/WelB ; 1.5) - razão entre momento plástico e elástico")
x.WriteLine("αpl = Min(" + Wpl.StrF + "/" + WelB.StrF + " ; 1.5) = " + αpl.StrF + " [--]")

'Propriedades da mola

x.WriteLine("")
x.WriteLine("Propriedades da mola:")

Ku= (2*Kser)/(3*γM) 'N/m3
x.WriteLine("Ku := (2*Kser)/(3*γM) - módulo de escorregamento instantâneo")
x.WriteLine("Ku = (2*" + Kser.StrF + ")/(3*" + γM.StrF + ") = " + Ku.StrF + " [N/m3]")
Kφ=2*Ku*Ip 'N*m
x.WriteLine("Kφ := 2*Ku*Ip - Mola relativa à rotação")
x.WriteLine("Kφ = 2*" + Ku.StrF + "*" + Ip.StrF + " = " + Kφ.StrF + " [N*m]")
Kx=2*Ku*Aef 'N/m
x.WriteLine("Kx := 2*Ku*Aef - Mola relativa à translação")
x.WriteLine("Kx = 2*" + Ku.StrF + "*" + Aef.StrF + " = " + Kx.StrF + " [N/m]")

'Verificação da capacidade resistente

x.WriteLine("")
x.WriteLine("Verificação da capacidade resistente da ligação:")

Fed=Sqrt (Ha^2 +Va^2) 'N
x.WriteLine("Fed := Sqrt(Ha^2 +Va^2) - força resultante efetiva de cálculo")
x.WriteLine("Fed = Sqrt(" + Ha.StrF + "^2 + " + Va.StrF + "^2) = " + Fed.StrF + " [N]")
Tfd=Fed/Aef 'N/m2
x.WriteLine("Tfd := Fed/Aef - tensão efetiva de cálculo")
x.WriteLine("Tfd = " + Fed.StrF + "/" + Aef.StrF + " = " + Tfd.StrF + " [N/m2]")
WplB=αpl*WelB
x.WriteLine("WplB := αpl*WelB - momento plástico")
x.WriteLine("WplB = " + αpl.StrF + "*" + WelB.StrF + " = " + WplB.StrF + " [--]")
Tmd=Ma/WplB 'N/m2
x.WriteLine("Tmd := Ma/WplB")
x.WriteLine("Tmd = " + Ma.StrF + "/" + WplB.StrF + " = " + Tmd.StrF + " [N/m2]")
α=ATan(Va/-Ha)*180/kPi 'deg
x.WriteLine("α := ATan(Va/-Ha) - ângulo da resultante em relação à direção principal da placa")
x.WriteLine("α = ATan(" + Va.StrF + "/" + "-" + Ha.StrF + ") = " + α.StrF + " [deg]")
β=dim_g+α 'deg
x.WriteLine("β := dim_g+α - ângulo da resultante em relação à direção das fibras")
x.WriteLine("β = " + dim_g.StrF + " + " + α.StrF + " = " + β.StrF + " [deg]")

Dim temp1, temp2, temp3 As String
If α < α0 Then
    faα0k=fa00k+k1*α
    temp1="<"
    temp2="faα0k := fa00k+k1*α - EN 1995-1-1 8.44"
    temp3 ="faα0k = " + fa00k.StrF + " + " + k1.StrF + "*" + α.StrF + " = " + faα0k.StrF + " [N/m2]"

```

```

Else
  fa0k=fa0k+k1*α+k2*(α-α0)
  temp1=">"
  temp2="fa0k := fa0k+k1*α+k2*(α-α0) - EN 1995-1-1 8.44"
  temp3="fa0k = " + fa0k.StrF + " + " + k1.StrF + "*" + α.StrF + " + " + k2.StrF + "*" + (α.StrF + "-" + α0.StrF + ") = " + fa0k.StrF + " [N/m2]"
End If

x.WriteLine("α (" + α.StrF + "°) " + temp1 + " α0 (" + α0.StrF + "°) , então:")
x.WriteLine(temp2)
x.WriteLine(temp3)

If β < 45 Then
  fa0k=Max (fa0k - (fa0k-fa9090k)*β/45 , fa0k - (fa0k-fa9090k)*Sin( Max( α*kPi/180 , β*kPi/180 ) ) )
  temp1="<"
  temp2="fa0k := Max (fa0k - (fa0k-fa9090k)*β/4/kPi ; fa0k - (fa0k-fa9090k)*Sin(Max(α;β)) ) - EN 1995-1-1 8.42 e 8.4"
  temp3="fa0k = Max(" + fa0k.StrF + " - " + (" + fa0k.StrF + " - " + fa9090k.StrF + ") * " + β.StrF + "/45 ; " + fa0k.StrF + " - (" + fa0k.StrF + " - " + fa9090k.StrF + ") * Sin(Max(" + α.StrF + " ; " + β.StrF + ")) = " + fa0k.StrF + " [N/m2]"
Else
  fa0k=fa0k - (fa0k-fa9090k)*Sin( Max( α*kPi/180 , β*kPi/180 ) )
  temp1=">"
  temp2="fa0k := fa0k - (fa0k-fa9090k)*Sin( Max(α*kPi/180 , β*kPi/180)) "
  temp3="fa0k = " + fa0k.StrF + " - (" + fa0k.StrF + " - " + fa9090k.StrF + ") * Sin(Max(" + α.StrF + " ; " + β.StrF + ")) = " + fa0k.StrF + " [N/m2]"
End If

x.WriteLine("β (" + β.StrF + "°) " + temp1 + " 45° , então:")
x.WriteLine(temp2)
x.WriteLine(temp3)

x.WriteLine("")
x.WriteLine("Resistências de cálculo:")

fa00d=fa00k*Kmod/γM 'N/m2
x.WriteLine("fa00d := fa00k*Kmod/γM")
x.WriteLine("fa00d = " + fa00k.StrF + "*" + Kmod.StrF + "/" + γM.StrF + " = " + fa00d.StrF + " [N/m2]")
fa0bd=fa0bk*Kmod/γM 'N/m2
x.WriteLine("fa0bd := fa0bk*Kmod/γM")
x.WriteLine("fa0bd = " + fa0bk.StrF + "*" + Kmod.StrF + "/" + γM.StrF + " = " + fa0bd.StrF + " [N/m2]")

x.WriteLine("")
x.WriteLine("Verificação da capacidade resistente da zona superior esquerda (nó A):")

Acapres=(Tfd/fa0bd)^2+(Tmd/fa00d)^2
x.WriteLine("Acapres := (Tfd/fa0bd)^2+(Tmd/fa00d)^2")
x.WriteLine("Acapres = (" + Tfd.StrF + "/" + fa0bd.StrF + ")^2 + (" + Tmd.StrF + "/" + fa00d.StrF + ")^2 = " + Acapres.StrF + " [--]")
Acapres=Acapres*100 '%
x.WriteLine("Acapres = " + Acapres.StrF + " %")

```

```

*****
'ZONA INFERIOR (NÓ B)

x.WriteLine("")
x.WriteLine("*****")
x.WriteLine("")
x.WriteLine("ZONA INFERIOR (NÓ B)")
x.WriteLine("")
x.WriteLine("Propriedades geométricas da zona:")

Aef= 0.03298 'm2
x.WriteLine("Aef := "+ Aef.StrF + " [m2] - Área efetiva")
Ix= 0.000009567 'm4
x.WriteLine("Ix := "+ Ix.StrF + " [m4] - Inércia na direção principal")
Iy=0.000858828 'm4
x.WriteLine("Iy := "+ Iy.StrF + " [m4] - Inércia na perpendicular à direção principal")
Ip=Ix+Iy 'm4
x.WriteLine("Ip := Ix+Iy - momento polar de inércia")
x.WriteLine("Ip = "+ Ix.StrF + " + " + Iy.StrF + " = " + Ip.StrF + " [m4] ")
rmax=0.281052486 'm
x.WriteLine("rmax := "+ rmax.StrF + " [m] - maior distância até o CG da zona")
WelB=Ip/rmax 'm3
x.WriteLine("WelB := Ip/rmax - módulo de rigidez elástico")
x.WriteLine("WelB = "+ Ip.StrF + "/" + rmax.StrF + " = " + WelB.StrF + " [m3]")
hef=0.059 'm
x.WriteLine("hef := "+ hef.StrF + " [m4] - maior altura efetiva de ancoragem perpendicular ao maior lado")
d=.Sqrt( (Aef/hef)^2+hef^2 ) 'm
x.WriteLine("d := Sqrt((Aef/hef)^2+hef^2) - EN 1995-1-1 8.49")
x.WriteLine("d = Sqrt((" + Aef.StrF + "/" + hef.StrF + ")^2 + " + hef.StrF + "^2) = " + d.StrF + " [m4]")
Wpl=af*d/4 'm3
x.WriteLine("Wpl := Aef*d/4 - Momento plástico EN 1995-1-1 8.48")
x.WriteLine("Wpl = "+ Aef.StrF + "*" + d.StrF + "/4 = " + Wpl.StrF + " [m3]")
apl=Min(Wpl/WelB,1.5)
x.WriteLine("apl := Min(Wpl/WelB ; 1.5) - razão entre momento plástico e elástico")
x.WriteLine("apl = Min(" + Wpl.StrF + "/" + WelB.StrF + " ; 1.5) = " + apl.StrF + " [--]")

'Propriedades da mola

x.WriteLine("")
x.WriteLine("Propriedades da mola:")

Ku= (2*Kser)/(3*γM) 'N/m3
x.WriteLine("Ku := (2*Kser)/(3*γM) - módulo de escorregamento instantâneo")
x.WriteLine("Ku = (2*" + Kser.StrF + ")/(3*" + γM.StrF + ") = " + Ku.StrF + " [N/m3]")
Kφ=2*Ku*Ip 'N*m
x.WriteLine("Kφ := 2*Ku*Ip - Mola relativa à rotação")
x.WriteLine("Kφ = 2*" + Ku.StrF + "*" + Ip.StrF + " = " + Kφ.StrF + " [N*m]")
Kx=2*Ku*Aef 'N/m
x.WriteLine("Kx := 2*Ku*Aef - Mola relativa à translação")
x.WriteLine("Kx = 2*" + Ku.StrF + "*" + Aef.StrF + " = " + Kx.StrF + " [N/m]")

```

'Verificação da capacidade resistente

```

x.WriteLine("")
x.WriteLine("Verificação da capacidade resistente da ligação:")

Fed=Sqrt (Hb^2 +Vb^2) 'N
x.WriteLine("Fed := Sqrt(Ha^2 +Va^2) - força resultante efetiva de cálculo")
x.WriteLine("Fed = Sqrt(" + Ha.StrF + "^2 + " + Va.StrF + "^2) = " + Fed.StrF + " [N]")
Tfd=Fed/Aef 'N/m2
x.WriteLine("Tfd := Fed/Aef - tensão efetiva de cálculo")
x.WriteLine("Tfd = " + Fed.StrF + "/" + Aef.StrF + " = " + Tfd.StrF + " [N/m2] ")
WplB=αpl*WelB
x.WriteLine("WplB := αpl*WelB - momento plástico")
x.WriteLine("WplB = " + αpl.StrF + "*" + WelB.StrF + " = " + WplB.StrF + " [--]")
Tmd=Mb/WplB 'N/m2
x.WriteLine("Tmd := Mb/WplB")
x.WriteLine("Tmd = " + Mb.StrF + "/" + WplB.StrF + " = " + Tmd.StrF + " [N/m2] ")
α=ATan(Va/-Ha)*180/kPi 'deg
x.WriteLine("α := ATan(Va/-Ha) - ângulo da resultante em relação à direção principal da placa")
x.WriteLine("α = ATan(" + Va.StrF + "/" + "-" + Ha.StrF + ") = " + α.StrF + " [deg]")
β=α 'deg
x.WriteLine("β := dim_g+α - ângulo da resultante em relação à direção das fibras")
x.WriteLine("β = " + dim_g.StrF + " + " + α.StrF + " = " + β.StrF + " [deg]")

If α < α0 Then
  faα0k=fa00k+k1*α
  temp1="<"
  temp2="faα0k := fa00k+k1*α - EN 1995-1-1 8.44"
  temp3 ="faα0k = " + fa00k.StrF + " + " + k1.StrF + "*" + α.StrF + " = " + faα0k.StrF + " [N/m2]"
Else
  faα0k=fa00k+k1*α+k2*(α-α0)
  temp1=">"
  temp2="faα0k := fa00k+k1*α+k2*(α-α0) - EN 1995-1-1 8.44"
  temp3 ="faα0k = " + fa00k.StrF + " + " + k1.StrF + "*" + α.StrF + " + " + k2.StrF + "*" + α.StrF + "-" + α0.StrF + " = " + faα0k.StrF + " [N/m2]"
End If

x.WriteLine("α (" + α.StrF + "°) " + temp1 + " α0 (" + α0.StrF + "°) , então:")
x.WriteLine(temp2)
x.WriteLine(temp3)

If β < 45 Then
  faαbk=Max (faα0k - (faα0k-fa9090k)*β/45 , fa00k - (fa00k-fa9090k)*Sin( Max( α*kPi/180 , β*kPi/180 ) ) )
  temp1="<"
  temp2="faαbk := Max (faα0k - (faα0k-fa9090k)*β*4/kPi ; fa00k - (fa00k-fa9090k)*Sin(Max(α;β)) ) - EN 1995-1-1 8.42 e 8.4"
  temp3="faαbk = Max(" + faα0k.StrF + " - " + "(" + faα0k.StrF + " - " + fa9090k.StrF + ")" + β.StrF + "/45 ; " + faα0k.StrF + " - (" + faα0k.StrF + " - " + fa9090k.StrF + ")*Sin(Max(" + α.StrF + " ; " + β.StrF + ")) = " + faαbk.StrF + " [N/m2]"
Else
  faαbk=faα0k - (faα0k-fa9090k)*Sin( Max( α*kPi/180 , β*kPi/180 ) )

```

```

temp1=">"
temp2="fa0bk := fa0k - (fa0k-fa9090k)*Sin( Max( $\alpha$ *kPi/180 ,  $\beta$ *kPi/180)) "
temp3="fa0bk = "+ fa0k.StrF + " - ( "+ fa0k.StrF + " - "+ fa9090k.StrF + ")*Sin(Max(" +  $\alpha$ .StrF + " ; "+  $\beta$ .StrF + ")) = "
+ fa0bk.StrF + " [N/m2]"
End If

x.WriteLine("β (" +  $\beta$ .StrF + "°) " + temp1 + " 45° , então:")
x.WriteLine(temp2)
x.WriteLine(temp3)

x.WriteLine("")
x.WriteLine("Resistências de cálculo:")

fa00d=fa0k*Kmod/ $\gamma$ M 'N/m2
x.WriteLine("fa00d := fa0k*Kmod/ $\gamma$ M")
x.WriteLine("fa00d = "+ fa0k.StrF + "*" + Kmod.StrF + "/" +  $\gamma$ M.StrF + " = "+ fa00d.StrF + " [N/m2]")
fa0bd=fa0bk*Kmod/ $\gamma$ M 'N/m2
x.WriteLine("fa0bd := fa0bk*Kmod/ $\gamma$ M")
x.WriteLine("fa0bd = "+ fa0bk.StrF + "*" + Kmod.StrF + "/" +  $\gamma$ M.StrF + " = "+ fa0bd.StrF + " [N/m2]")

x.WriteLine("")
x.WriteLine("Verificação da capacidade resistente da zona inferior (nó B):")

Bcapres=(Tfd/fa0bd)^2+(Tmd/fa00d)^2
x.WriteLine("Bcapres := (Tfd/fa0bd)^2+(Tmd/fa00d)^2")
x.WriteLine("Bcapres = (" + Tfd.StrF + "/" + fa0bd.StrF + ")^2 + (" + Tmd.StrF + "/" + fa00d.StrF + ")^2 = "+ Bcapres.StrF +
" [-]")
Bcapres=Bcapres*100 '%'
x.WriteLine("Bcapres = "+ Bcapres.StrF + " %")

*****
'ZONA SUPERIOR DIREITA (NÓ C)

x.WriteLine("")
x.WriteLine("*****")
x.WriteLine("")
x.WriteLine("ZONA SUPERIOR DIREITA (NÓ C)")
x.WriteLine("")
x.WriteLine("Propriedades geométricas da zona:")

Aef= 0.017088004 'm2
x.WriteLine("Aef := "+ Aef.StrF + " [m2] - Área efetiva")
Ix= 0.00000706 'm4
x.WriteLine("Ix := "+ Ix.StrF + " [m4] - Inércia na direção principal")
Iy=0.000094145 'm4
x.WriteLine("Iy := "+ Iy.StrF + " [m4] - Inércia na perpendicular à direção principal")
Ip=Ix+Iy 'm4
x.WriteLine("Ip := Ix+Iy - momento polar de inércia")
x.WriteLine("Ip = "+ Ix.StrF + " + "+ Iy.StrF + " = "+ Ip.StrF+ " [m4] ")
rmax=0.1876228 'm
x.WriteLine("rmax := "+ rmax.StrF + " [m] - maior distância até o CG da zona")

```

```

WelB=Ip/rmax 'm3
x.WriteLine("WelB := Ip/rmax - módulo de rigidez elástico")
x.WriteLine("WelB = " + Ip.StrF + "/" + rmax.StrF + " = " + WelB.StrF + " [m3]")
hef=0.079 'm
x.WriteLine("hef := " + hef.StrF + " [m4] - maior altura efetiva de ancoragem perpendicular ao maior lado")
d=Sqrt( (Aef/hef)^2+hef^2) 'm
x.WriteLine("d := Sqrt((Aef/hef)^2+hef^2) - EN 1995-1-1 8.49")
x.WriteLine("d = Sqrt((" + Aef.StrF + "/" + hef.StrF + ")^2 + " + hef.StrF + "^2) = " + d.StrF + " [m4]")
Wpl=aef*d/4 'm3
x.WriteLine("Wpl := Aef*d/4 - Momento plástico EN 1995-1-1 8.48")
x.WriteLine("Wpl = " + Aef.StrF + "*" + d.StrF + "/4 = " + Wpl.StrF + " [m3]")
αpl=Min(Wpl/WelB,1.5)
x.WriteLine("αpl := Min(Wpl/WelB ; 1.5) - razão entre momento plástico e elástico")
x.WriteLine("αpl = Min(" + Wpl.StrF + "/" + WelB.StrF + " ; 1.5) = " + αpl.StrF + " [--]")

```

'Propriedades da mola

```

x.WriteLine("")
x.WriteLine("Propriedades da mola:")

Ku= (2*Kser)/(3*γM) 'N/m3
x.WriteLine("Ku := (2*Kser)/(3*γM) - módulo de escorregamento instantâneo")
x.WriteLine("Ku = (2*" + Kser.StrF + ")/(3*" + γM.StrF + ") = " + Ku.StrF + " [N/m3]")
Kφ=2*Ku*Ip 'N*m
x.WriteLine("Kφ := 2*Ku*Ip - Mola relativa à rotação")
x.WriteLine("Kφ = 2*" + Ku.StrF + "*" + Ip.StrF + " = " + Kφ.StrF + " [N*m]")
Kx=2*Ku*Aef 'N/m
x.WriteLine("Kx := 2*Ku*Aef - Mola relativa à translação")
x.WriteLine("Kx = 2*" + Ku.StrF + "*" + Aef.StrF + " = " + Kx.StrF + " [N/m]")

```

'Verificação da capacidade resistente

```

x.WriteLine("")
x.WriteLine("Verificação da capacidade resistente da ligação:")

Fed=Sqrt (Hc^2 +Vc^2) 'N
x.WriteLine("Fed := Sqrt(Hc^2 +Vc^2) - força resultante efetiva de cálculo")
x.WriteLine("Fed = Sqrt(" + Hc.StrF + "^2 + " + Vc.StrF + "^2) = " + Fed.StrF + " [N]")
Tfd=Fed/Aef 'N/m2
x.WriteLine("Tfd := Fed/Aef - tensão efetiva de cálculo")
x.WriteLine("Tfd = " + Fed.StrF + "/" + Aef.StrF + " = " + Tfd.StrF + " [N/m2]")
WplB=αpl*WelB
x.WriteLine("WplB := αpl*WelB - momento plástico")
x.WriteLine("WplB = " + αpl.StrF + "*" + WelB.StrF + " = " + WplB.StrF + " [--]")
Tmd=Mc/WplB 'N/m2
x.WriteLine("Tmd := Mc/WplB")
x.WriteLine("Tmd = " + Mc.StrF + "/" + WplB.StrF + " = " + Tmd.StrF + " [N/m2]")
α=ATan(-Vc/Hc)*180/kPi 'deg
x.WriteLine("α := ATan(-Vc/Hc) - ângulo da resultante em relação à direção principal da placa")
x.WriteLine("α = ATan(" + Vc.StrF + "/" + "-" + Hc.StrF + ") = " + α.StrF + " [deg]")

```

$\beta = \alpha$ 'deg

x.WriteLine("β := α - ângulo da resultante em relação à direção das fibras")

x.WriteLine("β = " + α.StrF + " = " + β.StrF + " [deg]")

If $\alpha < \alpha_0$ Then

fa0k=fa0k+k1*α

temp1="<"

temp2="fa0k := fa0k+k1*α - EN 1995-1-1 8.44"

temp3="fa0k = " + fa0k.StrF + " + " + k1.StrF + "*" + α.StrF + " = " + fa0k.StrF + " [N/m2]"

Else

fa0k=fa0k+k1*α+k2*(α-α0)

temp1=">"

temp2="fa0k := fa0k+k1*α+k2*(α-α0) - EN 1995-1-1 8.44"

temp3="fa0k = " + fa0k.StrF + " + " + k1.StrF + "*" + α.StrF + " + " + k2.StrF + "*" + (α.StrF + "-" + α0.StrF + ") = " + fa0k.StrF + " [N/m2]"

End If

x.WriteLine("α (" + α.StrF + "°) " + temp1 + " α0 (" + α0.StrF + "°) , então:")

x.WriteLine(temp2)

x.WriteLine(temp3)

If $\beta < 45$ Then

fa0bk=Max (fa0k - (fa0k-fa9090k)*β/45 , fa0k - (fa0k-fa9090k)*Sin(Max(α*kPi/180 , β*kPi/180)))

temp1="<"

temp2="fa0bk := Max (fa0k - (fa0k-fa9090k)*β*4/kPi ; fa0k - (fa0k-fa9090k)*Sin(Max(α;β))) - EN 1995-1-1 8.42 e 8.4"

temp3="fa0bk = Max(" + fa0k.StrF + "-" + "(" + fa0k.StrF + "-" + fa9090k.StrF + ")" + β.StrF + "/45 ; " + fa0k.StrF + "-" + "(" + fa0k.StrF + "-" + fa9090k.StrF + ")"*Sin(Max(" + α.StrF + ";" + β.StrF + "))) = " + fa0bk.StrF + " [N/m2]"

Else

fa0bk=fa0k - (fa0k-fa9090k)*Sin(Max(α*kPi/180 , β*kPi/180))

temp1=">"

temp2="fa0bk := fa0k - (fa0k-fa9090k)*Sin(Max(α*kPi/180 , β*kPi/180)) "

temp3="fa0bk = " + fa0k.StrF + "-" + "(" + fa0k.StrF + "-" + fa9090k.StrF + ")"*Sin(Max(" + α.StrF + ";" + β.StrF + "))) = " + fa0bk.StrF + " [N/m2]"

End If

x.WriteLine("β (" + β.StrF + "°) " + temp1 + " 45° , então:")

x.WriteLine(temp2)

x.WriteLine(temp3)

x.WriteLine("")

x.WriteLine("Resistências de cálculo:")

fa00d=fa0k*Kmod/γM 'N/m2

x.WriteLine("fa00d := fa0k*Kmod/γM")

x.WriteLine("fa00d = " + fa0k.StrF + "*" + Kmod.StrF + "/" + γM.StrF + " = " + fa00d.StrF + " [N/m2]")

fa0bd=fa0bk*Kmod/γM 'N/m2

x.WriteLine("fa0bd := fa0bk*Kmod/γM")

x.WriteLine("fa0bd = " + fa0bk.StrF + "*" + Kmod.StrF + "/" + γM.StrF + " = " + fa0bd.StrF + " [N/m2]")

x.WriteLine("")


```

x.WriteLine("Verificação da capacidade resistente da zona superior direita (nó C):")

Ccapres=(Tfd/faαbd)^2+(Tmd/fa00d)^2
x.WriteLine("Ccapres := (Tfd/faαbd)^2+(Tmd/fa00d)^2")
x.WriteLine("Ccapres = (" + Tfd.StrF + "/" + faαbd.StrF + ")^2 + (" + Tmd.StrF + "/" + fa00d.StrF + ")^2 = " + Ccapres.StrF +
" [-]")
Ccapres=Ccapres*100 '%'
x.WriteLine("Ccapres = " + Ccapres.StrF + " %")

x.WriteLine("")

x.WriteLine("Resumo da capacidade resistente da ligação: ")
x.WriteLine("Acapres = " + Acapres.StrF + " %" + " ; Bcapres = " + Bcapres.StrF + " %" + " ; Ccapres = " + Ccapres.StrF +
" %")

*****
'Capacidade resistente da chapa

'LINHA A-B + C-B

'Comprimento efetivo da linha de ruptura
Lef=0.559 'm

'Menor distância entre o CG e a linha de ruptura
a=0.0345 'm

'Esforço efetivo na linha de ruptura
Mcentro=Hb*a-Mb 'N*m
'As demais forças (Horizontal e Vertical) são as próprias forças no nó

'Tensões na linha de ruptura
SigmaM=4*Mcentro/lef^2 'N/m
SigmaF=-Vb/Lef 'N/m
SigmaT=Hb/Lef 'N/m

'Força do binário correspondente à MEd
FmEd=2*(Mcentro)/Lef 'N

'Força efetiva no CG da placa
Fed=.Sqrt(Hb^2+Vb^2) 'N

'Ângulo da força resultante
α=ATan(Vb/-Hb) 'rad

'Ângulo entre a direção X da placa e a linha de ruptura
γ=0 'rad

'Forças atuantes na direção principal e perpendicular da linha de ruptura
'Principal
FxE1=Fed*cos(α)+2*FmEd*sin(γ) 'N
FxE2=Fed*cos(α)-2*FmEd*sin(γ) 'N

```

```
FxEd=Max(FxEd1,FxEd2) 'N
```

```
'Perpendicular
```

```
FyEd1=Fed*Sin(α)+2*FmEd*Cos(γ) 'N
```

```
FyEd2=Fed*Sin(α)-2*FmEd*Cos(γ) 'N
```

```
FyEd=Max(FyEd1,FyEd2) 'N
```

```
'Obtenção dos esforços resistentes de cálculo
```

```
If FxEd < 0 Then
```

```
    fn0k=fc0k 'N/m2
```

```
    k=1
```

```
Else
```

```
    fn0k=ft0k 'N/m2
```

```
    k=1+kv*Sin(2*γ)
```

```
End If
```

```
If FyEd < 0 Then
```

```
    fn90k=fc90k 'N/m2
```

```
Else
```

```
    fn90k=ft90k 'N/m2
```

```
End If
```

```
'Capacidade Resistente da placa
```

```
FxRk=Max(Abs( fn0k*Lef*Sin(γ-γ0*Sin(2*γ*kPi/180)) ), Abs( fv0k*Lef*Cos(γ*kPi/180) ) ) 'N
```

```
FxRd=FxRk/γM 'N
```

```
FyRk=Max( Abs( fn90k*Lef*Cos(γ*kPi/180) ), k*fv90k*Lef*Sin(γ*kPi/180) ) 'N
```

```
FyRd=FyRk/γM 'N
```

```
Bcapcha= ( FxEd/FxEd )^2 + ( FyEd/FyRd )^2
```

```
Bcapcha=Bcapcha*100 '%
```

```
x.Close
```

```
Dim c As Double
```

```
End Sub
```

```
Sub verif_cap_res_tipo2(x1 as double, x2 as double, x3 as double, x4 as double, x5 as double)
```

```
    'Verificação da capacidade resistente da ligação
```

```
    'Ligação Tipo 1 - Duas peças em ligação de extremidade
```

```
*****
```

'Definição de variáveis

```
Dim Va, Ha, Ma, Vb, Hb, Mb, Vc, Hc, Mc As Double
Dim Aef, Ix, Iy, Ip, rmax, WelB, hef, d, Wpl,  $\alpha$ pl, Ku, K $\phi$ , Kx As Double
Dim Fed, Tfd, WplB, Tmd,  $\alpha$ ,  $\beta$  As Double
Dim Acapres, Bcapres, Ccapres As Double
Dim Mcentro, SigmaM, SigmaF, SigmaT, a As Double
Dim Lef, FxEd1, FxEd2, FyEd1, FyEd2, FxEd, FyEd, FmEd As Double
Dim fn0k, fn90k, k,  $\gamma$  As Double
Dim FxRk, FxRd, FyRk, FyRd As Double
Dim Acapcha, Bcapcha, Ccapcha As Double
```

'Valores do exemplo resolvido (SI)

```
Dim f As FolderItem
Dim x As TextOutputStream
f = GetSaveFolderItem("", "relatorio-tipo1.txt")
x = TextOutputStream.Create(f)

Dim data As Xojo.Core.Date = Xojo.Core.Date.Now
x.WriteLine(data.ToText)
```

```
'x.WriteLine("RELATÓRIO DE CÁLCULO")
'x.WriteLine("Tipo de ligação: duas peças em extremidade (heel joint)")
'x.WriteLine
'x.WriteLine("*****")
'x.WriteLine("*****")
```

```
'x.WriteLine
'x.WriteLine("Dimensões da ligação (ver legenda):")
```

```
dim_a=0.160 'm
'x.WriteLine("dim_a := "+ dim_a.StrF + " [m]")
dim_b=0.160 'm
'x.WriteLine("dim_b := "+ dim_b.StrF + " [m]")
dim_c=0.88 'm
'x.WriteLine("dim_c := "+ dim_c.StrF + " [m]")
dim_d=0.64 'm
'x.WriteLine("dim_d := "+ dim_d.StrF + " [m]")
dim_e=0.350 'm
'x.WriteLine("dim_e := "+ dim_e.StrF + " [m]")
dim_f=0.210 'm
'x.WriteLine("dim_f := "+ dim_f.StrF + " [m]")
dim_g=22 'deg
'x.WriteLine("dim_g := "+ dim_g.StrF + " [deg]")
```

```
'x.WriteLine
'x.WriteLine("Propriedades da chapa:")
```

```

t=0.0015 'm
'x.WriteLine("t := " + t.StrF + " [m] - espessura")
kser=3500000 'N/m3
'x.WriteLine("kser := " + kser.StrF + " [N/m3] - modulo de escorregamento")
fa00k=2310000 'N/m2
'x.WriteLine("fa00k := " + fa00k.StrF + " [N/m2] - tensão resistente de ancoragem, para  $\alpha = 0^\circ$  e  $\beta = 0^\circ$ ")
fa9090k=1300000 'N/m2
'x.WriteLine("fa9090k := " + fa9090k.StrF + " [N/m2] - tensão resistente de ancoragem, para  $\alpha = 90^\circ$  e  $\beta = 90^\circ$ ")
k1=-22000 'N/deg.m2
'x.WriteLine("k1 := " + k1.StrF + " [N/deg.m2] - constante1")
k2=3100 'N/deg.m2
'x.WriteLine("k2 := " + k2.StrF + " [N/deg.m2] - constante2")
 $\alpha$ 0=38 'deg
'x.WriteLine(" $\alpha$ 0 := " +  $\alpha$ 0.StrF + " [deg] - constante3")

x.WriteLine
'x.WriteLine("Propriedades da madeira:")

ft0k=320000 'N/m
'x.WriteLine("ft0k := " + ft0k.StrF + " [N/m2] - tensão resistente de tração, paralelo às fibras")
ft90k=200000 'N/m
'x.WriteLine("ft90k := " + ft90k.StrF + " [N/m2] - tensão resistente de tração, perpendicular às fibras")
fc0k=210000 'N/m
'x.WriteLine("fc0k := " + fc0k.StrF + " [N/m2] - tensão resistente de compressão, paralelo às fibras")
fc90k=151000 'N/m
'x.WriteLine("fc90k := " + fc90k.StrF + " [N/m2] - tensão resistente de compressão, perpendicular às fibras")
fv0k=106000 'N/m
'x.WriteLine("fv0k := " + fv0k.StrF + " [N/m2] - tensão resistente de embutimento, paralelo às fibras")
fv90k=87000 'N/m
'x.WriteLine("fv90k := " + fv90k.StrF + " [N/m2] - tensão resistente de embutimento, perpendicular às fibras")
 $\gamma$ 0=16 'deg
'x.WriteLine(" $\gamma$ 0 := " +  $\gamma$ 0.StrF + " [deg] - ângulo característico da chapa")
kv=0.7
'x.WriteLine("kv := " + kv.StrF + " [--] - fator de redução para peças entalhadas")
kmod=0.9
'x.WriteLine("kmod := " + kmod.StrF + " [--] - fator de redução")
 $\gamma$ M=1.3

*****
'Capacidade resistente da chapa

LINHA A-B + C-B

'Comprimento efetivo da linha de ruptura
Lef=x5 'm

Forças atuantes na linha de ruptura
dim H,V,M as double

```

H=x1 'N
 V=x2 'N
 M=x3 ' N*m

'Momento atuante na linha de ruptura
 FmEd=M/Lef

'Ângulo entre a direção X da placa e a linha de ruptura
 γ =x4 'rad
 $22 \cdot k\pi/180$

'Força efetiva no CG da placa
 Fed=Sqrt(H^2+V^2) 'N

'Ângulo da força resultante
 α =ATan(-V/H) 'rad

'Forças atuantes na direção principal e perpendicular da linha de ruptura

'Principal
 FxEd1=Fed*Cos(α)+2*FmEd*Sin(γ) 'N
 FxEd2=Fed*Cos(α)-2*FmEd*Sin(γ) 'N
 FxEd=Max(FxEd1,FxEd2) 'N

'Perpendicular
 FyEd1=Fed*Sin(α)+2*FmEd*Cos(γ) 'N
 FyEd2=Fed*Sin(α)-2*FmEd*Cos(γ) 'N
 FyEd=Max(FyEd1,FyEd2) 'N

'Obtenção dos esforços resistentes de cálculo

If FxEd < 0 Then
 fn0k=fc0k 'N/m2
 k=1
 Else
 fn0k=ft0k 'N/m2
 k=1+kv*Sin(2* γ)
 End If

If FyEd < 0 Then
 fn90k=fc90k 'N/m2
 Else
 fn90k=ft90k 'N/m2
 End If

'Capacidade Resistente da placa

FxRk=Max(Abs(fn0k*Lef*Sin(γ - γ_0 *Sin(2* γ *kPi/180))), Abs(fv0k*Lef*Cos(γ *kPi/180))) 'N
 FxRd=FxRk/ γ M 'N

FyRk=Max(Abs(fn90k*Lef*Cos(γ *kPi/180)) , k*fv90k*Lef*Sin(γ *kPi/180)) 'N

```
FyRd=FyRk/γM 'N
```

```
Bcapcha= ( FxEd/FxRd )^2 + ( FyEd/FyRd )^2
```

```
x.WriteLine("Bcapcha := (FxEd/FxRd)^2+(FyEd/FyRd)^2")
```

```
x.WriteLine("Bcapcha = (" + FxEd.StrF + "/" + FxRd.StrF + ")^2 + (" + FyEd.StrF + "/" + FyRd.StrF + ")^2 = "+ Bcapcha.StrF +  
" [--]")
```

```
Bcapcha=Bcapcha*100 '%
```

```
x.WriteLine("Bcapcha = " + Bcapcha.StrF + " %")
```

```
x.WriteLine(FxEd.StrF)
```

```
x.WriteLine(FxRd.StrF)
```

```
x.WriteLine(FyEd.StrF)
```

```
x.WriteLine(FyRd.StrF)
```

```
x.Close
```

```
Dim c As Double
```

```
End Sub
```

Properties

```
dim_a As double
```

```
dim_b As double
```

```
dim_c As double
```

```
dim_d As double
```

```
dim_e As double
```

```
dim_f As double
```

```
dim_g As double
```

```
fa00d As Double
```

fa00k As double

fa9090k As double

fa α 0k As Double

fa α bd As Double

fa α bk As double

fc0k As double

fc90k As double

ft0k As double

ft90k As double

fv0k As double

fv90k As double

k1 As double

k2 As double

kmod As double

kser As double

kv As double

t As double

α_0 As double

γ_0 As double

γ_M As double

End Module